University of South Carolina
Scholar Commons

Theses and Dissertations

2018

Understanding The Adsorption And Nucleation Of Transition Metals On A Model Carbon Support

Grant S. Seuser
University of South Carolina

Follow this and additional works at: https://scholarcommons.sc.edu/etd

 Part of the Chemistry Commons

Recommended Citation

Seuser, G. S.(2018). *Understanding The Adsorption And Nucleation Of Transition Metals On A Model Carbon Support.* (Doctoral dissertation). Retrieved from https://scholarcommons.sc.edu/etd/4878

This Open Access Dissertation is brought to you by Scholar Commons. It has been accepted for inclusion in Theses and Dissertations by an authorized administrator of Scholar Commons. For more information, please contact dillarda@mailbox.sc.edu.

www.manaraa.com

UNDERSTANDING THE ADSORPTION AND NUCLEATION OF TRANSITION METALS ON A MODEL CARBON SUPPORT

by

Grant S. Seuser

Bachelor of Science
University of Houston, 2013

Submitted in Partial Fulfillment of the Requirements

For the Degree of Doctor of Philosophy in

Chemistry

College of Arts and Sciences

University of South Carolina

2018

Accepted by

Donna A. Chen, Major Professor

Vitaly Rassolov, Committee Member

Thomas M. Makris, Committee Member

John R. Regalbuto, Committee Member

Cheryl L. Addy, Vice Provost and Dean of the Graduate School

www.manaraa.com

© Copyright by Grant S. Seuser, 2018
All Rights Reserved.

www.manaraa.com

DEDICATION

I dedicate this work to my mother, father and brother.

www.manaraa.com

ACKNOWLEDGEMENTS

I would first like to express my appreciation for my advisor, Dr. Donna A. Chen, who has provided me with excellent guidance over the course of my graduate school career. I would also like to like to thank the current and former group members of Dr. Chen's research group who have helped me tremendously: Dr. Randima Galhenage, Dr. Audrey Duke, Dr. Kangmin Xie, Amy Brandt, Thathsara Maddumapatabandi, Deependra Shakya, Sharfa Farzandh, and Greg King.

I would also like to thank Dr. John R. Regalbuto, who I collaborated with extensively and with whom I learned much about the art and science of catalysts preparation. Of course, none of that work would have been possible without the help of the Regalbuto group members: Dr. Ritu, Banarjee, Dr. Huynh Ngoc Tien, Dr. John Tengco, Dr. Jayson Keels, Dr. Andrew Wang, Dr. Sonia Eskandari, Dr. Bahareh A. T. Mehrabadi, Dr. Fahad Almalki, Jeremiah Lipp, Sean Noble and Jessica Alers. I've also enjoyed my productive discussions with other chemistry and chemical engineering students, including Mevan Dissanayake, Nick Delucia, Victoria Bobo, José L. Contreras-Mora, Elizabeth Barlow, Nabi Shoukouri, Xinbin Yu and Greg Tate.

Last, but certainly not least, I'd like to thank professors and faculty members from whom I have learned so much, including Dr. Jochen Lauterbach, Dr. Chris Williams, Dr. S. Michael Angel, Dr. Myrick, Dr. Vitaly Rassolov, Dr. Stephen Morgan, Dr. Mark Berg, Dr. Andrew Greytak and Dr. Leslie Lovelace. And I would like to thank anyone who I may have inadvertently left out.

www.manaraa.com

ABSTRACT

Heterogeneous catalysis plays a vital role in the commercial production of chemicals. However, much is still unknown about the fundamental surface chemistry involved in catalyst preparation and the surface chemistry of the catalysts themselves. In the first part of this work, a surface science approach was employed to develop a fundamental understanding of the surface chemistry of strong electrostatic adsorption (SEA) of metal precursors on a model carbon support, highly oriented pyrolytic graphite (HOPG). SEA is a wet impregnation method in which anionic/cationic metal precursors are adsorbed onto positively/negatively charged functional groups by adjusting the pH of the solution above or below the point of zero charge of the support. The precursors are subsequently reduced to generate small, well-dispersed nanoparticles. Our findings show that hydroxyl groups on the surface of HOPG mediate the adsorption of Pt and Pd cationic precursors by deprotonating under basic conditions and accumulating a negative charge. In the case of Pt and Pd anionic precursors, hydroxyl groups did not mediate the adsorption of the precursors under acidic conditions. Moreover, the adsorption of the Pt anion was not purely electrostatic and most likely involves a chemical interaction with the support. The reduction of Pt precursors adsorbed onto HOPG lead to the formation of dendritic like clusters, indicative of Pt being highly mobile on the surface and having a weak interaction with the support. The addition of hydroxyl groups did not influence the nucleation of Pt for either precursor.

www.manaraa.com

In the second part of this work, model surfaces were prepared and characterized under ultra-high vacuum conditions, enabling excellent control over the surface composition and morphology of the sample. Re clusters of varying sizes were grown on HOPG to help distinguish between cluster size effects and chemical interactions between Re and oxygen on TiO_2(110). Our findings suggest there is indeed a strong chemical interaction that takes place between Re and oxygen on TiO_2(110). Lastly, the oxidation states of Re in PtRe catalysts may play an important role in the aqueous phase reforming of oxygenated hydrocarbons and the water gas shift reaction. To understand how the presence of Pt may facilitate the oxidation state of Re, XPS was used to determine the oxidation states that were present on Re films grown on Pt(111) after exposure to oxygen. Based on these studies, it was concluded that the presence of Pt does not facilitate the oxidation of Re films.

www.manaraa.com

TABLE OF CONTENTS

Dedication iii

Acknowledgements iv

Abstract v

List of Tables x

List of Figures xi

List of Abbreviations xvi

Chapter 1: Introduction 1

1.1 Heterogeneous catalysis 2

1.2 Surface Science – a model approach to catalysis 3

1.3 Motivation 3

1.4 References 9

Chapter 2: Instrumentation and techniques 16

2.1 X-ray photoelectron spectroscopy 17

2.2 Low energy ion scattering 18

2.3 Scanning probe microscopy 18

2.4 Transmission Fourier transform infrared spectroscopy 20

2.5 Inductively coupled plasma atomic emission spectroscopy 20

2.6 References 24

Chapter 3: Understanding uptake of Pt precursors during strong electrostatic adsorption On single-crystal carbon surfaces 27

www.manaraa.com

3.1 Introduction....28

3.2 Experimental....29

3.3 Results and Discussion....33

3.4 Conclusions....42

3.5 References....51

Chapter 4: Comparing strong electrostatic adsorption of Pt and Pd precursors on graphitic supports....57

4.1 Introduction....58

4.2 Experimental....60

4.3 Results and Discussion....64

4.4 Conclusions....74

4.5 References....86

Chapter 5: Nucleation of Re cluster on HOPG: distinguishing between cluster size effects and oxygen coordination....91

5.1 Introduction....92

5.2 Experimental....94

5.3 Results and Discussion....96

5.4 Conclusions....99

5.5 References....105

Chapter 6: Growth and oxidation of Re films on Pt(111)....111

6.1 Introduction....112

6.2 Experimental....114

6.3 Results and Discussion....115

6.4 Conclusions....124

www.manaraa.com

6.5 References.....131

Appendix A: Supplemental Table for Chapter 3 139

Appendix B: Permission to Print for Chapter 3 142

www.manaraa.com

LIST OF TABLES

Table 4.1: PZC and O(1s)/C(1s) ratios of GN-Alfa supports that underwent a different acid and reduction treatments 77

Table 5.1: Summary of the average Re cluster height, cluster density and the Re($4f_{7/2}$) peak position for each surface that Re was deposited onto HOPG and TiO_2(110) 101

Table 6.1: The integrated area and total fraction associated with each Re oxidation state for Re deposited onto TiO_2(110) and Pt(111) and then exposed to 250 torr O_2.....125

Table A.1: Experimental details for SEA studies 140

www.manaraa.com

LIST OF FIGURES

Figure 1.1: Strong electrostatic adsorption of Pt precursors onto an oxide support 8

Figure 1.2: Highly oriented pyrolytic graphite (HOPG) is a carbon single crystal that consists of graphene sheets stacked on top of one another 8

Figure 2.1: Diagram summarizing the concept of XPS 22

Figure 2.2: Depiction of low energy ion scattering 22

Figure 2.3: Scanning tunneling microscope operating in constant current mode 23

Figure 2.4: An atomic force microscope.....23

Figure 2.5: Schematic of a Fourier-transform infrared spectrometer 24

Figure 3.1: XPS data for the O(1s) regions for untreated and HCl treated: a) HOPG; and b) GNP surfaces.....44

Figure 3.2: Transmission infrared spectroscopy data for: a) Darco G60: i) before treatment; and ii) after HNO_3 treatment; and b) GNPs: i) before treatment; ii) after HNO_3 treatment; and iii) after HCl treatment.....44

Figure 3.3: Pt(4f) XPS data for SEA of $H_2[PtCl_6]$ on: a) HOPG; and b) GNP surfaces before and after treating with HCl 45

Figure 3.4: Uptake on untreated and acid-treated GNPs as a function of pH for a) chloroplatinic acid and b) tetraamine platinum (II) hydroxide 45

Figure 3.5: AFM images for SEA of $H_2[PtCl_6]$ on: a, b) HOPG reduction in H_2 at 200 °C on: a, b) HOPG; and c, d) HCl treated HOPG 46

Figure 3.6: STEM images for SEA of $H_2[PtCl_6]$ after reduction in H_2 at 200 °C on : a, b) GNPs; and c, d) HCl treated GNPs. 47

Figure 3.7: Pt(4f) XPS data for SEA of tetraamine platinum (II) on: a) HOPG; and b) GNP surfaces before and after treating with HCl. 48

www.manaraa.com

Figure 3.8: AFM images of $[Pt(NH_3)_4](OH)_2$ SEA after reduction in H_2 at 200 ° on a, b) HOPG; and c, d) HCl-treated HOPG 49

Figure 3.9: STEM images for $[Pt(NH_3)_4](OH)_2$ SEA after reduction in H_2 at 200 °C on: untreated GNPs; and b) HCl-treated GNPs.....50

Figure 3.10: Pt(4f) XPS data for: a) $Na_2[PtCl_4]$ SEA on: i) HOPG; ii) GNPs; iii) Darco G60; iv) Ketjen black; and b) $[Pt(NH_3)_4](OH)_2$ SEA on: i) Timrex HSAG 300; ii) Darco S51; and iii) Darco KBM 51

Figure 4.1: O(1s) region of untreated and HCl treated HOPG and their respective O(1s)/C(1s) ratios.....77

Figure 4.2: Comparison of Metal/C(1s) ratios of anionic (left) and cationic (right) Pt and Pd precursors. Anionic uptake experiments were conducted between a pH of 2-2.5 while the cationic uptake experiments were all conducted at a pH of 11 78

Figure 4.3: XPS of the Pd(3d) region for a) $[PdCl_4]^{2-}$ adsorbed onto untreated and HCl treated HOPG at a pH of 2.1 and b) $[Pd(NH_3)_4]^{2+}$ adsorbed onto HCl treated and untreated HOPG at a pH of 11 78

Figure 4.4: Comparison of Pd(3d)/C(1s) ratios of anionic and cationic Pt (right) and Pd (left) precursors on HOPG as a function of pH 79

Figure 4.5: 200 ppm $PdCl_2$ and 200 ppm $[Pd(NH_3)]Cl_2$ solutions as a function of pH. As NH_4OH is added to the $PdCl_2$ solution, the color the changes from yellow to clear, indicating the formation of the $[Pd(NH_3)_4]^{2+}$ species. As HCl is added to the $[Pd(NH_3)]Cl_2$ solution, the solution changes from clear to yellow, indicating the formation of the $[PdCl_4]^{2-}$ species.....79

Figure 4.6: The Pd (right) and Pt (left) precursor concentration as a function of pH.....80

Figure 4.7: Uptake of Pd precursors onto the washed and HCl treated GNP supports using the a) $[PdCl_4]^{2-}$ and b) $[Pd(NH_3)_4]^{2+}$ precursors 80

Figure 4.8: XPS of the Pd(3d) region for a) $[PdCl_4]^{2-}$ adsorbed onto the washed and HCl treated GNPs at a pH of 2 and b) $[Pd(NH_3)_4]^{2+}$ adsorbed at a pH of 11 81

Figure 4.9: SEA uptake of 200 ppm $[PtCl_6]^{2-}$ ($H_2[PtCl_6]$) and 300 ppm $[Pt(NH_3)_4]^{2+}$ ($[Pt(NH_3)_4](OH)_2$) onto GNPs 81

Figure 4.10: Temperature programmed reduction experiment of GN-Alfa support. The sample was heated at 5 °C/min in 10% H_2 balance Argon 82

www.manaraa.com

Figure 4.11: IR spectra of GN-alfa support that underwent different acid and reduction treatments: a) treated with HNO_3, treated with HCl, as received and b) as received, reduced at 500 °C, reduced at 500 °C followed by an HCl treatment, reduced at 500 °C followed by an HNO_3 treatment 82

Figure 4.12: O(1s) region of GN-Alfa supports subjected to various reduction and acid treatments (see legend). All O(1s) spectra are normalized with respect to the C(1s) signal of each sample. All reduction treatments were done in 20% H_2 balance Helium 83

Figure 4.13: Uptake of a) $[PtCl_6]^{2-}$, b) $[Pt(NH_3)_4]^{]2+}$, c) $[PdCl_4]^{2-}$ and d) $[Pd(NH_3)_4]^{2+}$ precursors on GN-Alfa supports of various PZCs. The green, blue and red traces corresponds to GN-Alfas prepared with a PZC = 10.5 (reduced 500 °C 2 hrs), 4.0 (as received), and 1.2 respectively (nitric acid treated). The uptakes of a and c were carried out at a surface loading of 500 m^2/gram while b and d were carried at a surface loading of 1000 m^2/gram.....84

Figure 4.14: Uptake plots of a) $[Pd(NH_3)_4]^{2+}$ and b) $[PdCl_4]^{2-}$ adsorbed onto GN-Alfa supports exposed to a variety of acid and reduction treatments at a surface loading of 500 m^2/gram.....85

Figure 4.15: The top graphs depict the adsorption of $[PdCl_4]^{2-}$ (left) and $[Pd(NH_3)_4]^{2+}$ (right) on a series of GN-alfa supports with varying levels of surface oxygen content, as expressed using the O(1s)/C(1s) ratio prior to uptake of Pd precursors. Uptake experiments were conducted at a pH of ~2.1 and 11 respectively.....85

Figure 4.16: XPS of the Pd(3d) region for $[PdCl_4]^{2-}$ (left) and $[Pd(NH_3)_4]^{2+}$ (right) on a series of GN-alfa supports with varying levels of surface oxygen content. Uptake experiments were conducted at a pH of ~2.1 and 11 respectively.....86

Figure 5.1: (a) Re(4f) region of for different monolayer coverages of Re deposited Ti(110) (b) Re($4f_{7/2}$) binding energy position as a function of coverage.....101

Figure 5.2: 0.25-0.22 ML of Re deposited onto HOPG that was sputtered for (a) 0 seconds, (b) 30 seconds, (c) 5 minutes, and (d) 10 minutes. The histogram below each image corresponds to the Re cluster height distribution of that surface.....102

Figure 5.3: 0.11 – 0.125 ML of Re deposited onto HOPG that was sputter for (a) 0 seconds, (b) 5 minutes, (c) 10 minutes, and (d) 20 minutes. The histograms below each image corresponds to the Re cluster height distribution for each image 102

Figure 5.4: Cluster height and density for 0.22-0.25 and 0.11-0.125 ML Re/HOPG as a function of sputtering time.....103

www.manaraa.com

Figure 5.5: (a) the O(1s) region of HOPG after annealing to 400 K to 3 minutes (O/C ratio of 0.0479) and after annealing to 950 K for 12 minutes (O/C ratio of 0.0176). By annealing at lower temperature, HOPG retains oxygen functionality (b) STM image of 0.22 ML of Re deposited onto the HOPG-O (c) the cluster height distribution of Re 104

Figure 5.6: Left panel, binding energy position of Re for the 0.22-0.25 ML Re coverages as a function of sputtering time on HOPG and TiO_2(110). HOPG-O refers to the surface that was only annealed to 400 K prior to the deposition of Re. Right panel, binding energy position of Re for the 0.11-0.125 ML Re coverages on HOPG and TiO_2 104

Figure 5.7: Binding Energy of Re($4f_{7/2}$) plotted against the cluster height of Re on HOPG-O, HOPG, and TiO_2(110). The dashed blue and green lines offer a guide to the indicate the general binding energy shift trends for Re grown on TiO_2(110) (blue) and HOPG (green) 105

Figure 6.1: Re films grown on Pt(111) surface at coverages of a) 0.4 ML, b) 0.9 ML and c) 1.9 ML 126

Figure 6.2: STM images of 1.0 ML Re films grown on Pt(111) at a) room temperature, b) 500 K and c) a 0.8 ML Re film at 600 K. The image shown in d) is the same surface as c) after annealing 600 K for 10 minutes 126

Figure 6.3: Low energy ion scattering (LEIS) data of 0.9 ML Re film deposited on Pt(111) followed by annealing to 500, 600, and 700 K for 1 minutes each.....127

Figure 6.4: XPS of the a) Pt(4f) and b) Re(4f) regions of 0.8 ML Re deposited at 500 K. The gold traces corresponds to the 0.8 ML Re film after deposition; the maroon traces was taken after annealing the film to 600 K for 5 minutes; and blue traces corresponds to the surface after annealing for an addition 5 minutes at 600 K 127

Figure 6.5: STM images of a) 0.8 ML Re film deposited at 500 K followed by annealing to 600 K for 10 minutes and b) addition 1.0 ML Re deposited onto the surface at 500 K followed by annealing to 600 K for 10 minutes 128

Figure 6.6: STM images of a) clean Pt(111) surface and b) Pt(111) + 1.9 ML Re annealed to 1000 K for 5 minutes 128

Figure 6.7: XPS done at a 26° off-normal for the a) Pt(4f) and b) Re(4f) regions following the formation of Pt-Re alloy formation process on Pt(111). Grazing angle XPS done at a 72°off-normal for the c) Pt(4f) and d) Re(4f) regions. The red traces correspond to the pristine Pt(111) surface, the blue traces are the 1.9 ML Re surface, and the green traces represent the 1.9 ML Re surface annealed to 1000 K for 5 minutes. 129

www.manaraa.com

Figure 6.8: XPS of a) Re(4f) and b) Pt(4f) region of a Pt(111) and a 1.9 ML Re/Pt(111) surface annealed to 1000 K before, purple and red traces respectively, and after exposure to 250 torr O_2, yellow-orange and blue traces respectively. All XPS measurements were taken using at 72° off-normal 130

Figure 6.9: XPS of the O(1s) region of Pt(111), 1.9 ML Re film annealed to 1000 K for 5 minutes, 0.8 ML Re film, and 1.8 ML Re exposed to 250 torr of O_2 for 2 hours.....130

Figure 6.10: XPS of Re(4f) pre and post exposure to 250 torr O_2 for 2 hours for the a) 0.8 ML Re and b) 1.8 ML Re films deposited on Pt(111).....131

www.manaraa.com

LIST OF ABBREVIATIONS

AFM ..... atomic force microscopy

AP-XPS ..... ambient pressure X-ray photoelectron spectroscopy

FTIR ..... Fourier-transform infrared spectroscopy

GNP ..... graphene nanoplatelet

HOPG ..... highly oriented pyrolytic graphite

ICP-AES ..... inductively coupled plasma atomic emission spectroscopy

LEIS ..... low energy ion scattering

PZC ..... point of zero charge

QCM ..... quartz crystal microbalance

RPA ..... revised physical adsorption model

SEA ..... strong electrostatic adsorption

STEM ..... scanning transmission electron microscopy

STM ..... scanning tunneling microscopy

TEM ..... transmission electron microscopy

TPR ..... temperature programmed reduction

UHV ..... ultra high vacuum

XPS ..... X-ray photoelectron spectroscopy

www.manaraa.com

CHAPTER 1

INTRODUCTION

www.manaraa.com

1.1 Heterogeneous catalysis

Catalysis performs an essential role in the global economy, helping to manufacture 60% of industrially produced chemicals[2] and contributing between 20-30% of total GDP in developed countries.[3] More specifically, heterogeneous catalysts are used to convert hydrocarbons into fertilizers,[4] fuels,[5-10] and plastics,[11, 12] all of which have shaped the development of civilization. Catalysts also assist in cleaning up pollutants generated by motor vehicles[13] and coal fired power plants.[14] Moreover, there is interest in developing catalysts for the production of fuels and other chemicals from biomass to create energy resources and chemical processes that are more sustainable.[15-17] However, the development of new catalyst technology is largely based on highly inefficient trial and error methodology.[18-20] To facilitate technological breakthroughs in catalysis, it is critical to develop a fundamental understanding of the properties that control the chemistry of heterogeneous catalysts.

Generally, heterogeneous catalysts used in industry are transition metal nanoparticles dispersed over a high surface area oxide or carbon support.[21, 22] The combination of high dispersion and porous support helps to maximize the surface area of the metal,[23] often thought of as the catalytically active site, while minimizing cost. In spite their prolific use in the chemical industry, there is still much about heterogeneous catalysis that is still not understood on the fundamental level.[21, 24, 25] While practical for the mass production of chemicals, the surfaces of industrial catalysts are ill defined and difficult to control, severely complicating studies that attempt to correlate surface structure and chemical composition with surface chemistry. To overcome these

www.manaraa.com

constraints, the field of surface science has attempted to answer these questions by studying model catalysts.

1.2 Surface Science – a model approach to catalysis

One of the primary aims of surface science is to elucidate surface structure-function relationships in the field of catalysis. The essence of the surface science approach to catalysis has been to construct and characterize model catalysts, which are far less complex than their "real world" counterparts.[23, 25, 26]. These model catalysts consist of planar, single crystals of metal or transition metal particles epitaxially grown on single crystal oxide or carbon surfaces.[24] By preparing these surfaces under ultra high vacuum (UHV) conditions, $\leq 10^{-10}$ torr, they can be characterized with an array of surface sensitive techniques in a pristine environment, providing a surface with a well-known chemical composition, structure and morphology. UHV studies have helped isolate a number of factors that influence the surface chemistry of catalysts, including the support material,[8] metal-support interactions,[27, 28] metal oxidation states,[29-31] particle size,[32] and the presence an additional metal.[33, 34] Indeed, the model approach has had great success in identifying specific surface sites, chemical composition, and surface morphologies that are responsible for controlling the activity, stability and selectivity of catalysts.

1.3 Motivation

Many bimetallic systems exhibit enhanced catalytic activity, selectivity, and stability compared to their monometallic counterparts.[34, 35] In general, the superiority of bimetallic catalysts has been attributed to changes in electronic structure (ligand effect), unique geometric arrangements of surface atoms (ensemble effects), or each metal

www.manaraa.com

playing a separate role in driving the reaction forward (bifunctional effects). Perhaps the simplest model approach to studying bimetallic systems is to prepare and characterize films of one metal grown onto a single crystal of the other metal. Doing so enables one to isolate the effects that are responsible for the enhanced activity.

Pt based catalysts have shown enhanced activity and stability for aqueous phase reforming (APR) of alcohols in the presence of rhenium,[17] though the exact mechanism responsible for this enhanced activity is still under dispute. Specifically, Pt/Carbon catalysts have demonstrated enhanced activity and stability for the aqueous phase reforming (APR) of alcohols when rhenium was added,[17] while PtRe/Titania catalysts show improved activity towards the water gas shift reaction when compared to its monometallic counterpart.[36] The presence of Re seems to reduce CO poisoning on Pt sites, however the mechanism by which this takes place is not well understood. The reduced CO poisoning of Pt has two possible explanations: a ligand effect[16, 37, 38] decreases the Pt-CO bond strength or ReO_x removes CO from Pt via the water gas shift reaction.[39] Because Re is oxidized upon exposure to air, it not clear how the presence of Pt influences the oxidation states of Re.[40] Using physical vapor deposition to grow metal clusters and films onto single crystals, particle size and surface morphology can be finely controlled. Re films were grown on Pt(111) in order to understand PtRe alloy formation and how the presence of Pt influences the oxidation states Re.

Another approach to studying bimetallic systems that more accurately represent "real world" catalysts is to grow bimetallic clusters on an oxide or carbon support. Previous work in our group focused on Pt-Re bimetallic clusters grown on TiO_2(110). However, the growth of Re onto the surface was complicated by metal-support

www.manaraa.com

interactions and particle size effects that could not be deconvoluted. To decouple these two effects, Re was deposited onto highly oriented pyrolytic graphite (HOPG), which is know to have weak electronic interactions with metal clusters grown on its surface.[41, 42] Re clusters were grown in vacuum in order to understand cluster size effects and determine the extent chemical interaction that Re has with surface oxygen species under UHV conditions.

While preparing model catalysts in vacuum enables excellent control over the surface morphology and surface composition, they do not accurately mirror the synthesis methods used to create "real world" catalysts. Most industrially relevant catalysts are prepared using wet chemical impregnation methods. Adapting these methods to the preparation of catalysts on a model support offers insight into the factors that control metal nucleation and the surface chemistry of industrially relevant synthesis methods. Dry impregnation is by far the most common technique used to make industrial catalyst, but can suffer from difficulties in providing control over particle size.[24] Alternatively, strong electrostatic adsorption (SEA) is a simple technique that has demonstrated the ability to generate small nanoparticles on oxide[43-45] and carbon supports,[46, 47] Creating small nanoparticles is of general interest in the field of heterogeneous catalysis given that small particles maximize the number of metal atoms available as active sites, and, in some cases, can enhance catalytic activity.

SEA is carried out by contacting a metal precursor solution with the support and then adjusting the pH above or below the point of zero charge (PZC) of the support in order to accumulate charge on surface functional groups. Figure 1.1 depicts the operating principle of SEA. At the point of zero charge (PZC), functional groups on the support

www.manaraa.com

have no charge, but when the pH is raised about the PZC of the support, functional groups on the surface can become negatively charge, enabling the adsorption of cationic metal precursors. Conversely, when the pH is decreased below the PZC, a positive charge accumulates on the surface, enabling the adsorption of an anionic metal precursor. After adsorption, the metal precursors are reduced using a thermal treatment to generate the metal nanoparticles. While the principle of electrostatic adsorption is well understood on oxide supports,[48-50] the factors that influence SEA adsorption and nucleation on carbon supports is still poorly understood.

The use of carbon as a support for metal nanoparticles is of great importance in the field of catalysis.[51] One of the interesting properties of carbon is that its surface chemistry can be manipulated through the introduction or removal of oxygen functionalities using simple acid or heat treatments. These functional groups can alter the PZC of the surface and act as nucleation sites, which in turn can be used to control the adsorption of metal precursors and the subsequent nucleation of metal nanoparticles. Therefore, elucidating how particular functional groups on carbon influence SEA adsorption and the nucleation of metals is of interest.

In this work, the adsorption of platinum and palladium precursors onto a model carbon support via the SEA method was studied. Platinum/carbon catalysts are used for hydrogenation reactions, fuel cells, and more recently in the synthesis of biofuels.[15, 52] Palladium is widely used in the field of homogenous catalysis for Suzuki coupling reactions, but has recently been shown to be particularly reactive and stable when Pd nanoparticles were supported on graphene nanoplatelets.[53] With a surface science approach in mind, highly oriented pyrolytic graphite (HOPG) was used as the model

www.manaraa.com

support to study the adsorption and nucleation of transition metal precursors. HOPG is a well-studied substrate with a known structure that can act as a model carbon support, as depicted in Figure 1.2. Preparation of HOPG samples involves a relatively simple procedure of cleaving the surface with Scotch tape, leaving a fresh graphite sheet on top of the crystal. Finally, the surface of HOPG is free of any oxygen functional groups, providing a clean substrate that can be systematically functionalized with oxygen groups to study the impact they have on adsorption and nucleation of metals.

www.manaraa.com

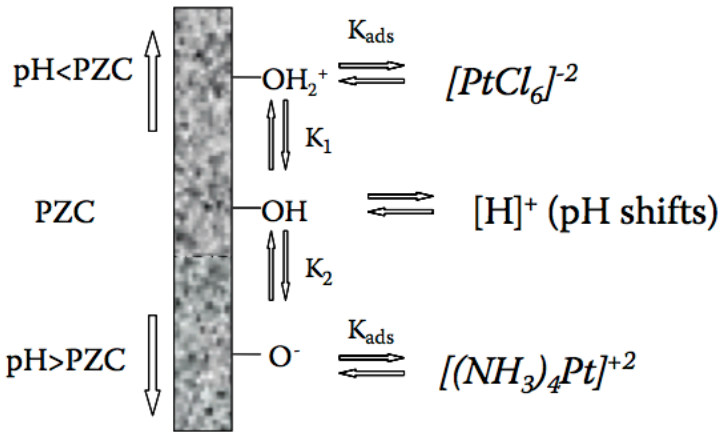

Figure 1.1: Strong electrostatic adsorption of Pt precursors onto an oxide support.

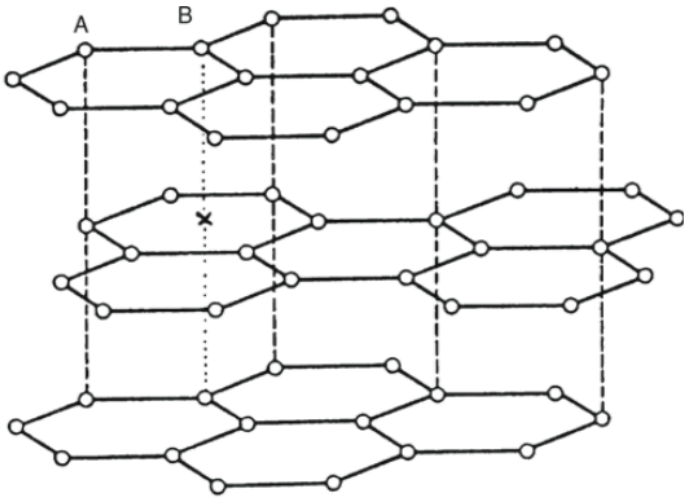

Figure 1.2: Highly oriented pyrolytic graphite (HOPG) is a carbon single crystal that consists of graphene sheets stacked on top of one another.[1]

www.manaraa.com

1.4 References

1. *Surface Analysis – The Principal Techniques*. 2nd ed.; John Wiley & Sons, Ltd: 2009.

2. Recognizing the Best in Innovation: Breakthrough Catalyst. *R&D Magazine* **2005,** *47* (9), 20.

3. Maxwell, I. E., Driving Forces for Innovation in Applied Catalysis. *11th Internation Congress on Catalysis - 40th Anniversary Studies in Surface Science and Catalysis* **1996,** *101*, 1-9.

4. Ertl, G., Primary steps in catalytic synthesis of ammonia. *Journal of Vacuum Science and Technology A* **1983,** *2*, 1247-1253.

5. Prestvik, R., Moljord, K., Grande, K., Holmen, A., Influence of Pretreatment on the Metal Function of a Commercial Pt-Re/Al2O3 Catalyst. *Journal of Catalysis* **1998,** *174*, 119-129.

6. Prestvik, R., Totdal, B., Lyman, C. E., Holmen, A., Bimetallic Particle Formation in Pt-Re/Al2O3 Reforming Catalyst Revealed by Energy-Dispersive X-Ray Spectrometry in the Analytical Electron Microscope. *Journal of Catalysis* **1998,** *176*, 246-252.

7. Rønning, M., Gjervan, Torbjørn, Prestvik, Rune, Nicholson, David G., Holmen, Anders, Influence of Pretreatment Temperature on the Bimetallic Interactions in Pt-Re/Al2O3 Reforming Catalysts Studied by X-Ray Absorption Spectroscopy. *Journal of Catalysis* **2001,** *204* (2), 292-304.

8. Trong On, D., Che, M., Bonneviot, L., Hydrogen Spillover on Bimetallic Supported Pt-Re Particles. *New Aspects of Spillover Effects in Catalysis* **1993**, 125-130.

www.manaraa.com

9. Xiao, J., Puddephatt, R. J., Pt-Re Clusters and Bimetallic Catalysts. *Coordination Chemistry Reviews* **1995,** *143*, 457-500.

10. Okal, J., Tylus, W., Kepinski, L., XPS study of oxidation of rhenium metal on γ-Al2O3 support. *Journal of Catalysis* **2004,** *225* (2), 498-509.

11. Monnier, J. R., The direct epoxidation of higher olefins using molecular oxygen. *Applied Catalysis A: General* **2001,** *221*, 73-91.

12. Brown, C.; Krzystek, J.; Achey, R.; Lita, A.; Fu, R.; Meulenberg, R. W.; Polinski, M.; Peek, N.; Wang, Y.; van de Burgt, L. J.; Profeta, S.; Stiegman, A. E.; Scott, S. L., Mechanism of Initiation in the Phillips Ethylene Polymerization Catalyst: Redox Processes Leading to the Active Site. *ACS Catalysis* **2015,** *5* (9), 5574-5583.

13. Kašpar, J.; Fornasiero, P.; Hickey, N., Automotive catalytic converters: current status and some perspectives. *Catalysis Today* **2003,** *77* (4), 419-449.

14. Li, J.; Chang, H.; Ma, L.; Hao, J.; Yang, R. T., Low-temperature selective catalytic reduction of NOx with NH3 over metal oxide and zeolite catalysts—A review. *Catalysis Today* **2011,** *175* (1), 147-156.

15. Cortright, R. D., R. R. Davda & J. A. Dumesic, Hydrogen from catalytic reforming of biomass-derived hydrocarbons in liquid water. *Nature* **2002,** *418*, 964-966.

16. Simonetti, D. A., E.L. Kunkes, J.A. Dumesic, Gas-phase conversion of glycerol to synthesis gas over carbon-supported platinum and platinum–rhenium catalysts. *Journal of Catalysis* **2007,** *247*, 298-306.

17. Kunkes, E. L., Dante A. Simonetti, James A. Dumesic, William D. Pyrz, Luis E. Murillo, Jingguang G. Chen, Douglas J. Buttrey, The role of rhenium in the conversion of

www.manaraa.com

glycerol to synthesis gas over carbon supported platinum–rhenium catalysts. *Journal of Catalysis* **2008,** *260*, 164-177.

18. Sani, Y. M., Wan Mohd Ashri Wan Dauda, A.R. Abdul Aziz, Activity of solid acid catalysts for biodiesel production: A critical review. *Applied Catalysis A: General* **2014,** *470*, 140-161.

19. Hansen, T. W., J B Wagner, P L Hansen, S Dahl, H Topsoe, C J Jacobsen, Atomic-resolution in situ transmission electron microscopy of a promoter of a heterogeneous catalyst. *Science* **2001,** *294* (5546), 1508-10.

20. Schwarz, J. A.; Contescu, C.; Contescu, A., Methods for Preparation of Catalytic Materials. *Chem. Rev.* **1995,** *95*, 477-510.

21. BaÈumer, M., Hans-Joachim Freund, Metal deposits on well-ordered oxide Films. *Surface Science* **1999,** *61*, 127-198.

22. Johns, J. E.; Hersam, M. C., Atomic Covalent Functionalization of Graphene. *Accounts of Chemical Research* **2013,** *46* (1), 77-86.

23. Bäumer, M., Hans-Joachim Freund, Metal deposits on well-ordered oxide Films. *Surface Science* **1999,** *61*, 127-198.

24. Gunter, P. L. J.; Niemantsverdriet, J. W.; Ribeiro, F. H.; Somorjai, G. A., Surface Science Approach to Modeling Supported Catalysts. *Catalysis Reviews* **1997,** *39* (1-2), 77-168.

25. Goodman, G. W., Catalysis: from "single crystal" to real world. *Surface Science* **1993,** *299*, 837-848.

26. Wallace, W. T., B. K. Min,; Goodman, D. W., The nucleation, growth, and stability of oxide-supported metal clusters. *Topics in Catalysis* **2005,** *34* (1-4), 17-30.

www.manaraa.com

27. Tauster, S., Strong Metal Support Interactions. *Accounts of Chemical Research* **1987,** *20*, 389-394.

28. Goodman, D., "Catalytically active Au on Titania'': yet another example of a Strong Metal Support Interaction (SMSI)? *Catalysis Letters* **2004,** *99*, 1-4.

29. de la Fuente, J. L. G.; Pérez-Alonso, F. J.; M. V. Martínez-Huerta; M. A. Peña, J. L. G. F.; Rojas, S., Identification of Ru phases in PtRu based electrocatalysts and relevance in the methanol electrooxidation reaction. *Catalysis Today* **2009,** *143* (1-2), 69-75.

30. Villullas, H. M., Flora I. Mattos-Costa, and Luis O. S. Bulho˜es, Electrochemical Oxidation of Methanol on Pt Nanoparticles Dispersed on RuO2. *J. Phys. Chem. B* **2004,** *108*, 12898-12903.

31. Stalnionis, G.; Tamašauskaitė-Tamašiūnaitė, L.; Pautienienė, V.; Sudavičius, A.; Jusys, Z., Modification of a Pt surface by spontaneous Sn deposition for electrocatalytic applications. *Journal of Solid State Electrochemistry* **2004,** *8* (11), 892-899.

32. Crampton, A. S.; Rotzer, M. D.; Ridge, C. J.; Schweinberger, F. F.; Heiz, U.; Yoon, B.; Landman, U., Structure sensitivity in the nonscalable regime explored via catalysed ethylene hydrogenation on supported platinum nanoclusters. *Nature communications* **2016,** *7*, 10389.

33. Campbell, C. T., Bimetallic Surface Chemistry. *Annu. Rev. Phys. Chem.* **1990,** *41*, 775-837.

34. Rodriguez, J. A., Physical and chemical properties of bimetallic surfaces. *Surface Science Reports* **1996,** *24*, 223-287.

www.manaraa.com

35. Rodriguez, J. A., Goodman, D. Wayne, Surface Science Studies of the Electronic and Chemical Properties of Bimetallic Systems. *J. Phys. Chem.* **1991,** *95*, 4196-4206.

36. Azzam, K., I. Babich, I., K. Seshan, L. Lefferts, A bifunctional catalyst for the single-stage water–gas shift reaction in fuel cell applications. Part 2. Roles of the support and promoter on catalyst activity and stability. *Journal of Catalysis* **2007,** *251* (1), 163-171.

37. Ramstad, A., F. Strisland, S. Raaen, A. Borg, C. Berg, CO and O2 adsorption on the Re/Pt(111) surface studied by photoemission and thermal desorption. *Surface Science* **1999,** *440*, 290-300.

38. Godey, D. J., G.A. Somorjai The Adsorption and Desorption of Hydrogen and Carbon Monoxide on Bimetallic Re-Pt Surfaces. *Surface Science* **1988,** *204*, 301-318.

39. Zhang, L., Ayman M. Karim, Mark H. Engelhard, Zhehao Wei, David L. King, Yong Wang, Correlation of Pt–Re surface properties with reaction pathways for the aqueous-phase reforming of glycerol. *Journal of Catalysis* **2012,** *287*, 37-43.

40. King, D. L., Zhang, Liang, Xia, Gordon, Karim, Ayman M., Heldebrant, David J., Wang, Xianqin, Peterson, Tom, Wang, Yong, Aqueous phase reforming of glycerol for hydrogen production over Pt–Re supported on carbon. *Applied Catalysis B: Environmental* **2010,** *99* (1-2), 206-213.

41. Nielsen, R. M., S. Murphy , C. Strebel, M. Johansson, J.H. Nielsen,I. Chorkendorff, A comparative STM study of Ru nanoparticles deposited on HOPG by mass-selected gas aggregation versus thermal evaporation. *Surface Science* **2009,** *608*, 3420-3430.

www.manaraa.com

42. Lee, H. B., S. H. Baeck, T. F. Jaramillo, S.F. Bent, Growth of Pt nanowires by atomic layer deposition on highly ordered pyrolytic graphite. *Nano letters* **2013,** *13* (2), 457-63.

43. Spieker, W. A.; Liu, J.; Miller, J. T.; Kropf, A. J.; Regalbuto, J. R., An EXAFS study of the co-ordination chemistry of hydrogen hexachloroplatinate(IV) 1. Speciation in aqueous solution. *Applied Catalysis A: General* **2002,** *232*, 219-235.

44. Spieker, W. A.; Liu, J.; Hao, X.; Miller, J. T.; Kropf, A. J.; Regalbuto, J. R., An EXAFS study of the coordination chemistry of hydrogen hexachloroplatinate (IV) 2. Speciation of complexes adsorbed onto alumina. *Applied Catalysis A: General* **2002,** *243*, 53-66.

45. *Catalyst Preparation Science and Engineering*. CRC Press Taylor and Francis Group: 2007.

46. Hao, X.; Barnes, S.; Regalbuto, J. R., A fundamental study of Pt impregnation of carbon: Adsorption equilibrium and particle synthesis. *Journal of Catalysis* **2011,** *279*, 48-65.

47. Banerjee, R. The Oxidation And Decoration Chemistry Of Platinum And Palladium on Carbon Supports. University of South Carolina, 2016.

48. Park, J.; Regalbuto, J. R., A Simple, Accurate Determination of Oxide PZC and the Strong Buffering Effect of Oxide Surfaces at Incipient Wetness. *Journal of colloid and interface science* **1995,** *175*, 239-252.

49. Agashe, K. B.; Regalbuto, J. R., Revised physical adsorption model. *Journal of colloid and interface science* **1997,** *185*, 174-189.

www.manaraa.com

50. Hao, X.; Spieker, W. A.; Regalbuto, J. R., A further simplification of the revised physical adsorption (RPA) model. *Journal of colloid and interface science* **2003,** *267* (2), 259-264.

51. Rodriguez-Reinoso, F., The role of carbon materials in heterogeneous catalysis. *Carbon* **1998,** *36* (3), 159-175.

52. Lam, E.; Luong, J. H. T., Carbon Materials as Catalyst Supports and Catalysts in the Transformation of Biomass to Fuels and Chemicals. *ACS Catalysis* **2014,** *4* (10), 3393-3410.

53. Gilliland, S. E.; Tengco, J. M. M.; Yang, Y.; Regalbuto, J. R.; Castano, C. E.; Gupton, B. F., Electrostatic adsorption-microwave synthesis of palladium nanoparticles on graphene for improved cross-coupling activity. *Applied Catalysis A: General* **2018,** *550*, 168-175.

www.manaraa.com

CHAPTER 2

INSTRUMENTATION AND TECHNIQUES

www.manaraa.com

2.1 X-ray photoelectron spectroscopy

X-ray photoelectron spectroscopy (XPS) is widespread technique used for chemical identification and quantification of surfaces. XPS utilizes the photoelectric effect, the ejection of electrons form a surface when light is shined onto it, to identify chemicals by measuring the kinetic energy of the ejected electrons. Due to the short mean free path of electrons through solids, only electrons from the top 0-10 nm of the surface can be detected, making XPS an inherently surface sensitive technique.

In practice, X-rays of a known wavelength, usually an Al K_α or Mg K_α source, are used to eject both valence band and core shell electrons form a sample surface while and a hemispherical analyzer is used to measure the kinetic energy of the ejected electrons. Because the energy of the X-ray source is known, the binding energy of the ejected electrons can be calculated with the following equation:

$$BE = h\nu - KE - \Phi$$

Where BE is the binding energy of the electron, KE is its kinetic energy, h is Planck's constant, ν is the frequency of the x-ray source and Φ is the work function of the sample. The electrons from a particular core level appear as peaks in the spectrum at a specific binding energy (see Figure 2.1), allowing for chemical identification and quantification. XPS analysis can also extract information about the chemical environment, oxidation state, alloy formation[5-9] and nanoparticle size,[10] based on binding energy shifts.

www.manaraa.com

2.2 Low energy ion scattering

Low energy ion scattering is used to detect the atomic composition of the topmost layer of the surface. Ions, typically He^+, Ne^+, or Ar^+, with energies that range between 500 – 5 kV are sputtered onto the surface. As depicted in Figure 2.2, the incident ion elastically scatters off the scattering atom on the surface. The kinetic energy of the incident ion is then measured with a hemispherical analyzer to determine the mass of the scattering atom, thereby revealing its chemical identity. LEIS is sensitive to the topmost layer of the surface because ions that penetrate beneath the first layer are neutralized,[4] meaning they cannot be detected when using a hemispherical analyzer.

2.3 Scanning probe microscopy

Scanning tunneling microscopy (STM) is used to provide information about the surface morphology and metal particle size of model catalysts. After being invented in 1982 by Binnig and Rohrer,[11] STM has provided an instrumental tool for surface scientists to study model catalysts.[12] The basic operation of an STM in constant current mode is depicted in Figure 2.3. First, a voltage is applied between the atomically sharp conductive tip and a conductive surface. The tip is then brought within a few angstroms of the surface in order to establish a tunneling current between the tip and the sample. Once the tunneling junction is established, the tip is rastered across the surface while a piezotube is used to adjust the height of the tip to keep the tunneling current constant. The height information is then used to create a map of the surface.

While STM is limited to conductive surfaces, it is an incredibly powerful technique that has a vertical resolution of up to 0.01 A and a lateral resolution of 0.1 A.[4]

www.manaraa.com

The high vertical resolution provided by STM is due to the exponential relationship between the tunneling current and distance give in the equation below:

$$I \propto e^{-2kd}$$

where I is the current, k is associated with the work function, and d is the distance between the tip and the surface. In practice, the lateral resolution in STM experiments tends to suffer when imaging particles due tip convolution effects,[12] making the height information more reliable.

Atomic force microscopy (AFM) is another scanning probe technique that was used to gain insight into surface morphology. Unlike STM, AFM can be used on both conductive and nonconductive surfaces and is better at imaging rough surfaces. Instead of measuring a current, the AFM tip is brought into contact with a surface and the force normal between the tip and the sample is measured. As depicted in Figure 2.4, the force is measured using a laser to track the deflections of the tip. These deflections are then used to calculate the height using the following equation:

$$F_N = -k_N \Delta z$$

where F_N is the force normal to the surface, k_N is the spring constant normal to the sample surface, and Δz is the change in height. A typical AFM can measure forces in the range of $10^{-9} – 10^{-6}$ N.[4] The lateral resolution is generally determined by the diameter of the tip[13] while the vertical resolution tends to be subnanometer.

www.manaraa.com

2.4 Transmission Fourier-transform infrared spectroscopy

Transmission Fourier-transform infrared spectroscopy (FTIR) is used to provide qualitative information about the oxygen functional groups present on high surface area carbon supports.[14] A depiction of an FTIR spectrometer operating in transmission mode is shown in Figure 2.5. IR spectroscopy is capable of detecting the vibrational modes of molecules that absorb infrared light. The vibrational modes of functional groups are quantized and are capable of absorbing light in the mid-infrared region (4000 – 200 cm^{-1}) at a specific wavelength, enabling for the identification of the functional group. However, only vibrational modes that undergo a change dipole during the vibration are capable of adsorbing IR light.[3] Transmission FTIR samples are prepared by mixing the adsorbing material with an IR transparent material, usually KBr, enabling high surface area materials like carbon to be characterized.

2.5 Inductively coupled plasma atomic emission spectroscopy

Inductively coupled plasma atomic emission spectroscopy (ICP-AES) was utilized to measure the concentration of transition metal precursors and determine the amount of metal adsorbed onto the surface of high surface area materials. ICP-AES utilizes an argon plasma torch as an excitation source to atomize and induce atomic emissions for different analytes in a given solution. As the solution enters the flame, the molecules and elements in the solution are atomized and emit light at specific wavelengths in the UV-Vis spectrum,[3] enabling the identification of a particular element. The light is emitted as outer-shell electrons transition from high to low energy atomic orbitals.[3] The quantification of transition metals in solution is made possible through

www.manaraa.com

commercially available standard solutions that can be used for calibration. The adsorption of metal precursors onto the surface of high surface area materials was determined by measuring the concentration of the metal in solution before and after it was contacted with the high surface area material.[15] This methodology assumes that the decrease in concentration of a particular metal after contact is the result of metal adsorbing onto the surface of the high surface area material.

www.manaraa.com

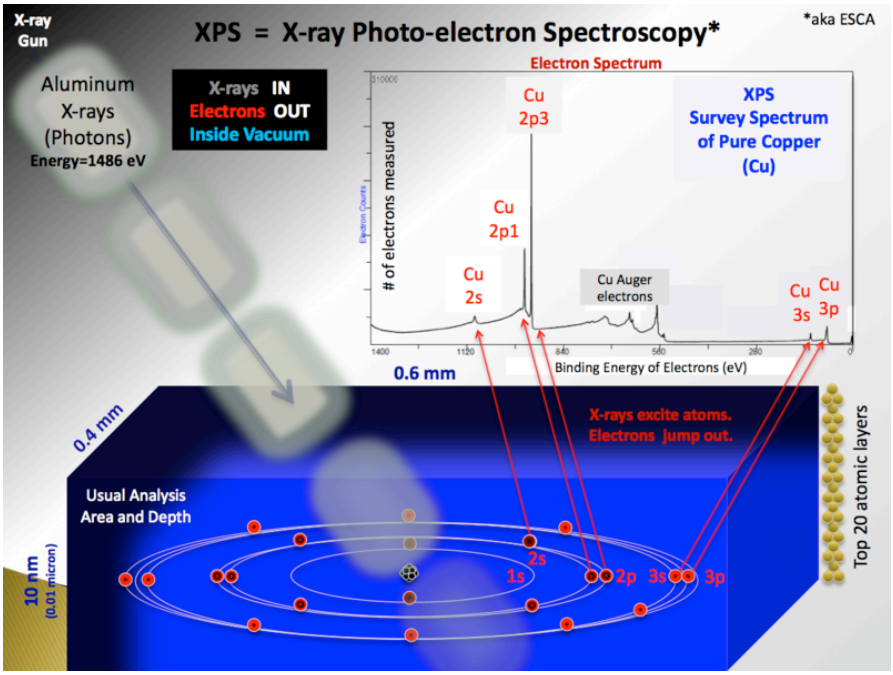

Figure 2.1: Diagram summarizing the concept of XPS.[1]

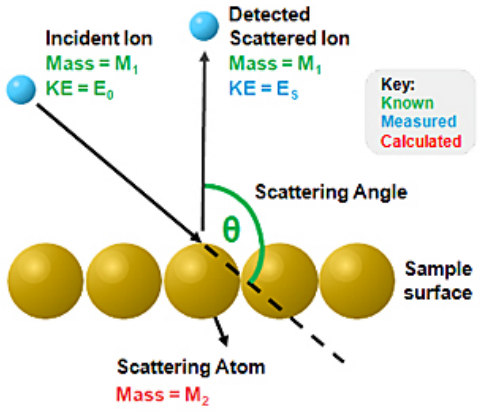

Figure 2.2: Depiction of low energy ion scattering.

www.manaraa.com

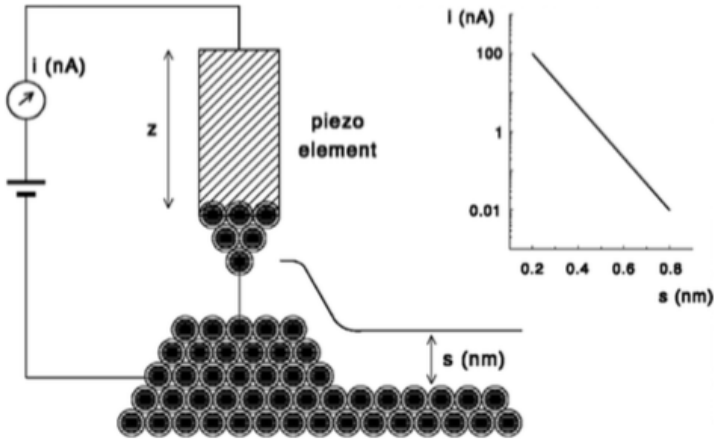

Figure 2.3: Scanning tunneling microscope (STM) operating under constant current mode.[2]

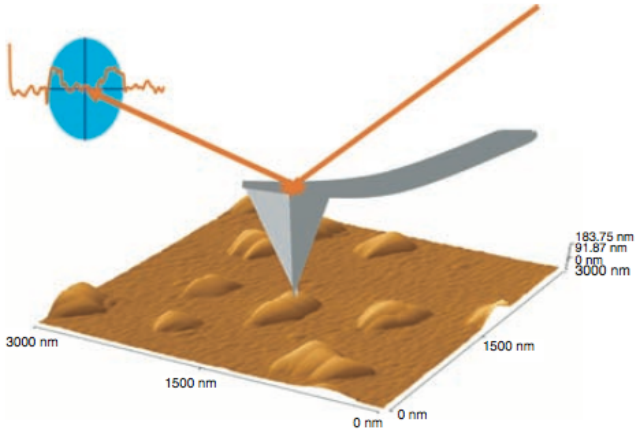

Figure 2.4: An atomic force microscope being scanned across the surface. A laser beam is track the deflection of the tip, providing height information about the surface.[4]

www.manaraa.com

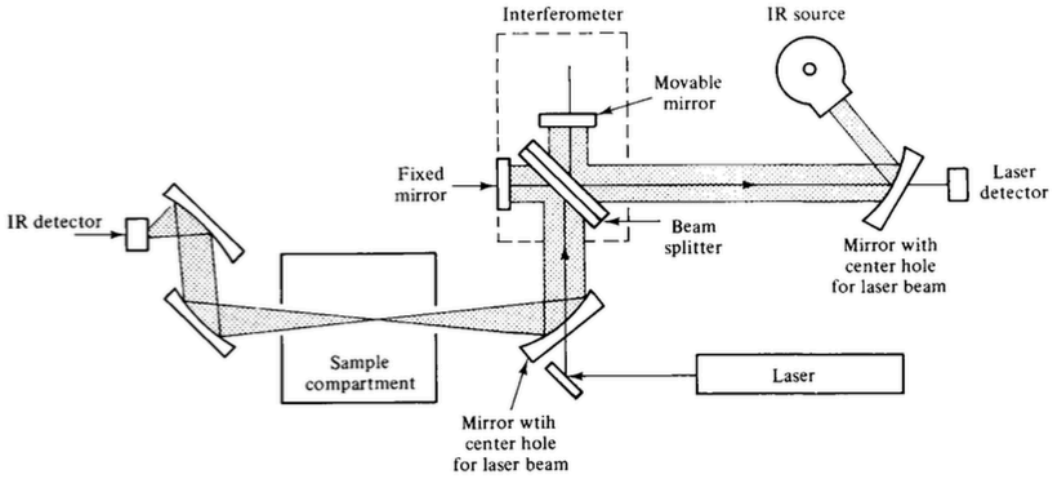

Figure 2.5: Schematic of a Fourier-transform infrared spectrometer operating in transmission mode.[3]

2.6 References

1. X-ray Photoelectron Spectroscopy. https://en.wikipedia.org/wiki/X-ray_photoelectron_spectroscopy#/media/File:XPS_PHYSICS.png (accessed February 2, 2018).

2. Niemantsverdriet, J. W., *Spectroscopy in Catalysis*. 3rd ed.; WILEY-VCH Verlag GmbH & Co. KGaA: 2007.

3. James D. Ingle, J.; Crouch, S. R., *Spectrochemical Analysis*. Prentice-Hall Inc.: Englewood Cliffs, New Jersey, 1988.

4. *Surface Analysis – The Principal Techniques*. 2nd ed.; John Wiley & Sons, Ltd: 2009.

5. Godey, D. J., G.A. Somorjai The Adsorption and Desorption of Hydrogen and Carbon Monoxide on Bimetallic Re-Pt Surfaces. *Surface Science* **1988,** *204*, 301-318.

www.manaraa.com

6. Somorjai, G. A., Godbey, D. J., The Preparation and Characterization of Rhenium Modified Pt(111) and Pt(100), and Platinum Modified Re(0001) Single Crystal Surfaces. *Surface Science* **1988,** *202*, 204-226.

7. Ramstad, A., F. Strisland, S. Raaen, T. Worren, A. Borg, C. Berg, Growth and alloy formation studied by photoelectron spectroscopy and STM. *Surface Science* **1999,** *425*, 57-67.

8. Ramstad, A., F. Strisland, S. Raaen, A. Borg, C. Berg, CO and O2 adsorption on the Re/Pt(111) surface studied by photoemission and thermal desorption. *Surface Science* **1999,** *440*, 290-300.

9. Duke, A. S.; Galhenage, R. P.; Tenney, S. A.; Sutter, P.; Chen, D. A., In Situ Studies of Carbon Monoxide Oxidation on Platinum and Platinum–Rhenium Alloy Surfaces. *The Journal of Physical Chemistry C* **2015,** *119* (1), 381-391.

10. Yang, D.-Q.; Sacher, E., Initial- and final-state effects on metal cluster/substrate interactions, as determined by XPS: copper clusters on Dow Cyclotene and highly oriented pyrolytic graphite. *Applied Surface Science* **2002,** *195*, 187-195.

11. Binnig, G.; Rohrer, H.; Gerber, C.; Weibel, E., Surface Studies by Scanning Tunneling Microscopy. *Physical Review Letters* **1982,** *49* (1), 57-61.

12. Bowker, M., Catalysis resolved using scanning tunnelling microscopy. *Chemical Society reviews* **2007,** *36* (10), 1656-73.

13. Wong, S. S.; Harper, J. D.; Peter T. Landsbury, J.; Lieber, C. M., Carbon Nanotube Tips: High-Resolution Probes for Imaging Biological Systems. *Journal of the American Chemical Society* **1998,** *120*, 603-604.

www.manaraa.com

14. C. Moreno-Castilla, M. A. F.-G., J. P. Joly, I. Bautista-Toledo, F. Carrasco-Marin, and J. Rivera-Utrilla, Activated Carbon Surface Modifications by Nitric Acid, Hydrogen Peroxide, and Ammonium Peroxydisulfate Treatments. *Langmuir* **1995,** *1995*, 4386-4392.

15. *Catalyst Preparation Science and Engineering*. CRC Press Taylor and Francis Group: 2007.

www.manaraa.com

CHAPTER 3

UNDERSTANDING UPTAKE OF PT PRECURSORS DURING STRONG ELECTROSTATIC ADSORPTION ON SINGLE-CRYSTAL CARBON SURFACES

Reprinted with permission from Springer Customer Service Centre GmbH : Springer Nature, *Topics in Catalysis*, "Understanding uptake of Pt precursors during strong electrostatic adsorption on single-crystal carbon surfaces", Grant S. Seuser, Ritubarna Banerjee, Gift Metavarayuth, Amy J. Brandt, Thathsara D. Maddumapatabandi, Stavros Karakalos, Ye Lin, John R. Regalbuto and Donna A. Chen, **2018**, Copyright 2018

www.manaraa.com

3.1 Introduction

One of the key goals in catalyst synthesis is the preparation of supported metal clusters with controlled sizes and size distributions. Specifically, the ability to prepare small, uniformly sized clusters of precious metals that retain their high dispersion during reaction is a topic of great interest in the catalysis community. Previous work by the Regalbuto group has demonstrated that highly dispersed metal particles can be deposited on carbon as well as oxide supports via strong electrostatic adsorption (SEA).[1-3] In this method, cationic/anionic metal precursors are electrostatically adsorbed onto negatively/positively charged functional groups whose charges can be controlled by varying the pH values above or below the point of zero charge (PZC) for the support. Therefore, the functional groups on the support act as nucleation sites in the SEA process and determine the value of the PZC for the support. However, very little is known about the fundamental processes occurring during nucleation of the ionic metal precursors in SEA and the factors that govern the sizes of the resulting metal clusters formed after reduction of the ionic precursors.

The nucleation and growth of Pt clusters on carbon supports is of particular interest since Pt on carbon catalysts are used in a variety of chemical processes,[4-8] such as hydrogenation reactions,[6, 9, 10] and as catalysts in proton exchange membrane fuel cells.[4, 11, 12] Furthermore, recent studies by the Gupton group have demonstrated unusual activity in the Suzuki reaction for precious metal catalysts supported on graphene nanoplatelets (GNPs).[13] In this work, single-crystal carbon surfaces (highly oriented pyrolytic graphite, HOPG) and GNPs with the same well-defined graphitic surface structures are employed as model supports. Since both supports contain almost no functional groups in their

www.manaraa.com

native forms, they provide surfaces on which the role of functional groups can be systematically studied. The HOPG single-crystal surfaces are nearly atomically clean after cleaving and can be studied by traditional surface science techniques like X-ray photoelectron spectroscopy (XPS) and atomic force microscopy (AFM). Complementary XPS and transmission electron microscopy (TEM) studies can be carried out on the GNPs, which also have surface areas high enough for the PZC and uptake experiments typically used to characterize supported metal catalysts.

In the studies reported here, the deposition of Pt clusters by SEA on well-defined graphitic surfaces was investigated as a function of selective introduction of surface hydroxyl groups. Adsorption of $PtCl_6^{2-}$ under acidic conditions was found to be dominated by protonated aromatic ring sites so that Pt uptake was high even in the absence of surface functional groups, and the addition of protonated hydroxyl groups did not increase adsorption. In contrast, adsorption of $Pt(NH_3)_4^{2+}$ under basic conditions was significantly increased by hydroxylation, which provided negatively charged adsorption sites via the deprotonation of the hydroxyl groups. For the cationic precursor, adsorption on hydroxylated surfaces resulted in lower cluster densities of metallic Pt clusters after reduction in H_2 compared to the untreated surface. For the anionic precursor, smaller clusters were formed on the hydroxylated surface after precursor reduction.

3.2 Experimental

Highly oriented pyrolytic graphite surfaces were obtained from Nanoscience Instruments (ZYH grade, 5x5x2mm^3), and clean HOPG surfaces were prepared by cleaving the top layers with adhesive tape. Graphene nanoplatelets were purchased from Strem Chemical (CAS #06-0222, 2-10 nm thick, ~5 microns wide). Chloroplatinic acid

www.manaraa.com

($H_2[PtCl_6]$, 99.9%), tetraammine platinum(II) hydroxide ($[Pt(NH_3)_4](OH)_2$, 99.999%), sodium tetrachloroplatinate ($Na_2[PtCl_4]$, 99.9%) and tetraammine platinum(II) chloride ($[Pt(NH_3)_4](Cl)_2$, 99.99%)were all obtained from Sigma Aldrich. Vendors for the other powdered supports are given in the supplemental section.

Uptake measurements on the GNPs as a function of pH were conducted at a surface loading of 500 m^2/L. The extent of Pt adsorption was determined from the difference in Pt concentration in solution before and after adsorption, and Pt concentrations were measured using a Perkin-Elmer Optima 2000 DV for inductively coupled plasma (ICP) optical emission spectroscopy. The GNP surface area was taken as 40 m^2/g, which is at the high end of the range reported by the manufacturer, given that this surface area results in maximum uptake values for chloroplatinic acid that are consistent with those in the literature for adsorption on carbon supports.[3]

Acid treatment of the HOPG was carried out by placing a drop of 37% HCl (Aldrich) or 67% HNO_3 (Aldrich) on the face of the HOPG for 3 hours. After the treatment, the surface was thoroughly washed with DI water and dried in air. For the GNPs, acid treatment was carried out by heating at 90 °C in concentrated acid for 3 hours. The residual counterions from the acid were removed by washing the GNPs in DI water using a vacuum filter until the pH of the filtrate was the same as untreated DI water (5.5).

SEA on the HOPG surface was carried out by immersing the substrate for 1 hour into 50 mL of the Pt precursor solution. During this time, the solution was vigorously agitated with a Teflon-coated stir bar. For SEA on the GNPs and other high surface area carbon supports, the support was exposed to the solution of the Pt precursor and sonicated for 1 hour. $H_2[PtCl_6]$ and $[Pt(NH_3)_4](OH)_2$ adsorption were carried out at pHs of 2.5-3 and 11-

www.manaraa.com

11.5, respectively, which roughly corresponded to the maximum uptake of the GNPs as a function of pH. The pH for $Na_2[PtCl_4]$ adsorption was set at 3, based on the maximum in the uptake vs. pH curve for other anions like $PtCl_6^{2-}$ on the GNPs. For all of the HOPG samples, a Pt precursor concentration of 100 ppm was used, and concentrations of 300 ppm were used for SEA on the GNPs. For all of the samples studied, the exact pH values and Pt precursor concentrations, as well as the PZC for the supports, are given in Table 3.1. After adsorption, the GNPs were vacuum filtered and allowed to dry in air at room temperature for 24-48 hours, and the HOPG substrates were also dried in air at room temperature. Reduction of the platinum precursors was carried out in a quartz tube at 200 ºC in a flowing gas mixture of 10-20% H_2/balance He for 1 hour, unless otherwise specified.

The PZC of the GNPs was measured using a variation of the pH shift method, which has been described in detail elsewhere.[1, 2] Deionized water (DI) with an initial pH of 3, 6, and 9 was added to a sample of GNPs until incipient wetness, at which point the final pH was measured with a spear-tipped pH probe. The final pHs over these initial pH ranges represent the PZC of the support.

XPS experiments were conducted on a Kratos AXIS Ultra DLD instrument equipped with a monochromatic Al Kα source, charge neutralizer, a hemispherical analyzer, load lock and catalysis cell.[14] All spectra were collected with a charge neutralizer using a step size of 0.06 eV and pass energy of 40 eV. Samples could be transferred directly from the XPS chamber to the catalysis cell, where the samples were exposed to a flow of pure H_2 (Airgas, UHP 99.999%) at 200 °C for 1 hour in order to reduce the Pt precursors. The C(1s) binding energy for freshly cleaved HOPG was

www.manaraa.com

284.4±0.1 eV with the charge neutralizer on and did not shift when the charge neutralizer was turned off. Similarly, the GNPs also exhibited a C(1s) peak at 284.4±0.1 eV using the charge neutralizer, and therefore no binding energy correction was applied to either the HOPG or GNP samples since there was no evidence for peak shifts due to charging. For all reported XPS ratios, the intensities were corrected by the atomic sensitivity factors associated with each element.[15] For some of the batches of GNPs, there was a shoulder that appeared around 537.5 eV in the O(1s) region. After the GNPs were washed with DI water, the intensity of the shoulder decreased almost to zero. This feature is tentatively assigned to NO_3^- contamination since a peak at 1385 cm^{-1} attributed to nitrate[16] was also observed in the transmission IR spectrum. Notably, this same 537.5 eV species is observed on other carbon surfaces like Darco G60.[17]

Peak fitting of the XPS data was carried out using CasaXPS software for the Pt(4f) region and XPSPEAK 4.1 for the O(1s) region. The Pt(4f) peaks had Lorentzian-asymmetric peak shapes while the O(1s) peaks had Gaussian-Lorentzian peak shapes. The Pt($4f_{7/2}$) and Pt($4f_{5/2}$) peaks were fixed with peak area ratio of 4:3, respectively, with identical peak widths and a splitting of 3.3 eV, which is the value reported for Pt^{+2} and Pt^{+4} species.[18, 19]

AFM experiments were performed on a Nanoscope IIIa using a silicon, n-type tip. All experiments were conducted in tapping mode with scan rates varying between 1-2 Hz. For each experiment, multiple regions of the HOPG surface were imaged to establish that the images were representative of the entire surface. Average cluster heights were based on measurements of 30 clusters for each surface.

www.manaraa.com

STEM images were collected with an aberration-corrected JOEL 2100F scanning transmission electron microscope using Z-contrast imaging. Sample preparation involved ultrasonication of the sample in ethanol, followed by addition of a drop of this suspension to a copper TEM grid with a thin holey carbon coating. Average cluster diameters for $[Pt(NH_3)_4](OH)_2$ SEA experiments were from measurements of 1,153 clusters on untreated GNPs, and 1,175 clusters on HCl-treated GNPs using the software program Particule2, which was obtained from Dr. Catherine Louis at Universite Pierre et Marie Curie.

Transmission infrared spectroscopy experiments were conducted using a Nexus 470 spectrometer (Thermo Nicolet), which was purged with dry air. The sample pellet compositions were 0.2-0.5 weight percent carbon powder mixed with optical grade KBr, which was heated in an oven at 110-120 °C for 12 hours to remove water. Pellets were pressed at 8000 psi for 5 minutes.

3.3 Results and Discussion

3.3.1 Selective functionalization of graphitic carbon surfaces

Both the HOPG and GNP surfaces were functionalized with hydroxyl groups by treating the surface with concentrated HCl. The untreated HOPG surface had almost no surface oxygen, whereas the HCl-treated surface exhibited a single oxygen species with a binding energy of 532.8 eV, which has been assigned in the literature to OH groups on HOPG (Figure 3.1a).[20, 21] Treatment of the HOPG surface with concentrated HNO_3 also resulted in exclusively OH groups on the surface, but the O:C ratio was 25% lower compared with HCl treatment even though HNO_3 acid is commonly used to oxidize high surface area carbon supports.[3, 22] The untreated GNPs had a variety of oxygen species on

www.manaraa.com

the surface, with peaks at 531.0, 532.3, 533.5 and 535.5 eV. The 535.5 eV feature is probably associated with a contaminant, which was mostly removed from the surface after washing the GNPs in DI water. The 532.3 eV peak is tentatively assigned to OH groups even though the binding energy is on the low side, while the 533.5 eV species is consistent with C-O-C groups.[23] There is no clear assignment for the species corresponding to 531.0 eV, but it could be attributed to oxygen at the edges of the graphene nanoplatelets since these undercoordinated sites should be the most active for oxidation. After HCl treatment, the main surface species has a binding energy of 533.0 eV and is assigned to hydroxyl groups (Figure 3.1b), but other oxygen species also remain on the surface. Although the HCl-treated GNPs exhibited approximately the same O:C ratio as the untreated GNPs, it was difficult to accurately compare the O:C ratios for the GNPs because different samples had O:C ratios that varied by as much as 25%. PZC measurements for the GNPs clearly illustrated that there was a change in surface functional groups after HCl treatment. Specifically the PZC for untreated GNPs was 7-8, whereas after HCl treatment the PZC decreased to 3, and this decrease in PZC is characteristic of the addition of oxygen-containing functional groups.[3, 24]

For activated carbons such as Darco G60, treatment with HNO_3 results in the appearance of a peak at 1725 cm^{-1} in the transmission IR spectrum from the C=O stretch in carboxylic acid groups (Figure 3.2). However, neither HNO_3 nor HCl-treated GNPs exhibited evidence of C=O functionality from the infrared spectrum (Figure 3.2), and this is consistent with the addition of OH groups rather than C=O groups upon acid treatment. Furthermore, it was difficult to remove all of the nitrate ions from the GNPs even after extensively washing the GNPs with deionized water, given that the HNO_3-treated GNPs

www.manaraa.com

exhibited a peak at 1385 cm^{-1} in the transmission IR spectrum attributed to NO_3^-.[16] Therefore, HCl was considered to be a better choice for oxidizing the GNPs even though the O:C ratio was slightly higher with HNO_3.

3.3.2 SEA of chloroplatinic acid

SEA of the anionic $PtCl_6^{2-}$ precursor was achieved by exposing the surfaces to chloroplatinic acid at a pH of 2.5-3. The relative uptakes of Pt on the graphitic carbon surfaces before and after HCl-treatment were determined from the integrated Pt(4f) XPS signals (Figure 3.3). For both the HOPG and GNP surfaces, HCl-treatment decreased the Pt uptake by 46%. On all surfaces, the two Pt species were observed with Pt($4f_{7/2}$) peaks around 74.7 eV and 72.3 eV. The high binding energy species is assigned to Pt^{4+} and represents the main Pt species, whereas the lower binding energy peak is consistent with Pt^{2+}.[15] The presence of Pt^{2+} is attributed to reductive Pt^{4+} adsorption, which has been previously reported in EXAFS studies of chloroplatinic acid on carbon.[25] Heating the precursor in flowing H_2 at 200 °C for 1 hour in the *in situ* XPS cell resulted in complete reduction to metallic Pt, which had a Pt($4f_{7/2}$) binding energy of 71.2 eV. Since the untreated HOPG surface has almost no oxygen-containing functional groups, there are few protonated hydroxyl groups that can serve as sites for the electrostatic adsorption of the Pt anion. One possibility to explain the observed Pt adsorption is that the pi bonds in the aromatic rings that comprise the graphite surface become protonated under acid conditions and serve as sites for electrostatic anion adsorption.[5, 6, 26] Note that almost no uptake is observed under basic conditions when the aromatic rings are not protonated (Figure 3.4a). This explanation is consistent with the decreased Pt uptake after the surface is treated with HCl since the presence of oxygen functional groups have an electron-

www.manaraa.com

withdrawing effect that inhibits surface protonation.[6] Thus, the protonated rings appear to be the dominant electrostatic adsorption site, given that the number of protonated hydroxyl groups should increase after HCl treatment, but the HCl-treated surface showed less uptake than the untreated. For the untreated HOPG surfaces, the O(1s) region after $PtCl_6^{2-}$ adsorption exhibited a peak centered at 531.5 eV with an O:Pt ratio of 1.4. The oxygen surface species are attributed to residual or dissociated water from the spheres of hydration associated with the Pt ions in solution, and in general, the oxygen signal increased with Pt uptake. For the HCl treated surfaces, the O(1s) region was dominated by the hydroxyls initially present on the surface.

Platinum uptake on the untreated and HCl-treated GNPs as a function of pH were also measured by ICP (Figure 3.4a). However, the ICP uptake was not in agreement with the XPS results given that uptake on the HCl-treated surface was greater than on the untreated. This discrepancy can be explained by partial exfoliation of the GNPs after acid treatment, which would then increase the apparent uptake by increasing the surface area. Complete separation of graphitic layers is known to occur after exposure to concentrated acid[27, 28] followed by sonication or heating. Partial exfoliation in solution after acid exposure only would explain why the uptake on the HCl-treated GNPs is greater than the reported maximum value of 1.6 μmol/m^2 observed for the same precursor on other carbon surfaces.[3] The Pt deposited on the partially exfoliated layers would be difficult to detect by XPS because these layers would no longer be exposed after drying.

Pt cluster sizes and size distributions were characterized by AFM on the HOPG surfaces and STEM on the GNPs after SEA and subsequent reduction of the precursors (Figure 3.5). The exposure of HOPG to HCl resulted in the formation of raised features

www.manaraa.com

that were previously observed by Davies and coworkers and attributed to delamination of the surface layers that are held together by weak van der Waals forces.[29] However, the raised features were no longer observed after the HCl-treated surface was subjected to reduction conditions. For chloroplatinic acid on untreated HOPG, AFM images showed clusters with average heights of 4.1±0.6 nm, and these clusters tended to aggregate into dendritic structures (Figure 3.5a,b). Previous STM studies of Pt,[30, 31] as well as other metals like Pd[32] and Au[33], on HOPG surfaces have reported similar dendritic aggregates of three dimensional particles. The branched shapes of the aggregates are attributed to a combination of long diffusion lengths for the metal atoms on HOPG, which is a surface that contains very few defects to trap diffusing metal atoms, and irreversible binding of a diffusing atom when it encounters an existing cluster. Dendritic growth of metals on single-crystal metal surfaces have also been observed under these conditions.[34-37] This type of growth is known as diffusion-limited-aggregation, and simulations demonstrate that dendritic structures form when either atoms or clusters diffuse on the surface via a random walk and irreversibly attach to an existing cluster.[6, 38, 39] For the HCl-treated surface, the lower Pt coverage resulted in less extended aggregates of clusters, but the continued presence of the dendritic aggregates indicates that the surface hydroxyls do not inhibit diffusion. The Pt clusters exhibited the same average height (4.1±0.6 nm) as on the untreated surface (Figure 3.5c,d), which also implies that HCl treatment does not change the diffusion length for Pt atoms. Due to the weak interaction between the Pt clusters and the HOPG surface,[30, 31, 40] it was difficult to image the smaller aggregates, especially at the large image sizes, without displacing the clusters with the AFM tip. Interaction of the AFM tip with clusters caused streaks to appear in the images as the

www.manaraa.com

clusters were moved on the surface; these streaks can be seen in Figure 3.5d but also occur to a lesser extent in Figure 3.5b where the aggregates are larger and less likely to be displaced by the AFM tip.

STEM images for chloroplatinic acid on the GNPs also showed dendritic structures on untreated GNPs (Figure 3.6). On the HCl-treated GNPs, the main difference was the lower Pt coverage, which prevented extended dendritic structures from forming, but diffusion was still high enough for some larger islands to appear. Thus, the nucleation and growth of Pt clusters via SEA is very similar on single-crystal HOPG surfaces and the higher surface area GNPs.

3.3.3 SEA of tetraammine platinum(II) hydroxide

For the adsorption of the cationic $Pt(NH_3)_4^{2+}$ precursor, the surfaces were exposed to $[Pt(NH_3)_4](OH)_2$ at a pH of 11-11.5. The Pt(4f) XPS data for the untreated and HCl-treated HOPG surfaces illustrated that surface hydroxylation increased the Pt uptake by a factor of 1.6 (Figure 3.7a). Likewise, the uptake of Pt on the HCl-treated GNPs increased by a factor of 2.3 compared to on the untreated GNPs (Figure 3.7b). The lower Pt coverage on the untreated surface is attributed to an SEA mechanism in which the deprotonated hydroxyl groups provide negatively charged sites for the adsorption of the cationic Pt precursor. Thus, the surfaces hydroxylated by HCl have more nucleation sites for precursor adsorption and higher uptake is observed. Furthermore, ICP analysis for the uptake of $Pt(NH_3)_4^{2+}$ on the untreated GNPs indicated that the amount of Pt adsorbed on the surface was approximately a factor of five lower than for chloroplatinic acid uptake (Figure 3.4b). The relatively low concentration of hydroxyl groups on the untreated GNPs resulted in low uptake of the cationic precursor compared to the anionic precursor,

www.manaraa.com

which does not require oxygen-containing functional groups for adsorption. The unexpected presence of Pt^{4+} at 73.0 eV and 75.0 eV on HOPG for the adsorption of the Pt^{2+} precursor on all surfaces is discussed in the following section.

AFM images for $Pt(NH_3)_4^{2+}$ reduced on untreated HOPG demonstrated that the number of Pt clusters on the surface was lower than for SEA of $PtCl_6^{2-}$ (Figure 3.8a,b), and this behavior was consistent with the lower Pt uptake for the cationic precursor. The average cluster height of 3.1±0.7 nm was smaller than that of $PtCl_6^{2-}$ SEA, and particles at the step edges were relatively small (2.6±0.3 nm) whereas the particles on the terraces were significantly larger (3.7±0.5 nm). The majority of particles were situated at the step edges, as expected given that oxygen functionality is most likely to occur at the undercoordinated step edge sites. On the HCl-treated surface, Pt clusters after reduction had greater dispersion with an average height of only 1.3±0.4 nm (Figure 3.8c,d). Furthermore, a significant number of clusters appeared on the terraces, implying that HCl-induced hydroxylation of the surface introduces OH groups at terrace sites that serve as nucleation sites during SEA. The increased dispersion on the HCl-treated surface is more likely to be from higher nucleation densities rather than reduced diffusion because diffusion rates still appear to be high for chloroplatinic acid SEA on the HCl-treated surface. The larger images (Figure 3.8b,d) more clearly showed the propensity for Pt clusters to be situated at the step edges on untreated HOPG, and the high fraction of Pt clusters that exist on the terraces for the HCl-treated HOPG. However, the streaks in Figure 3.8b indicate that it was easy to displace the small clusters with the AFM tip; it was not possible to collect larger images of this surface due to strong interactions between the sample and tip. For the $Pt(NH_3)_4^{2+}$ on HCl-treated HOPG, displacement of

www.manaraa.com

clusters by the AFM tip was less of a problem because the Pt clusters existed as larger aggregates (Figure 3.8d). STEM images for $Pt(NH_3)_4^{2+}$ on GNPs (Figure 3.9) demonstrated that higher dispersion was achieved on the HCl-treated surfaces; the average cluster diameters were 2.1±0.7 nm on the untreated GNPs compared to 1.7±0.4 nm on the HCl-treated GNPs. However, the cluster densities were not uniform across the GNP surfaces, and some of the imaged regions had significantly lower cluster densities. Histograms for the measured cluster sizes (Figure 3.9, bottom) showed that the size distribution was significantly broader on the untreated GNPs, and much larger cluster sizes were observed. For example, the fraction of clusters greater than 2.7 nm was 17% on the untreated GNPs compared to less than 1% on the HCl-treated GNPs. In addition, clusters as large as 4.8 nm were observed on the untreated surface, whereas no cluster larger than 3.0 nm was found on the HCl-treated surface.

3.3.4 Oxidative adsorption of Pt^{2+} precursors

When $Pt(NH_3)_4^{2+}$ was adsorbed onto the HOPG surface, ~40% of the Pt was in the +4 oxidation state instead of the expected +2 state (Figure 3.7a). To our knowledge, oxidative adsorption of metal ions has not been previously reported in the literature, but there have also been almost no XPS studies of Pt^{2+} ions adsorbed on surfaces. Moreover, the adsorbed Pt^{+4} species were reduced back to Pt^{2+} when the surfaces were heated in air at 100-120 °C, which is a treatment typically employed to remove water from high surface area supports. Therefore, it would be less likely to observe oxidation of Pt^{+2} when the precursors are dried on the surface at elevated temperatures. On the GNPs, a slightly higher percentage of Pt (~60%) was observed as Pt^{4+} (Figure 3.7b). Adsorption was also carried out with the anionic Pt^{2+} precursor $PtCl_4^{2-}$ so that the adsorption could occur in an

www.manaraa.com

acidic rather than basic environment, and so that SEA could be conducted on other supports with higher PZCs. Adsorption of $PtCl_4^{2-}$ still occurred on HOPG and GNP surfaces, and the fraction of Pt^{4+} was approximately 50% in both cases (Figure 3.10a). For other carbon supports, at least 35% conversion to Pt^{4+} was observed for $PtCl_4^{2-}$ on Darco G60 and Ketjen black, and at least 20% Pt^{4+} was observed for SEA of $Pt(NH_3)_4^{2+}$ on Timrex HSAG 300, Darco S51 and Darco KBM (Figure 3.10b). Furthermore, oxidative adsorption was not limited to carbon surfaces since this behavior was observed for SEA of $PtCl_4^{2-}$ on alumina. In addition, the lack of Pt^{4+} oxidation for $[Pt(NH_3)_4]Cl_2$ SEA on silica demonstrated that oxidation did not occur on all supports.

Regarding the species that serves as the oxidizing agent for Pt^{2+}, the reduction of oxygen in O_2 to H_2O has an energetically favorable standard reduction potential of +1.23 V.[41] Since the oxidation of Pt^{2+} in $PtCl_4^{2-}$ to $PtCl_6^{2-}$ has a potential of -0.68 V,[41] the overall redox reaction should be spontaneous. The only other species available for reduction are H_2O to H_2 and Cl^- to Cl_2, but both of these are very energetically unfavorable with reduction potentials of -0.83 V and -1.36 V, respectively.[41] Surface oxygen cannot be responsible for oxidation of Pt^{2+} on the HOPG since there is almost no oxygen initially detected on the surface, while HOPG exhibits one of the highest fractions of Pt^{4+}. The following experiment was conducted to explore the role of dissolved O_2: SEA of $Pt(NH_3)_4^{2+}$ on HOPG was carried out by bubbling O_2 gas into the solution for one hour prior to SEA and during SEA. The resulting surface had a Pt^{4+} contribution that was slightly higher (13%) than without bubbling O_2 gas. This experiment does not provide conclusive evidence that dissolved O_2 acts as the oxidizing agent since the initial concentration of dissolved O_2 may already be sufficient to promote Pt^{2+} oxidation upon

www.manaraa.com

adsorption. It is also possible that the Pt^{2+} is oxidized in air after the surface is removed from solution, but this seems less likely since extended exposure to air for a week did not increase the fraction of Pt^{4+}. Furthermore, precursor oxidation cannot occur in solution before adsorption because oxidation is not observed for SEA on all surfaces; thus, it appears that the surface plays a role in catalyzing Pt^{2+} oxidation. Additional experiments are needed to better understand the oxidation of the Pt^{2+} precursors upon adsorption.

3.4 Conclusions

The nucleation of Pt particles by SEA on well-defined, model carbon surfaces is significantly influenced by introducing functional groups onto the supports. HOPG and GNP model surfaces were selectively functionalized with hydroxyl groups by exposing the supports to concentrated HCl. For the anionic precursor $PtCl_6^{2-}$, sites for electrostatic adsorption are believed to be the protonated aromatic rings of the carbon support based on the high uptake on surfaces with no oxygen functional groups. The presence of hydroxyl groups decreased Pt uptake during SEA because the protonation of the aromatic rings is inhibited by surface oxygen species. However, there was no evidence for decreased diffusion of Pt on the hydroxylated HOPG surfaces, given that the Pt particles sizes were the same as on the untreated surfaces. For the SEA of the cationic precursor $Pt(NH_3)_4^{2+}$, the deprotonated hydroxyl groups provided negatively charged sites for the electrostatic adsorption of the cationic precursor. Consequently, uptake was increased on the hydroxylated surface, and more highly dispersed clusters were formed due to the increased number of nucleation sites. Pt^{2+} precursors were found to be oxidized to Pt^{4+} immediately after SEA on both HOPG and GNPs, as well as alumina and other carbon supports. The fact that the same behavior was observed on functionalized single-crystal

www.manaraa.com

surfaces and high surface area GNPs demonstrates that the detailed understanding gained on the model single-crystal surfaces can be applied to catalytically relevant high surface area supports.

For Pt clusters on graphitic carbon, the interaction between Pt and the oxygen-containing functional groups is not strong enough to prevent the high diffusion rates on the surface that lead to the formation of large clusters. However, for other metals with stronger metal-oxygen bonds, it should be possible to control the diffusion rates of the metal atoms by surface functionalization so that higher dispersions may be achieved to provide a greater number of active sites for catalytic reaction on the supported clusters.

Acknowledgements

We gratefully acknowledge financial support from the National Science Foundation Industry/University Collaborative Research Center grant (IIP 1464595) and the National Science Foundation (CHE 1300227). G.S.S. and A.J.B. also acknowledge funding from a National Science Foundation IGERT grant (DGE 1250052).

www.manaraa.com

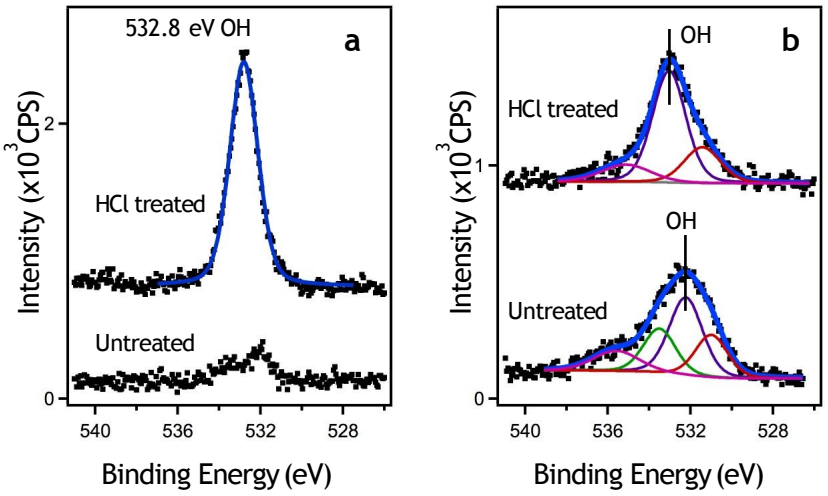

Figure 3.1:XPS data for O(1s) regions for untreated and HCl treated: a) HOPG; and b) GNP surfaces.

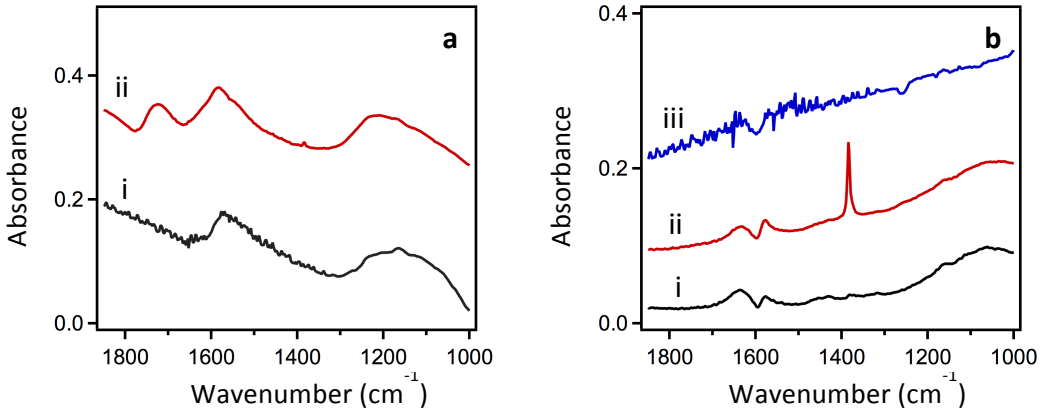

Figure 3.2: Transmission infrared spectroscopy data for: a) Darco G60: i) before treatment; and ii) after HNO_3 treatment; and b) GNPs: i) before treatment; ii) after HNO_3 treatment; and b) GNPs: i) before treatment; ii) after HNO_3 treatment; and iii) after HCl treatment. The apparent "noise" in the spectrum of (b, iii) is due to the unusually high water background for this experiment. Peaks at 1570 cm^{-1} are assigned to the C=C stretch associated with the aromatic rings.

www.manaraa.com

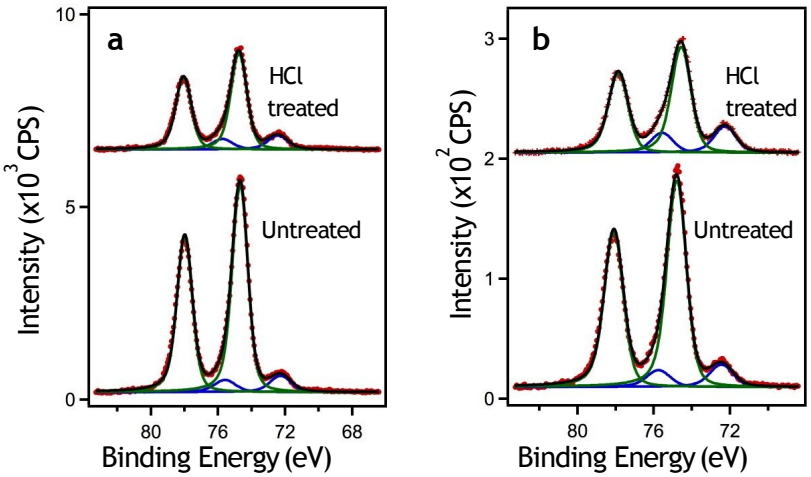

Figure 3.3: Pt(4f) XPS data for SEA of $H_2[PtCl_6]$ on: a) HOPG; and b) GNP surfaces before and after treating with HCl.

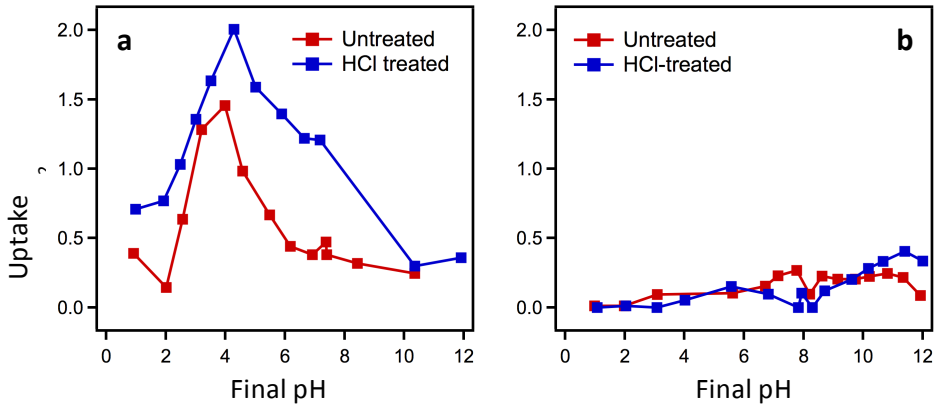

Figure 3.4: Uptake of untreated and acid-treated GNPs as a function of pH for: a) chloroplatinic acid and b) tetraamine platinum (II) hydroxide. The platinum precursor concentrations were 300 ppm.

www.manaraa.com

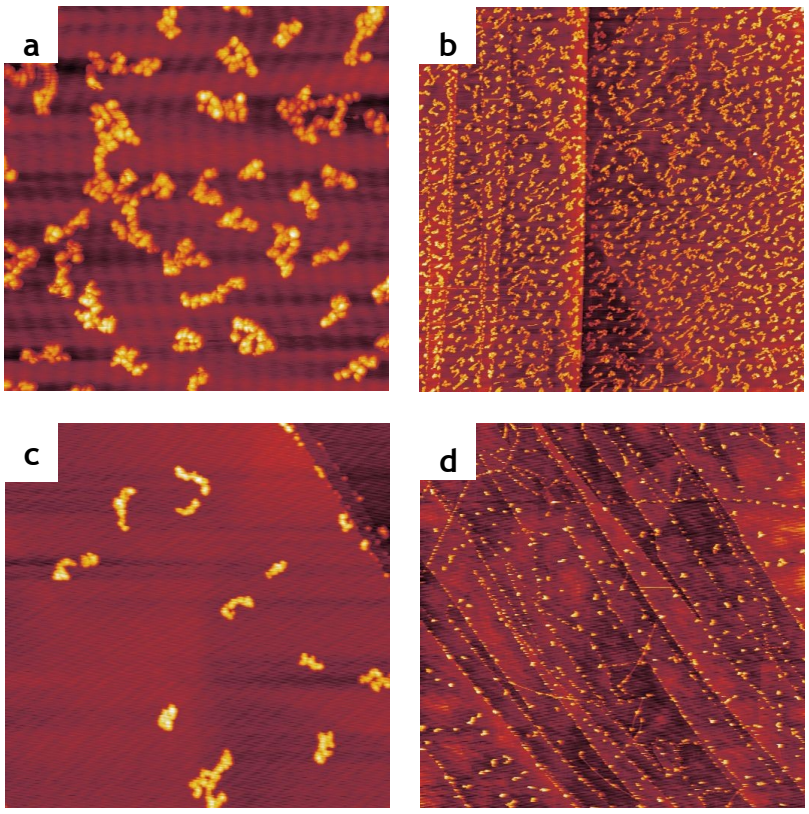

Figure 3.5: AFM images for SEA of $H_2[PtCl_6]$ on: a, b) HOPG reduction in H_2 at 200 °C on: a, b) HOPG; and c, d) HCl-treated HOPG. Images (a) and (c) are 1 μm x 1 um, and (b) and (d) are 5μm x 5 μm.

www.manaraa.com

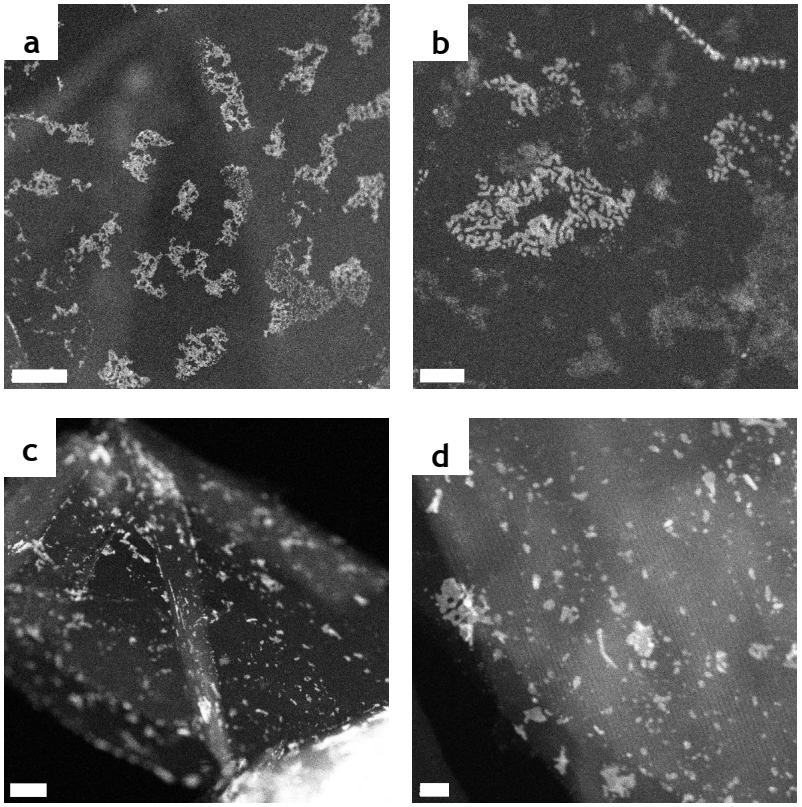

Figure 3.6: STEM images for SEA of $H_2[PtCl_6]$ after reduction in H_2 at 200 °C on : a, b) GNPs; and c, d) HCl treated GNPs. The scale bars are 0.1 μm in (a), 0.05 μm in (c) and 20 nm in (b) and (d).

www.manaraa.com

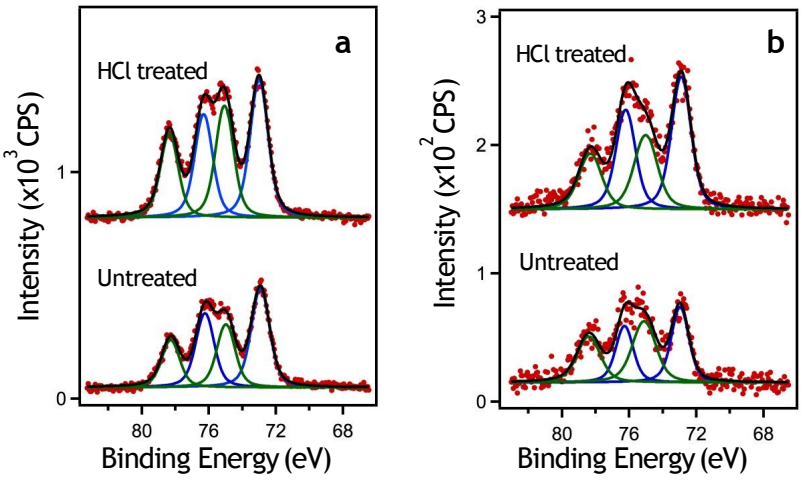

Figure 3.7: Pt(4f) XPS data for SEA of tetraamine platinum (II) hydroxide on: a) HOPG; and b) GNP surfaces before and after treating with HCl.

www.manaraa.com

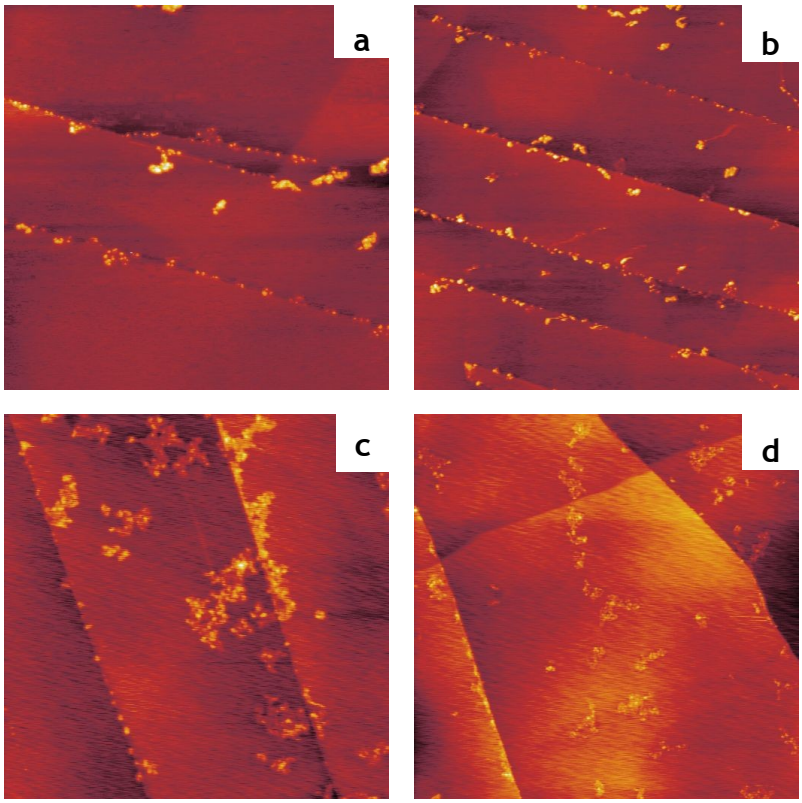

Figure 3.8: AFM images of $[Pt(NH_3)_4](OH)_2$ SEA after reduction in H_2 at 200 °C on: a, b) HOPG; and c, d) HCl-treated HOPG. Image sizes are 1μm x 1μm for (a) and (c) and 2 μm x 2 μm for (b) and (d).

www.manaraa.com

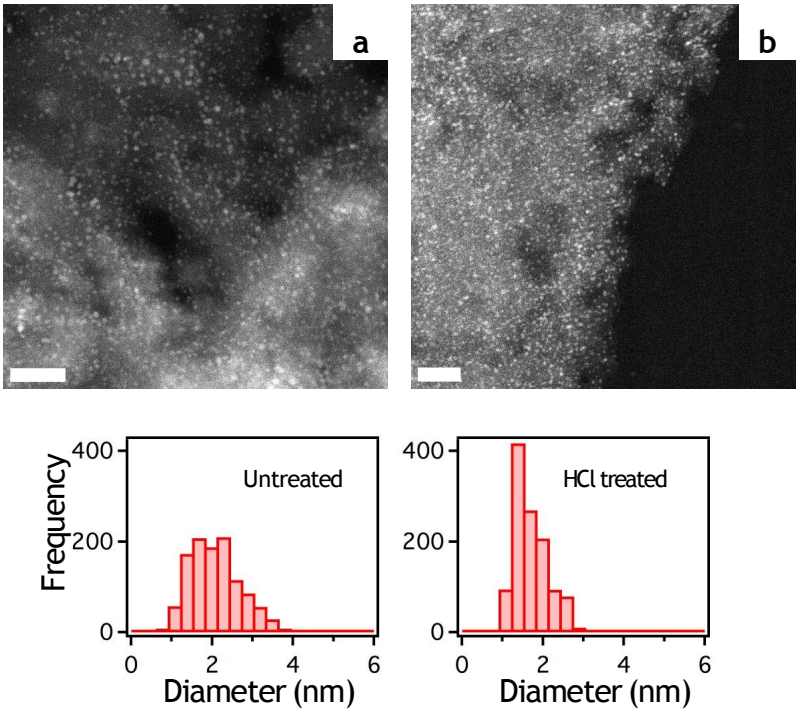

Figure 3.9: STEM images for $[Pt(NH_3)_4](OH)_2$ SEA after reduction in H_2 at 200 °C on: a) untreated GNPs; and b) HCl-treated GNPs. The scale bars are 20 nm. Histograms of Pt particles sizes are shown below each image.

www.manaraa.com

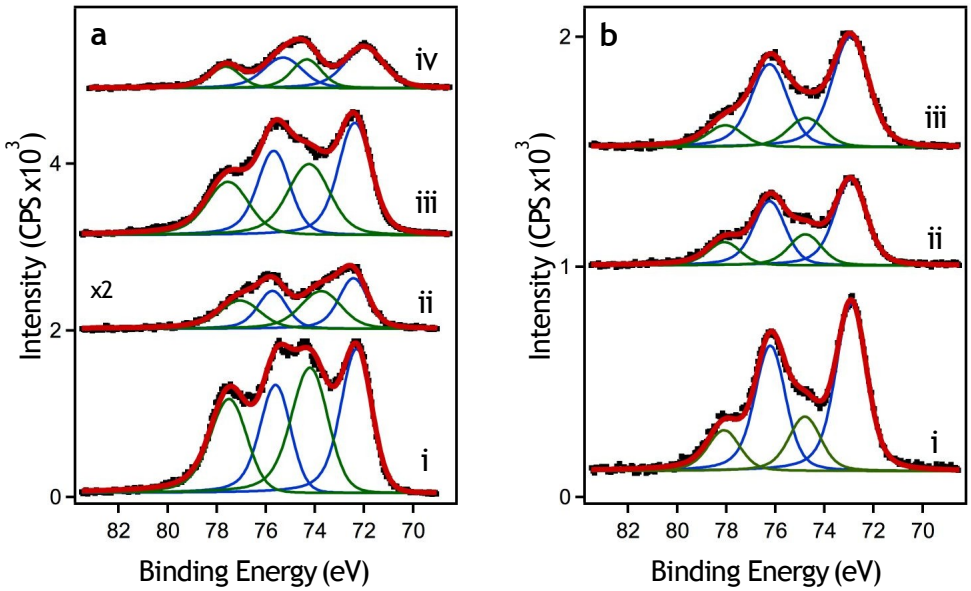

Figure 3.10: Pt(4f) XPS data for: a) $Na_2[PtCl_4]$ SEA on: i) HOPG; ii) GNPs; iii) Darco G60; and iv) Ketjen black; and b) $[Pt(NH_3)_4](OH)_2$ SEA on: i) Timrex HSAG 300; ii) Darco S51; and iii) Darco KBM.

3.5 References

1. Regalbuto, J. R., Strong Electrostatic Adsorption of Metals onto Catalyst Supports. In *Catalyst Preparation: Science and Engineering*, Regalbuto, J. R., Ed. Taylor and Francis: Boca Raton, FL, 2007.

2. Raciti, D.; Kubal, J.; Ma, C.; Barclay, M.; Gonzalez, M.; Chi, M. F.; Greeley, J.; More, K. L.; Wang, C., Pt_3Re alloy nanoparticles as electrocatalysts for the oxygen reduction reaction. *Nano Energy* **2016,** *20*, 202-211.

3. Hao, X.; Barnes, S.; Regalbuto, J. R., A fundamental study of Pt impregnation of carbon: Adsorption equilibrium and particle synthesis. *J. Catal.* **2011,** *279* (1), 48-65.

4. Cameron, D. S.; Cooper, S. J.; Dodgson, I. L.; Harrison, B.; Jenkins, J. W., Carbon as supports for precious metal catalysts. *Catal. Today* **1990,** *7* (10), 113-137.

www.manaraa.com

5. Radovic, L. R.; Rodriguez-Reinoso, F., Carbon materials in catalysis. In *Chemistry and Physics of Carbon, Vol 25*, Thrower, P. A., Ed. Marcel Dekker: New York, 1997; Vol. 25, pp 243-358.

6. Rodriguez-Reinoso, F., The role of carbon materials in heterogeneous catalysis. *Carbon* **1998,** *36* (3), 159-175.

7. Rodriguez-Reinoso, F., In *Porosity in Carbons*, Patrick, J. W., Ed. Wiley: Chichester (UK), 1995.

8. Auer, E.; Freund, A.; Pietsch, J.; Tacke, T., Carbons as supports for industrial precious metal catalysts. *Appl. Catal. A* **1998,** *173* (2), 259-271.

9. Coloma, F.; Sepulveda-Escribano, A.; Fierro, J. L. G.; Rodriguez-Reinoso, F., Gas phase hydrogenation of crotonaldehyde over Pt/activated carbon catalysts. Influence of the oxygen surface groups on the support. *Appl. Catal. A* **1997,** *150* (1), 165-183.

10. Job, N.; Pereira, M. F. R.; Lambert, S.; Cabiac, A.; Delahay, G.; Colomer, J. F.; Marien, J.; Figueiredo, J. L.; Pirard, J. P., Highly dispersed platinum catalysts prepared by impregnation of texture-tailored carbon xerogels. *J. Catal.* **2006,** *240* (2), 160-171.

11. Gasteiger, H. A.; Gu, W.; Makharia, R.; Mathias, M. F.; Sompalli, B., *Handbook of Fuel Cells: Fundamentals, Technology and Applications*. Wiley: Chichester (UK), 2003; Vol. 3.

12. Antolini, E., Carbon supports for low-temperature fuel cell catalysts. *Appl. Catal. B* **2009,** *88* (1-2), 1-24.

13. Gillilland, S.; Regalbuto, J. R.; Gupton, F., **in preparation**.

www.manaraa.com

14. Duke, A. S.; Dolgopolova, E. A.; Galhenage, R. P.; Ammal, S. C.; Heyden, A.; Smith, M. D.; Chen, D. A.; Shustova, N. B., Active Sites in Copper-Based Metal Organic Frameworks: Understanding Substrate Dynamics, Redox Processes, and Valence Band Structure. *J. Phys. Chem. C* **2015,** *119* (49), 27457-27466.

15. Wagner, C. D.; Riggs, W. M.; Davis, L. E.; Moulder, J. F., *Handbook of X-ray Photoelectron Spectroscopy*. Perkin Elmer Corporation: Eden Prairie, MN, 1979.

16. Chalmers, J. M., Mid-infrared Spectroscopy: Anomalies, Artifacts and Common Errors. In *Handbook of Vibrational Spectroscopy*, Chalmers, J. M.; Griffiths, P. R., Eds. John Wiley and Sons Chichester, 2002; Vol. 3, pp 2327-2347.

17. Banerjee, R. The Oxidation and Decoration Chemistry of Platinum and Palladium Nanoparticles on Carbon Supports. Ph.D. Thesis, University of South Carolina, Columbia, SC, 2016.

18. Peuckert, M.; Coenen, F. P.; Bonzel, H. P., XPS study of the electrochemical surface oxidation of platinum in 1N H_2SO_4 acid electrolyte. *Electrochim. Acta* **1984,** *29* (10), 1305-1314.

19. Battistoni, C.; Giuliani, A. M.; Paparazzo, E.; Tarli, F., Platinum complexes of the methyl-esters of dithiocarbazic acid and 3-phenyldithiocarbazic acid. *J. Chem. Soc. Dalton Trans.* **1984,** *7*, 1293-1299.

20. Buono, C.; Davies, P. R.; Davies, R. J.; Jones, T.; Kulhavy, J.; Lewis, R.; Morgan, D. J.; Robinson, N.; Willock, D. J., Spectroscopic and atomic force studies of the functionalisation of carbon surfaces: new insights into the role of the surface topography and specific chemical states. *Faraday Discuss.* **2014,** *173*, 257-272.

www.manaraa.com

21. Burgess, R.; Buono, C.; Davies, P. R.; Davies, R. J.; Legge, T.; Lai, A.; Lewis, R.; Morgan, D. J.; Robinson, N.; Willock, D. J., The functionalisation of graphite surfaces with nitric acid: Identification of functional groups and their effects on gold deposition. *J. Catal.* **2015,** *323*, 10-18.

22. van Dam, H. E.; van Bekkum, H., Preparation of Platinum on activated carbon. *J. Catal.* **1991,** *131* (2), 335-349.

23. Vickerman, J. C., *Surface Analysis: The Principal Techniques*. John Wiley and Sons: New York, 1997.

24. Hao, X.; Quach, L.; Korah, J.; Spieker, W. A.; Regalbuto, J. R., The control of platinum impregnation by PZC alteration of oxides and carbon. *J. Mol. Catal. A* **2004,** *219* (1), 97-107.

25. Hao, X. On the science of catalyst preparation: platinum impregnation over carbon. Ph.D. Thesis, University of Illinois, Chicago, 2004.

26. Leon, C.; Solar, J. M.; Calemma, V.; Radovic, L. R., Evidence for the protonation of basal plane sites on carbon. *Carbon* **1992,** *30* (5), 797-811.

27. Yu, A. P.; Ramesh, P.; Itkis, M. E.; Bekyarova, E.; Haddon, R. C., Graphite nanoplatelet-epoxy composite thermal interface materials. *J. Phys. Chem. C* **2007,** *111* (21), 7565-7569.

28. Ramesh, P.; Sampath, S., Electrochemical characterization of binderless, recompressed exfoliated graphite electrodes: Electron-transfer kinetics and diffusion characteristics. *Anal. Chem.* **2003,** *75* (24), 6949-6957.

www.manaraa.com

29. Bouleghlimat, E.; Davies, P. R.; Davies, R. J.; Howarth, R.; Kulhavy, J.; Morgan, D. J., The effect of acid treatment on the surface chemistry and topography of graphite. *Carbon* **2013,** *61*, 124-133.

30. Kalinkin, A. V.; Sorokin, A. M.; Smirnov, M. Y.; Bukhtiyarov, V. I., Size effect in the oxidation of platinum nanoparticles on graphite with nitrogen dioxide: An XPS and STM study. *Kinet. Catal.* **2014,** *55* (3), 354-360.

31. Howells, A. R.; Hung, L.; Chottiner, G. S.; Scherson, D. A., Effects of substrate defect density and annealing temperature on the nature of Pt clusters vapor deposited on the basal plane of highly oriented pyrolytic graphite. *Solid State Ionics* **2002,** *150* (1-2), 53-62.

32. Yuan, Z.; Hanf, M. C.; Stephan, R.; Dulot, F.; Denys, E.; Florentin, A.; Harbich, W.; Wetzel, P., Growth of palladium nanoparticles on nanostructured highly ordered pyrolytic graphite. *Surf. Interface Anal.* **2015,** *47* (1), 82-86.

33. Blum, B.; Salvarezza, R. C.; Arvia, A. J., Vapor-deposited gold film formation on highly oriented pyrolitic graphite. A transition from pseudo-two-dimensional branched island growth to continuous film formation. *J. Vac. Sci. Technol. B* **1999,** *17* (6), 2431-2438.

34. Hwang, R. Q.; Bartelt, M. C., Scanning-Tunneling Microscopy Studies of Metal On Metal Epitaxy. *Chemical Reviews* **1997,** *97* (#4), 1063-1082.

35. Hwang, R. Q.; Schroder, J.; Gunther, C.; Behm, R. J., Fractal Growth of 2-Dimensional Islands : Au On Ru(0001). *Phys. Rev. Lett.* **1991,** *67* (#23), 3279-3282.

36. Peuckert, M.; Bonzel, H. P., Characterization of oxidized platinum surfaces by X-ray photoelectron spectroscopy. *Surf. Sci.* **1984,** *145* (1), 239-259.

www.manaraa.com

37. Legare, P.; Hilaire, L.; Maire, G., Interaction of polycrystalline platinum and a platinum silicon alloy with oxygen - an XPS study. *Surf. Sci.* **1984,** *141* (2-3), 604-616.

38. Witten, T. A.; Sander, L. M., Diffusion-limited aggregation, a kinetic critical phenomenon. *Phys. Rev. Lett.* **1981,** *47* (19), 1400-1403.

39. Meakin, P.; Witten, T. A., Growing interface in diffusion-limited aggregation. *Phys. Rev. A* **1983,** *28* (5), 2985-2989.

40. Galhenage, R. P.; Xie, K.; Diao, W.; Tengco, J. M. M.; Seuser, G. S.; Monnier, J. R.; Chen, D. A., Platinum-ruthenium bimetallic clusters on graphite: a comparison of vapor deposition and electroless deposition methods. *Phys. Chem. Chem. Phys.* **2015,** *17* (42), 28354-28363.

41. Weast, R. C., *CRC Handbook of Chemistry and Physics*. 70th ed.; CRC Press, Inc.: Boca Raton, FL, 1989-1990.

www.manaraa.com

CHAPTER 4

COMPARING STRONG ELECTROSTATIC ADSORPTION OF PT AND PD PRECURSORS ON GRAPHITIC SUPPORTS

www.manaraa.com

4.1 Introduction

Synthesizing small, well-dispersed transition metal particles over high surface area supports is a topic of interest in the field of catalysis. Small particles use the metal in the most efficient way possible, since nearly all the metal atoms reside at the surface of the nanoparticle, and in some cases can actually enhance the activity of the catalysts.[1] Strong electrostatic adsorption (SEA) is a simple wet impregnation method that can generate small, well-dispersed metal nanoparticles over both oxide and carbon supports. Anionic/cationic metal precursors are adsorbed onto functional groups that accumulate a positive/negative charge by varying the pH below or above the point of zero charge (PZC) of the support. The SEA process has been well modeled by the revised physical adsorption (RPA) model on a variety of oxide supports.[2, 3] On oxide supports, the surface oxygen functional groups on supports like alumina are modeled as being amphoteric and can therefore accumulate either a positive or negative charge. The ability of the oxygen groups to accumulate charge depends on the pK_a values associated with protonating or deprotonating that oxygen group.[2-5]

$$[MOH_2^+] \overset{K_{a1}}{\longleftrightarrow} [MOH] + [H^+]$$

$$[MOH] \overset{K_{a2}}{\longleftrightarrow} [MO^-] + [H^+]$$

In contrast to oxide supports, carbon supports can have a variety of functional groups on the surface. For example, graphitic carbon surfaces consist of aromatic rings, while oxygenated carbon supports like graphene oxide have a wide range of oxygen functionalities on the surface, such as alcohols, carboxylic acids, and ketones.[6] The functional groups that are present on the surface of carbon dictate the adsorption of metal precursors onto the surface. Anionic Pt precursors adsorb readily onto carbon supports

www.manaraa.com

that have little to no oxygen content, such as graphitic surfaces[7] and carbon supports with a high PZC.[8] It has been proposed the adsorption of anionic Pt precursors on high PZC carbon supports is mediated by the protonation of aromatic rings on the surface.[8-12] The aromatic ring is not amphoteric, and is therefore only capable of accumulating a positive charge, consistent with the minimal amount of cationic adsorption on these surfaces. On the other hand, carbon supports that contain a variety of oxygen functional groups, like graphene oxide, tend to have a low PZC and are better at adsorbing cations than anions.[13] In fact, when oxygen functional groups are added to a high PZC carbon support with an acid treatment, the PZC of the carbon decreases, suppressing the adsorption of Pt anions and increasing the adsorption of Pt cations.[8, 14] These general trends suggest that the pK_a of these oxygen functional groups is low enough for deprotonation to occur under basic conditions, but not low enough to become protonated under acidic conditions. However, the pK_a values of oxygen function groups on high surface area carbon supports cannot be experimentally determined due to difficulties in obtaining reliable qualitative and quantitative information about the surface functional groups.[15-19] Therefore, much is still unknown about the functional groups that mediate SEA on carbon supports.

To gain more insight into the SEA process onto carbon supports, Pt and Pd precursors were chosen for study. Pt based catalysts have a wide variety of applications, including hydrogenation reaction,[20] naphtha reforming,[21] and catalytic converters.[22] Recently, it was found that Pd based catalysts synthesized using SEA on graphene nanoplatelets were highly active for Suzuki coupling.[13]

In this study, three different graphitic supports were chosen to study the SEA mechanism of Pd and Pt precursors. HOPG is a model single crystal carbon surface with

www.manaraa.com

a graphitic structure that is essentially free of any oxygen functional groups on the surface. Additionally, HOPG can be selectively functionalized with hydroxyl groups, enabling us to understand the role that hydroxyl groups play in mediating SEA. Graphene nanoplatelets (GNPs) from Strem chemical were used as a high surface area (40 m^2/gram) analog to HOPG. Lastly, graphene nanoplatelets (GN-Alfa) obtained through Alfa Aesar (500 m^2/gram) were chosen for study due to the ability to tune the surface oxygen content using a combination of reduction and acid treatments.

For the cationic precursors, it was found that the adsorption of both Pt and Pd was mediated by the presence of oxygen functional groups on the surface. In the case of HOPG, increasing the concentration of hydroxyl groups on the surface increased the adsorption of the cationic precursors. These results suggest that under basic conditions, hydroxyl groups on the surface on HOPG become deprotonated and act as adsorption sites for cationic precursors. For the GN-Alfa support, cationic adsorption increased with increasing surface oxygen content, which included a variety of oxygen functionalities on the surface such as hydroxyl groups and carboxylic acids. However, Pt and Pd anions appear to adsorb onto the surface of HOPG via a different mechanism. Based on XPS results, we suggest that the adsorption of Pt anions is partially mediated by a chemical reaction with the graphitic surface.

4.2 Experimental

Highly oriented pyrolytic graphite crystals were purchased from Nanoscience Instruments (ZYH grade, 5x5x2 mm^3). A clean HOPG surface was generated by exfoliating both sides of the HOPG crystal with adhesive tape. Low surface area graphene nanoplatelets, referred to as GNP, were obtained from Strem Chemical (CAS

www.manaraa.com

#06-0222, 2-10 nm thick, ~5 microns wide). High surface area graphene nanoplatelets, referred to as GN-Alfa, were obtained through Alfa Aesar (CAS #7782-42-5). Chloroplatinic acid ($H_2[PtCl_6]$, 99.9%), tetraamine platinum(II) hydroxide ($[Pt(NH_3)_4(OH)_2]$,99.99%), palladium(II) chloride ($PdCl_2$,99.9%), sodium tetrachloropalladate(II) ($Na_2[PdCl_4]$, 99.99%) tetraamine palladium(II) chloride ($[Pd(NH_3)_4]Cl_2$, 99.99%) were all obtained from Sigma Aldrich. $PdCl_2$ was dissolved into deionized water at a 1:5.6 molar ratio with HCl in order to stabilize the salt in solution and form the $[PdCl_4]^{2-}$ precursor.[23-26]

All uptake experiments with the GNPs and GN-Alfa supports were conducted as a function of pH with a surface loading of 500 m^2/L, unless stated otherwise. The adsorption of Pt and Pd precursors onto the surface was determined from the difference in metal concentration before and after adsorption. The metal concentrations were measured using a Perkin-Elmer Optima 2000 DV for inductively coupled plasma (ICP) optical emission spectroscopy. The GNP surface area was taken to be 40 m^2/gram, as reported by the manufacturer. The surface area of all the GN-Alfa supports used in these studies was assumed to be 500 m^2/gram, as reported by the manufacturer.

Acid treatment of the HOPG was conducted by placing a drop of 37% HCl (Aldrich) on the face of the HOPG crystal for 3 hours. After the treatment, the surface was washed using deionized (DI) water to remove residual HCl and Cl ion from the surface and dried in air. Acid treatments of the GNPs and GN-Alfa support were administered by heating the support in 37% HCl or 67% HNO_3 (Aldrich) at 90 °C for 3 hours. After the acid treatment, the GNPs or GN-Alfa supports were vacuum filtered and

www.manaraa.com

then washed with DI water until the pH of the filtrate was the same as the untreated DI water (5.5). The GNPs were washed with copious amounts of DI water prior to use.

To remove oxygen from the GN-Alfa supports were reduced in 20% H_2 balance He at 500 °C for 2 hours, unless otherwise specified. Temperature programmed reduction experiments were conducted in a custom TPX system connected to an Inficon Transpector 2 Mass Spectrometer that has been described previously.[27] The reduction was carried out using a 5 °C/min ramp rate in 10% H_2 balance Ar at a flow rate of 20 cc/min.

Strong electrostatic adsorption on HOPG was conducted by immersing the crystal into a 50 mL of a Pt or Pd precursor solution for 1 hour while stirring the solution with a Teflon-coated stir bar. For SEA experiments on the GNPs and GN-Alfa supports, the support was contacted with the Pt or Pd precursor and shaken for 1 hour in a high-density polyethylene container using an automated shaker. The adsorption of $PdCl_2$ and $[Pd(NH_3)_4]Cl_2$ on the GNPs and GN-Alfa supports were carried out at a pH between 2-2.2 and 11-11.1 respectively. The pH of the solutions containing $PdCl_2$ or $Na_2[PdCl_4]$ salts were adjusted using HCl or NH_4OH. NaOH was not used due to precipitation of the Pd salts. The pH of the $[Pd(NH_3)_4]Cl_2$ solution was adjusted with HCl, NH_4OH and/or NaOH. The pH of the Pt precursor solutions was adjusted with HCl and NaOH. The GNPs and GN-Alfa supports were allowed to dry at room temperature in air for 24-48 hours.

The PZC of the GNPs and GN-Alfa support were measured using a variation of the pH shift method.[4] Deionized water with an initial pH of 3, 6, and 9 was added to a

www.manaraa.com

sample of GNPs or GN-Alfa until incipient wetness at which point the final pH was measured with a spear-tipped pH probe. The final pHs are the PZC of the support.

X-ray photoelectron spectroscopy (XPS) experiments were conducted in a Kratos AXIS Ultra DLD instrument equipped with a monochromatic Al Kα source, charge neutralizer, a hemisphereical analyzer, load lock and catalysis cell. All spectra were collected with a charge neutralizer using a step size of 0.06 eV and a pass energy of 40 eV. The metal/C(1s) XPS ratios were calculated using the following equation:

$$\frac{A_M/ASF_M}{A_C/ASF_C}$$

where A_M and A_C are the integrated areas of the metal (Pt(4f) or Pd(3d)) and C(1s) regions respectively and ASF_M and ASF_C are the atomic sensitivity factors of the metal and C(1s) regions respectively.[28] To determine the integrated area, a linear background subtraction was applied to each spectrum prior to integration. All XPS peak fits of the Pd(3d) region were carried out using CasaXPS using a Shirley background and a Lorentzian-asymmetric peak shape. The peak splitting between Pd($3d_{7/2}$) and Pd($3d_{5/2}$) was fixed at 5.25 eV,[28] the area ratio between was set to 3:2 and peak widths were set equal to one another.

Transmission infrared spectroscopy experiments were conducted using a Nexus 470 spectrometer (Thermo Nicolet) that was purged with dry air. The sample pellet compositions were kept between 0.1-0.02 weight percent carbon powder mixed with optical grade KBr to ensure that the pellets remained transparent. The KBr was kept in an oven at 110-120 °C for 12 hours to remove water prior to use. Pellets were pressed with 8000 psi for 5 minutes.

www.manaraa.com

4.3 Results and Discussion

4.3.1 HOPG

The HOPG surface was functionalized with hydroxyl groups using an HCl treatment. The untreated HOPG surface has virtually no oxygen functionality while the HCl treated HOPG has a significant, single oxygen peak centered at 532.8 eV (Figure 4.1). In previous work, it was established that this oxygen peak corresponds to hydroxyl groups that form on the surface,[7] consistent with other studies in the literature.[29]

Strong electrostatic adsorption experiments on HOPG using the cationic Pt and Pd precursors, $[Pt(NH_3)_4]^{2+}$ and $[Pd(NH_3)_4]^{2+}$, were conducted at a pH of 11. The Pt/C and Pd/C ratios calculated from a series of XPS experiments are shown on the right side of Figure 4.2. In the case of both Pt and Pd, the addition of hydroxyl groups to the surface of HOPG lead to an increase in cationic adsorption by a factor of 1.8 for both precursors. These results suggest that cationic adsorption is mediated by hydroxyl groups on the surface of HOPG, which deprotonate under basic conditions enabling them to act as nucleation sites. Moreover, the increase in cationic adsorption upon the addition of oxygen functionality to the surface is consistent with a general trend for SEA conducted on high surface area carbon supports: treating the carbon support with acid increases the oxygen content on the surface and decreases its point of zero charge (PZC), which in turn leads to an increase in cationic adsorption.[8, 14] While the pK_a values of the oxygen functional groups on the surface are not known, theoretical calculations predicted the pK_a of carboxylic acid groups attached to graphene fall in the range between 3.16-3.44,[19] which is slightly more acidic than benzoic acid.[30] These results suggest that the pK_a values for model organic molecules can be a useful guide for determining the likelihood

www.manaraa.com

that an oxygen group will protonate or deprotonate in a given pH range. While the pK_a of hydroxyl groups on HOPG is unknown, organic molecules like phenol have a pK_a of around 10,[30] therefore it seems reasonable for hydroxyl groups on HOPG would be deprotonated at a pH of 11.

SEA experiments on HOPG for the anionic Pt and Pd precursors, $[PtCl_6]^{2-}$ and $[PdCl_4]^{2-}$, were conducted at a pH of 2.5 and 2.1, respectively. In the case of $[PtCl_6]^{2-}$, the HCl treatment decreased the Pt/C ratio by 54%, (left hand graph in Figure 4.2). Comparatively, the Pd signal of the $[PdCl_4]^{2-}$ precursor did not decrease after HOPG was treated with HCl. The same trend was also observed when $[PdCl_4]^{2-}$ was adsorbed at a pH of 3. Furthermore, the metal/C ratio of $[PdCl_4]^{2-}$ adsorbed onto the untreated HOPG was 18-19 times smaller than that of $[PtCl_6]^{2-}$. We previously attributed the SEA mechanism for Pt anions on the surface of HOPG to the adsorption of protons to delocalized pi electrons on the surface of HOPG,[7] which accumulate a positive charge on the surface capable of adsorbing Pt anions. Hydroxylating the surface disrupts the pi bonding network on the surface of HOPG, in turn leading to a decrease in anionic Pt adsorption. The fact that hydroxyl groups were not the principal mediator of Pt anion adsorption is consistent with protonated cationic hydroxyl groups having negative pK_a values,[30] meaning that they would be difficult to protonate. If the interaction between Pt and Pd anions with the surface of HOPG was purely electrostatic, then the same trend in adsorption should have been observed for both species.

Another possibility is that there is a chemical component to the adsorption of $[PtCl_6]^{2-}$ to the surface of HOPG. Previous work by our group demonstrated that when $[PtCl_6]^{2-}$ is adsorbed onto HOPG, Pt exists in both the Pt^{4+} and Pt^{2+} oxidation state.[7] The

www.manaraa.com

presence of Pt^{2+} demonstrates that Pt^{4+} becomes reduced when contacted with HOPG. On the other hand, both $[PdCl_4]^{2-}$ or $[Pd(NH_3)_4]^{2+}$ remain in the Pd^{2+} oxidation state when adsorbed onto HOPG (Figure 4.3a-b), suggesting a lack of chemical interaction with the surface. The reduction of $[PtCl_6]^{2-}$ on high surface area carbon supports has also been reported in the literature.[8, 31] Hoa et al. suggested that the reduction of $[PtCl_6]^{2-}$ occurs slowly, as evidenced by unpublished EXAFS results.[8] The reduction of $[PtCl_6]^{2-}$ on HOPG suggests that the interaction between the two is not purely electrostatic, but has a chemical component as well.

To test if there was an electrostatic component to the adsorption of the Pt and Pd anions, $[PdCl_4]^{2-}$ and $[PtCl_6]^{2-}$ were adsorbed onto HOPG as a function of pH (Figure 4.4). The Pt/C ratio decreases with increasing pH, consistent with the Pt adsorption having an electrostatic component. For $[PdCl_4]^{2-}$ adsorption, both $PdCl_2$ and $Na_2[PdCl_4]$ salts were used. For both Pd salts, there was little to no adsorption of Pd under acidic conditions. Under basic conditions, there was still Pd present on the surface. Similar experiments were conducted with the $[Pd(NH_3)_4]^{2+}$ solutions under both basic and acidic conditions. Surprisingly, there was significantly more adsorption of the $[Pd(NH_3)_4]^{2+}$ under acidic conditions than $[PdCl_4]^{2-}$.

These unexpected results of Pd adsorption on HOPG can be explained by stability issues with both the $[PdCl_4]^{2-}$ and $[Pd(NH_3)_4]^{2+}$ precursors, which are not a problem for the Pt precursors.[32, 33] For $[PdCl_4]^{2-}$, the use of NH_4OH to increase the pH of the $[PdCl_4]^{2-}$ solution can cause the chlorine ligands of $[PdCl_4]^{2-}$ to exchange with ammonia to form $[Pd(NH_3)_4]^{2+}$.[23] In fact, the adsorption observed under basic conditions is from $[Pd(NH_3)_4]^{2+}$ rather than $[PdCl_4]^{2-}$, given that the formation of $Pd(NH_3)_4^{2+}$ can be

www.manaraa.com

observed when $[PdCl_4]^{2-}$ solution changes from yellow to clear as NH_4OH is added, as shown in Figure 4.5. Similarly, the addition of HCl to $[Pd(NH_3)_4]^{2+}$ changes the color of the solution from clear to yellow, indicating the formation of the $[PdCl_4]^{2-}$ species. Separate ICP experiments were conducted to measure the concentration of both Pt and Pd precursors as a function of pH (Figure 4.6). The concentration of all the Pt and Pd precursors are relatively stable across the entire pH range with the exception of $[Pd(NH_3)_4]^{2+}$, which has a sharp decrease in concentration under acidic conditions. These results suggest that Pd precipitates out of the $[Pd(NH_3)_4]^{2+}$ solution as HCl is added to it; therefore the increase Pd/C ratio on HOPG when it was contacted with the $[Pd(NH_3)_4]^{2+}$ solution under acidic conditions is attributed to the precipitation of Pd. Due to the instability of both Pd precursors, it was not possible to test the electrostatic nature of Pd adsorption onto HOPG as a function of pH.

4.3.2 *GNP*

The SEA of Pt and Pd was also studied using GNPs, a high surface area analog of HOPG. In addition to being able to determine the amount of metal deposited using XPS, the adsorption of metals could also be measured by a typical uptake experiment, which enables the adsorption of metals onto the GNPs to be tracked as a function of pH. In our previous work, the GNPs were found to have low oxygen content, as indicated by a O(1s)/C(1s) ratio of 0.022 and a PZC of ~8. Treating the GNPs with HCl increased the number of hydroxyl groups on the surface, but only led to a slight increase in oxygen that was too small to be reliably quantified by XPS.[7]

The uptake of $[PdCl_4]^{2-}$ and $[Pd(NH_3)_4]^{2+}$ onto the GNPs are shown in Figure 4.7. In the case of the $[Pd(NH_3)_4]^{2+}$ uptake, there was almost no adsorption of Pd on the

www.manaraa.com

washed or HCl treated GNPs. For the $[PdCl_4]^{2-}$ uptake, the HCl treatment did not decrease the uptake of Pd. The uptake maxima for $[PdCl_4]^{2-}$ on the washed GNPs appeared at 0.5 μmol/m^2, a third of the amount of $[PtCl_6]^{2-}$ that adsorbed onto the GNPs (Figure 4.8). These results are similar to what was observed with HOPG, which showed significantly more $[PtCl_6]^{2-}$ adsorption than $[PdCl_4]^{2-}$ adsorption under acidic conditions. Furthermore, the adsorption maximum occurred at a pH of 2, the "natural" pH of the $[PdCl_4]^{2-}$ solution, i.e. no additional acid or base was added to the solution prior to contact with the support. The position of the maximum uptake on the washed GNPs are in line with previous observation that have made for $[PdCl_4]^{2-}$ on other carbon supports,[24-26] and was also true for the GN-Alfa support (see section 4.3.3.2). On the other hand, the maximum uptake for HCl treated GNPs occurred at a pH of around 1. These results are surprising in light of the fact that the ionic strength of the solution at a pH of 1 should suppress the adsorption of $[PdCl_4]^{2-}$. A possible explanation for the increase in adsorption is the partial exfoliation of the GNPs after the acid treatment,[7] which would increase the surface area onto which the Pd precursor could adsorb.

XPS experiments were conducted on washed and HCl treated GNPs that were exposed to $[PdCl_4]^{2-}$ pH of 2.1 or $[Pd(NH_3)_4]^{2+}$ at a pH of 11, (Figure 4.8). The XPS of $[PdCl_4]^{2-}$ (Figure 4.8a) showed that there was an order of magnitude less Pd adsorbed onto the GNPs as compared with $[PtCl_6]^{2-}$,[7] in agreement with the uptake results that demonstrated less adsorption of the Pd anion than the Pt anion (Figure 4.9). According to the XPS results, a comparable amount of $[PdCl_4]^{2-}$ was adsorbed onto the washed GNPs as compared with the HCl treated GNPs, in agreement with the uptake data collected at around a pH of 2. These results mirror what was observed on HOPG: significantly less

www.manaraa.com

adsorption of $[PdCl_4]^{2-}$ compared to $[PtCl_6]^{2-}$ regardless of whether the surface was treated with HCl. For the cationic adsorption (Figure 4.8b), essentially no $[Pd(NH_3)_4]^{2+}$ adsorbed onto the washed or HCl treated GNPs, in agreement with the uptake experiments. There is arguably a very small Pd signal on the HCl treated, but it is barely above the noise. The lack of adsorption of $[Pd(NH_3)_4]^{2+}$ onto the GNPs suggests that there is not a sufficient number of oxygen groups on the surface to mediate cationic adsorption. Overall, the trend of there being little adsorption of both cation and anionic Pd precursors is consistent with what was observed on HOPG.

4.3.3 GN-Alfa

4.3.3.1 Adding and removing oxygen functionalities from GN-Alfa

To better address the nature of Pd and Pt ion adsorption, we have conducted a series of SEA experiments on a graphene nanoplatelet support (GN-Alfa) and attempted to selectively remove and add oxygen functional groups in order to adjust the point of zero charge (PZC) and the O(1s)/C(1s) ratio (oxygen content) of the support. Table 4.1 provides a list of all the treatments that were used along with the measured oxygen content and PZC of the support. Variable amounts of oxygen were removed from the GN-Alfa support by annealing the support in 20% H_2 at a temperature that varied from 350 – 500 °C for 2 hours. Heating to 350 °C decreased the oxygen content by 31%; further reduction up to 500 °C decreased the oxygen content by 85%, removing essentially all the oxygen from the surface. The reduction at 500 °C increased the PZC of the GN-Alfa support from 4.0 to 10.5. A temperature programmed reduction (TPR) experiment was performed to confirm that the GN-Alfa support did not undergo methanation during the reduction treatment (Figure 4.10), which could cause structural

www.manaraa.com

changes to the material. The major desorption products were carbon monoxide and carbon dioxide, consistent with the removal of oxygen groups from the surface.[34] Methanation did occur, but not until above 550 °C, well above the reduction temperature of 500 °C. An additional TPR experiment confirmed that no methanation occurred when the GN-Alfa sample was reduced at 500 °C for 2 hours. Thus, we were successfully able to remove oxygen functionalities and increase the PZC of the GN-Alfa support using a simple reduction treatment in H_2.

To add oxygen functionality to the surface, the GN-alfa support was heated to 90 °C in HCl or HNO_3. Treating the GN-Alfa in HCl only increased the O(1s)/C(1s) ratio by only 13%, indicating that the HCl treatment added relatively little oxygen to the surface. Reduction of the GN-Alfa support at 500 °C followed by an HCl treatment almost doubled the oxygen content. However, there was still less than a third as much oxygen on the surface as compared to the as received GN-Alfa support, demonstrating again that the HCl treatment was not very effective at adding oxygen functionality to the surface. No new oxygen functionality features appeared in the FTIR spectra after any of the HCl treatments (Figure 4.11). Treating the GN-Alfa support in nitric acid more than doubled the oxygen content and decreased the PZC from 4.0 to 1.2. Furthermore, FTIR experiments on the nitric acid treated samples (Figure 4.11) revealed that the nitric acid treatment added carboxylic acid groups to the surface, as indicated by the absorption peak at 1725 cm^{-1}.[34] In an attempt to selectively functionalize the GN-Alfa support with HNO_3, the GN-Alfa support was first reduced to remove all the oxygen from the surface and then subjected to the HNO_3 treatment. Subsequent FTIR experiments confirmed that carboxylic acid groups were added to the surface; however the O(1s) peak shape

www.manaraa.com

remained rather broad (Figure 4.12), which is indicative of more than one oxygen surface species. Thus, the HNO_3 treatment of reduced GN-Alfa was not able to populate the surface with exclusively carboxylic acid groups.

4.3.3.2 Pt and Pd uptake on GN-Alfa

As received, nitric acid treated and GN-Alfas reduced at 500 °C were used to compare the adsorption of Pt and Pd precursors. The uptake experiments with the anionic precursors were carried out with a surface loading of 500 m^2/L, while the surface loading for cationic uptakes were carried out at 1000 m^2/L. As shown in Figure 4.13, both $[PtCl_6]^{2-}$ and $[Pt(NH_3)_4]^{2+}$ follow the expected adsorption trends predicted by the revised physical adsorption (RPA) model.[6] Namely, as the PZC of the GN-Alfa support increased, the adsorption of the anionic Pt precursors increased while the adsorption of the cation decreased. It has previously been speculated that oxygen groups on carbon can protonate to generate a cationic oxygen species that act as a nucleation site for anionic precursors. However, the HNO_3 treated GN-Alfa support, which contained the most oxygen functionalities, adsorbed no $[PtCl_6]^{2-}$. The lack of adsorption is consistent with the fact that most protonated oxygen functional groups attached to an aromatic ring, such as carboxylic acids or alcohols, have a negative pK_a, making them difficult to protonate.[30] On the other hand, the broad adsorption of $[Pt(NH_3)_4]^{2+}$ must be due to acidic oxygen functional groups that can deprotonate under acidic conditions. There are only two oxygen functional groups that are capable of being deprotonated and holding a negative charge, alcohols and carboxylic acid groups. Given that the pK_a values of molecules like phenol and benzoic acid are 10.02 and 4.21 respectively,[30] it is most likely that

www.manaraa.com

carboxylic acid groups mediate the adsorption of cationic precursors under acidic conditions.

In the case of Pd, the adsorption did not follow the expected trends predicted by the RPA model due in part to the instability of the Pd precursors in solution. Under basic conditions, the adsorption of $[Pd(NH_3)_4]^{2+}$ onto the various GN-Alfa supports follows the expected trends predicted by the RPA model. These same trends were also observed when the surface loading of the GN-Alfa support was kept at 500 m^2/L (Figure 4.14a). At a pH<5, there was some unexpected adsorption of Pd onto the as received and reduced GN-Alfa support due to the formation of $[PdCl_4]^{2-}$ and precipitation of an unknown Pd species. Precipitation was deduced by a decrease in Pd concentration as the pH of the $[Pd(NH_3)_4]^{2+}$ solution decreased below 5 (see Figure 4.5).

For $[PdCl_4]^{2-}$ uptake, the maximum uptake on the as received and the reduced GN-Alfa supports was narrower than that of $[PtCl_6]^{2-}$ (Figure 4.14b). Furthermore, the maximum uptake occurred at a pH = 2, the same peak maximum that was observed with the GNPs. The decrease in adsorption above a pH of 2 suggests that the addition of NH_4OH reduces the concentration of $[PdCl_4]^{2-}$ species available to absorb onto the surface.[23] This hypothesis is further supported by the adsorption trend of $[PdCl_4]^{2-}$ on the nitric acid treated GN-Alfa (low PZC) support, which increases above a pH of 2. In fact, the $[PdCl_4]^{2-}$ uptake on the nitric acid treated GN-Alfa mirrors the uptake of $[Pd(NH_3)_4]^{2+}$, consistent with the formation of the cationic Pd species. Surprisingly, the as received and reduced GN-Alfa supports adsorbed the same amount of $[PdCl_4]^{2-}$. Moreover, the calculated uptake of $[PdCl_4]^{2-}$ is 2-3 times higher than what was observed on the GNPs. These results may point to the GN-Alfa support having additional sites

www.manaraa.com

capable of accumulating charge or Pd precursors chemically react with the GN-Alfa support.

To correlate the Pd uptake to the amount of Pd deposited onto the surface of the GN-Alfa supports with varying levels of oxygen content, a separate set of uptake and XPS experiments were conducted. The GN-Alfa supports that were used received the following treatments, listed in order of increasing oxygen content: reduced at 500 °C, reduced at 500 °C followed by an HCl treatment, as received, reduced at 500 °C followed by an HNO_3 treatment, and treated in HNO_3. The O(1s)/(C1s) ratio (oxygen content) of the GN-Alfa supports was measured prior to adsorption of any Pd precursors, but after the reduction or acid treatments. $[PdCl_4]^{2-}$ adsorption was conducted at a pH of 2.1 on each GN-Alfa support, while $[Pd(NH_3)_4]^{2+}$ adsorption was conducted at a pH of 11. The results can be found in Figure 4.15.

For the $[Pd(NH_3)_4]^{2+}$, the Pd(3d)/C(1s) ratio directly correlated with the uptake data, which both increased with increasing surface oxygen content. There was more than a five fold increase in $[Pd(NH_3)_4]^{2+}$ adsorbed onto the GN-Alfa support with the most oxygen content as compared with that which has the least oxygen. Also, the adsorbed $[Pd(NH_3)_4]^{2+}$ species were found to reside in the Pd^{2+} oxidation state (Figure 4.16b). These findings are in line with the adsorption trends observed for all the $[Pd(NH_3)_4]^{2+}$ uptake experiments conducted on the GN-Alfa supports and the adsorption trend of cationic precursors on HOPG, which are all mediated by oxygen functional groups.

In the case of $[PdCl_4]^{2-}$ (Figure 4.15a), the uptake decreases with increasing oxygen content, while the Pd(3d)/C(1s) ratio first decreases and then flattens out. In both cases, the addition of oxygen groups to the surface did not lead to an increase in $[PdCl_4]^{2-}$

www.manaraa.com

adsorption. For the $[Pd(NH_3)_4]^{2+}$ (Figure 4.15b), the Pd(3d)/C(1s) ratio directly correlated with the uptake data, which both increased with increasing surface oxygen content. There was more than a five fold increase in $[Pd(NH_3)_4]^{2+}$ adsorbed onto the GN-Alfa support with the most oxygen content as compared with that which has the least oxygen. These findings are in line with the adsorption trends observed for all the $[Pd(NH_3)_4]^{2+}$ uptake experiments conducted on the GN-Alfa supports and the adsorption trend of cationic precursors on HOPG, which are all mediated by oxygen functional groups.

The discrepancy between the $[PdCl_4]^{2-}$ uptake and the XPS results maybe due to the assumption that the surface area of all the supports was 500 m^2/L, as reported by the manufacturer. BET experiments yielded a surface area of around 250 m^2/gram for the nitric acid treated GN-Alfa, half of the surface area measured for the reduced and as received GN-Alfa supports. By overestimating the surface area, the $[PdCl_4]^{2-}$ uptake for the nitric acid treated GN-Alfa support was underestimated. In addition, a closer examination of the XPS results (Figure 4.16a) reveal that that $[PdCl_4]^{2-}$ was partially reduced to Pd^0, a phenomena that has been noted by others as well.[13, 35] The adsorbed $[Pd(NH_3)_4]^{2+}$ species were found to reside in the Pd^{2+} oxidation state (Figure 4.16b) and were not reduced to Pd^0. The mechanism by which the reduction of $[PdCl_4]^{2-}$ occurs is still unknown. No such reduction was observed on HOPG or the GNPs, and therefore the reduction appears to be unique to the GN-Alfa support.

4.4 Conclusions

SEA adsorption of Pt and Pd cationic precursors is mediated by oxygen functional groups on the graphitic supports. On HOPG, increasing the concentration of hydroxyl groups increased the adsorption of both cationic precursors. For the GNPs, hydroxylating

www.manaraa.com

the surface increased the amount of $[Pt(NH_3)_4]^{2+}$ that adsorbed to the surface, but there was almost no adsorption of $[Pd(NH_3)_4]^{2+}$. The lack of $[Pd(NH_3)_4]^{2+}$ adsorption on the surface was attributed to the support not having sufficient oxygen functional groups on the surface. Lastly, for the GN-Alfa supports, functionalizing the surface with hydroxyl and carboxylic acid groups increased the adsorption of both cation precursors. In the case of $[Pd(NH_3)_4]^{2+}$, there was a direct correlation between the amount of Pd adsorbed and the surface oxygen content of the GN-Alfa, demonstrating that these oxygen functionalities act as nucleation sites for the cationic precursor.

The anionic adsorption of Pt on HOPG and the GNPs is not purely electrostatic and includes a chemical component as well. Significantly less $[PdCl_4]^{2-}$ adsorbed onto the surface of HOPG and the GNPs as compared to $[PtCl_6]^{2-}$. Furthermore, XPS showed that Pt^{4+} in $[PtCl_6]^{2-}$ was partially reduced to the 2+ oxidation state while Pd^{2+} in $[PdCl_4]^{2-}$ was not reduced, indicating that adsorption of $[PtCl_6]^{2-}$ is in part due to a chemical interaction with the graphitic support. Uptake experiments conducted on HOPG, GNPs, and the GN-Alfa supports all indicate that the adsorption of $[PtCl_6]^{2-}$ is at least partly electrostatic, since its adsorption depends on the pH of the solution and the oxygen content of the support. 2-3 times more $[PdCl_4]^{2-}$ was adsorbed onto the GN-Alfa support as compared to the GNPs, but the reason for this discrepancy is still not understood. Additionally, $[PdCl_4]^{2-}$ was shown to reduce to the metallic state on the GN-Alfa support, but the mechanism by which this occurs remains unknown.

www.manaraa.com

Acknowledgments

I would like to thank Dr. Ritu Banerjee, Dr. Huynh Ngoc Tien and Greg King for helping with some of the Pt and Pd uptake experiments that appear in this work. I would also like to thank Dr. Stavros Karakalos and Amy Brandt for conducting the XPS experiments.

www.manaraa.com

Table 4.1: PZC and O(1s)/C(1s) ratios of GN-Alfa supports that underwent a different acid and reduction treatments.

Treatment	PZC	O/C Ratio
HNO_3	1.2	0.0718
500 °C 2 hrs 20% hydrogen + HNO_3	2.1	0.0525
HCl	2.8	0.0371
As Received	4.0	0.0328
350 °C 2 hrs 20% hydrogen	4.5	0.0225
500 °C 2 hrs 20% hydrogen + HCl	6.4	0.0099
425 °C 2 hrs 20% hydrogen	7.3	0.0171
500 °C 2 hrs 20% hydrogen	10.5	0.0049

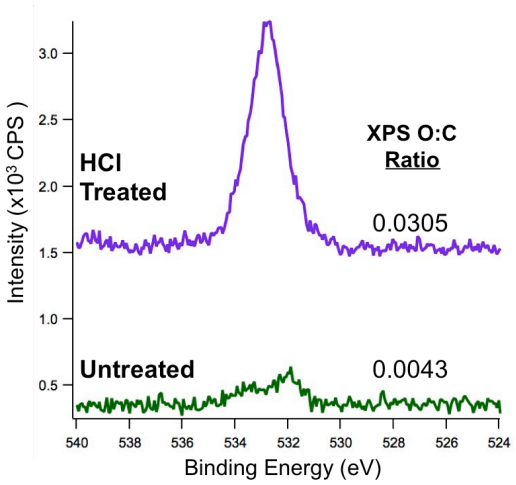

Figure 4.1: O(1s) region of untreated and HCl treated HOPG and their respective O(1s)/C(1s) ratios.

www.manaraa.com

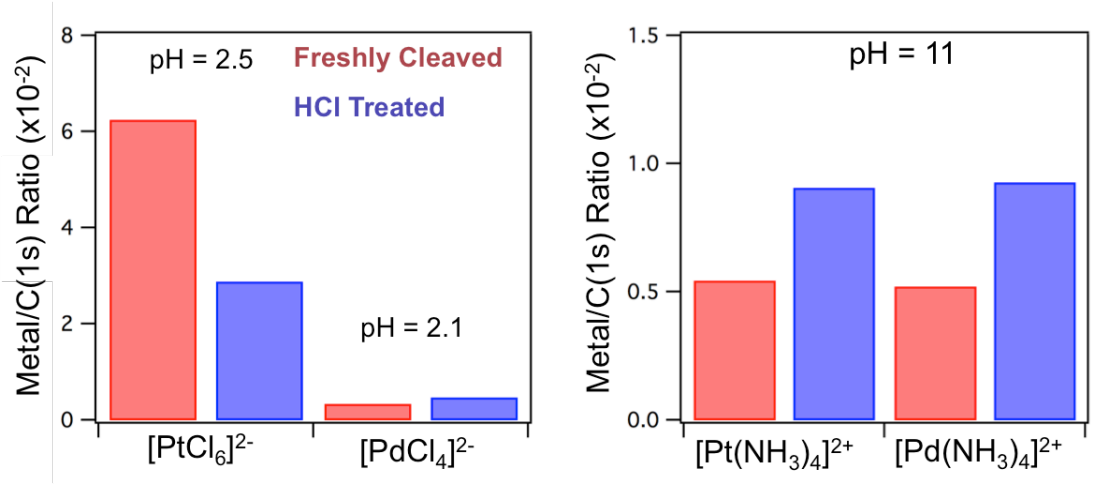

Figure 4.2: Comparison of Metal/C(1s) ratios of anionic (left) and cationic (right) Pt and Pd precursors. Anionic uptake experiments were conducted between a pH of 2-2.5 while the cationic uptake experiments were all conducted at a pH of 11.

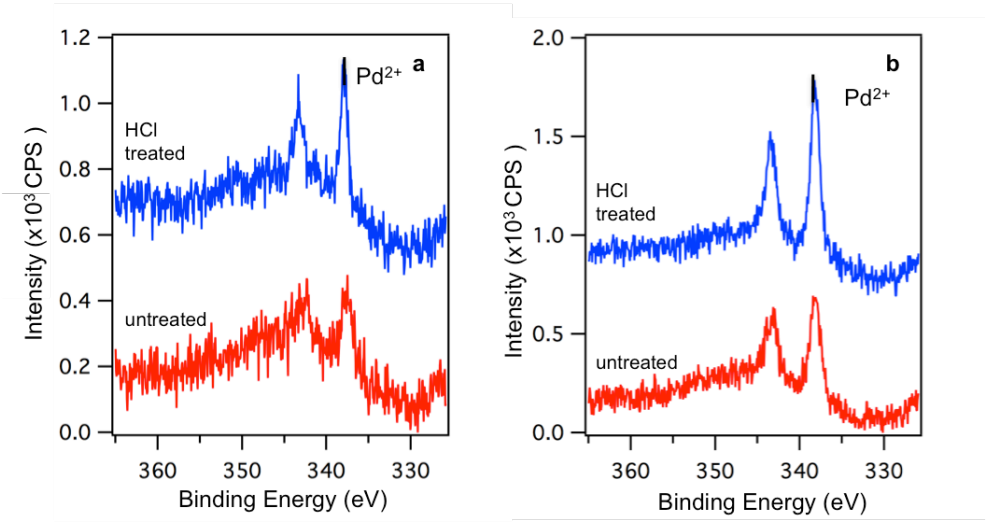

Figure 4.3: XPS of the Pd(3d) region for a) $[PdCl_4]^{2-}$ adsorbed onto untreated and HCl treated HOPG at a pH of 2.1 and b) $[Pd(NH_3)_4]^{2+}$ adsorbed onto HCl treated and untreated HOPG at a pH of 11.

www.manaraa.com

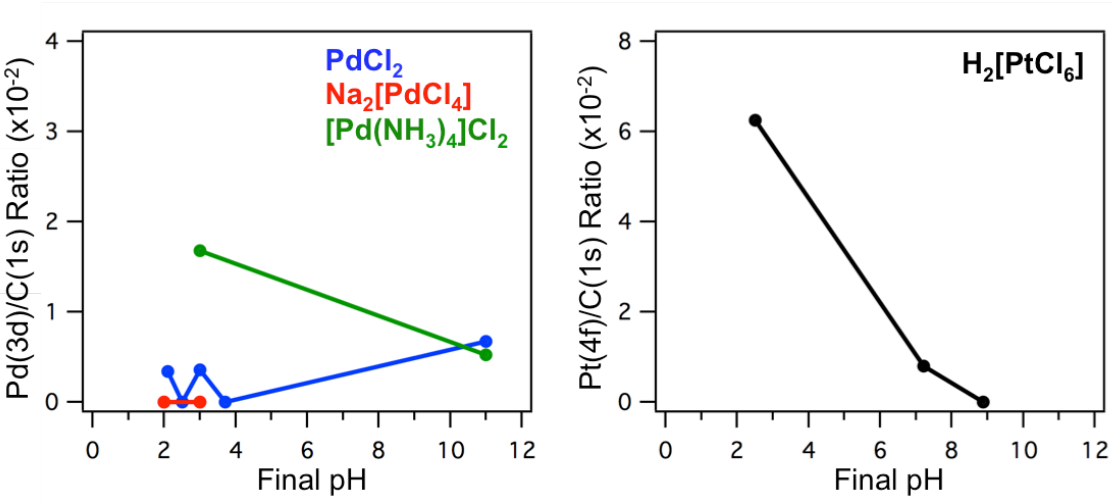

Figure 4.4: Comparison of Pd(3d)/C(1s) ratios of anionic and cationic Pt (right) and Pd (left) precursors on HOPG as a function of pH.

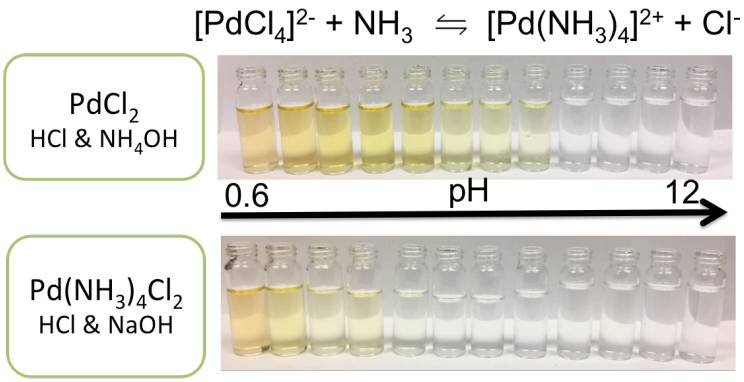

Figure 4.5: 200 ppm $PdCl_2$ and 200 ppm $[Pd(NH_3)]Cl_2$ solutions as a function of pH. As NH_4OH is added to the $PdCl_2$ solution, the color the changes from yellow to clear, indicating the formation of the $[Pd(NH_3)_4]^{2+}$ species. As HCl is added to the $[Pd(NH_3)]Cl_2$ solution, the solution changes from clear to yellow, indicating the formation of the $[PdCl_4]^{2-}$ species.

www.manaraa.com

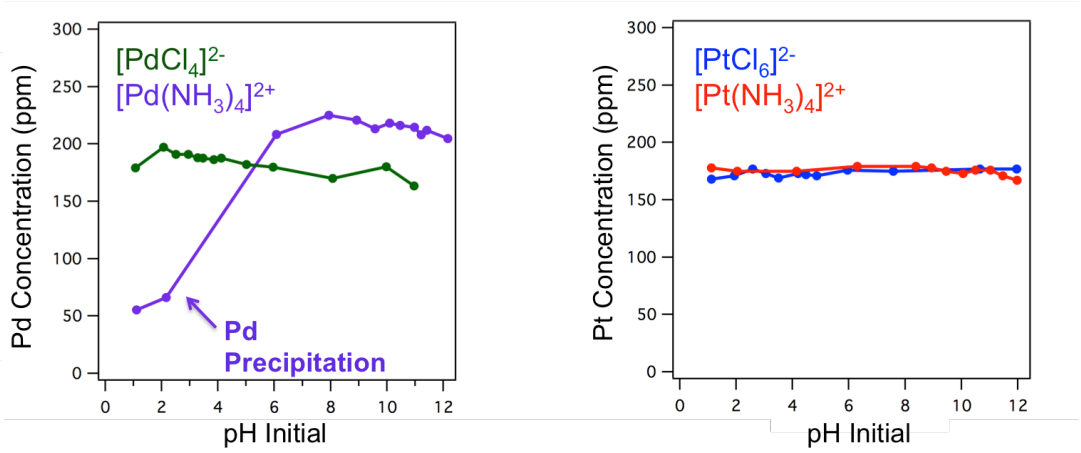

Figure 4.6: Stability of the Pd (right) and Pt (left) precursor concentration as a function of pH.

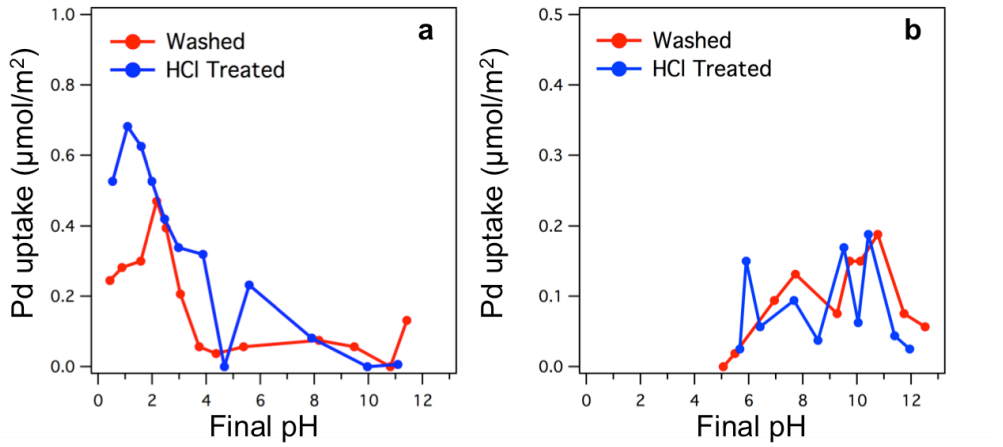

Figure 4.7: Uptake of Pd precursors onto the washed and HCl treated GNP supports using the a) $[PdCl_4]^{2-}$ and b) $[Pd(NH_3)_4]^{2+}$ precursors.

www.manaraa.com

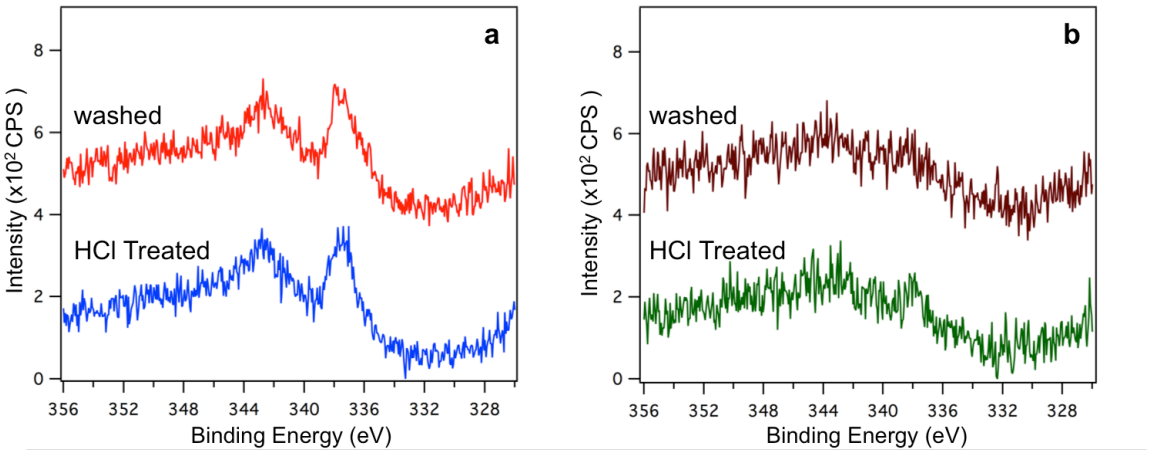

Figure 4.8: XPS of the Pd(3d) region for a) $[PdCl_4]^{2-}$ adsorbed onto the washed and HCl treated GNPs at a pH of 2 and b) $[Pd(NH_3)_4]^{2+}$ adsorbed at a pH of 11.

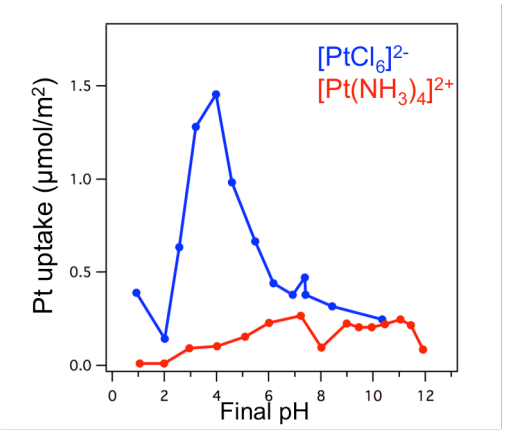

Figure 4.9: SEA uptake of 200 ppm $[PtCl_6]^{2-}$ ($H_2[PtCl_6]$) and 300 ppm $[Pt(NH_3)_4]^{2+}$ ($[Pt(NH_3)_4](OH)_2$) onto GNPs.

www.manaraa.com

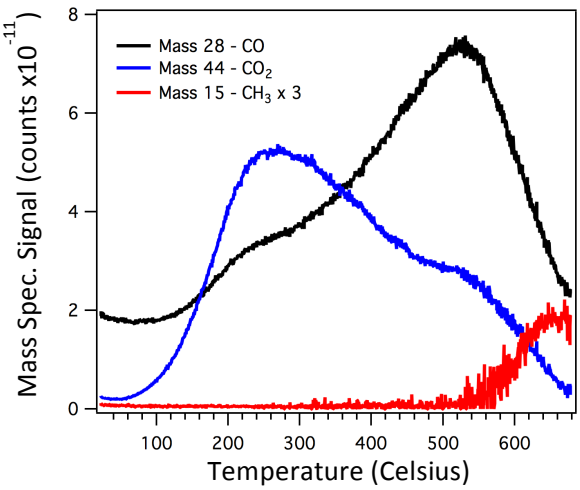

Figure 4.10: Temperature programmed reduction experiment of GN-Alfa support. The sample was heated at 5 °C/min in 10% H_2 balance Argon.

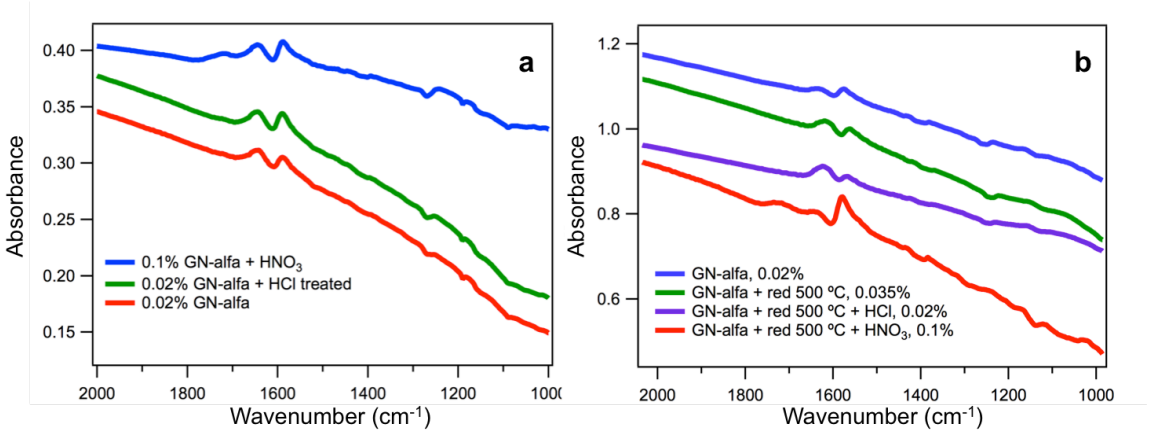

Figure 4.11: IR spectra of GN-Alfa support that underwent different acid and reduction treatments: a) treated with HNO_3, treated with HCl, as received and b) as received, reduced at 500 °C, reduced at 500 °C followed by an HCl treatment, reduced at 500 °C followed by an HNO_3 treatment.

www.manaraa.com

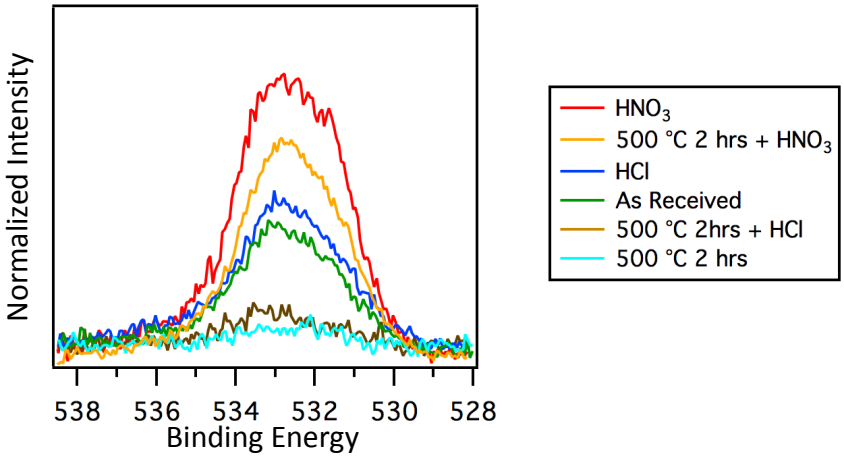

Figure 4.12: O(1s) region of GN-Alfa supports subjected to various reduction and acid treatments (see legend). All O(1s) spectra are normalized with respect to the C(1s) signal of each sample. All reduction treatments were done in 20% H_2 balance He.

www.manaraa.com

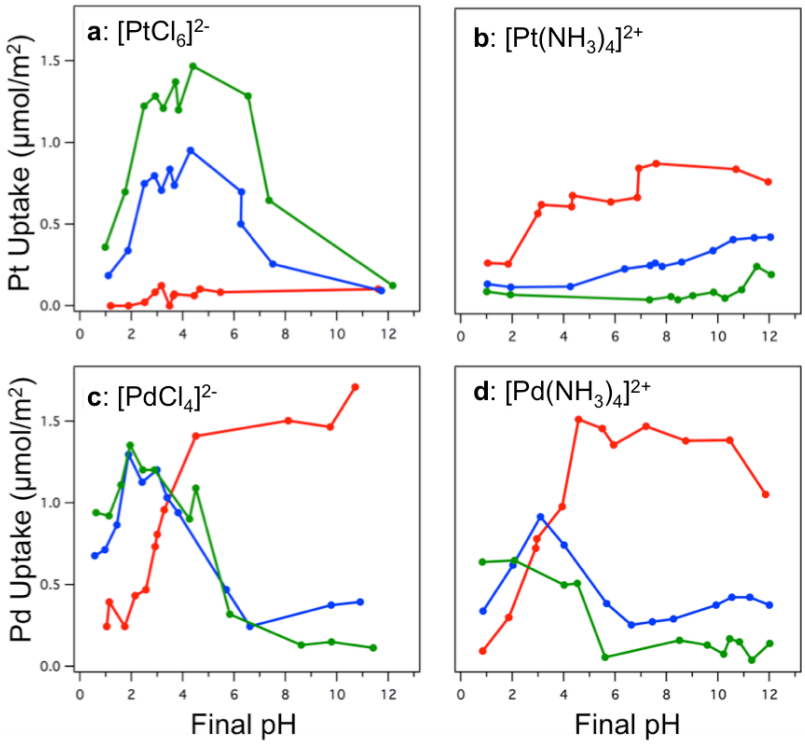

Figure 4.13: Uptake of a) $[PtCl_6]^{2-}$, b) $[Pt(NH_3)_4]^{2+}$, c) $[PdCl_4]^{2-}$ and d) $[Pd(NH_3)_4]^{2+}$ precursors on GN-Alfa supports of various PZCs. The green, blue and red traces corresponds to GN-Alfas prepared with a PZC = 10.5 (reduced 500 °C 2 hrs), 4.0 (as received), and 1.2 respectively (nitric acid treated). The uptakes of a) and c) were carried out at a surface loading of 500 m^2/gram while b) and d) were carried at a surface loading of 1000 m^2/gram.

www.manaraa.com

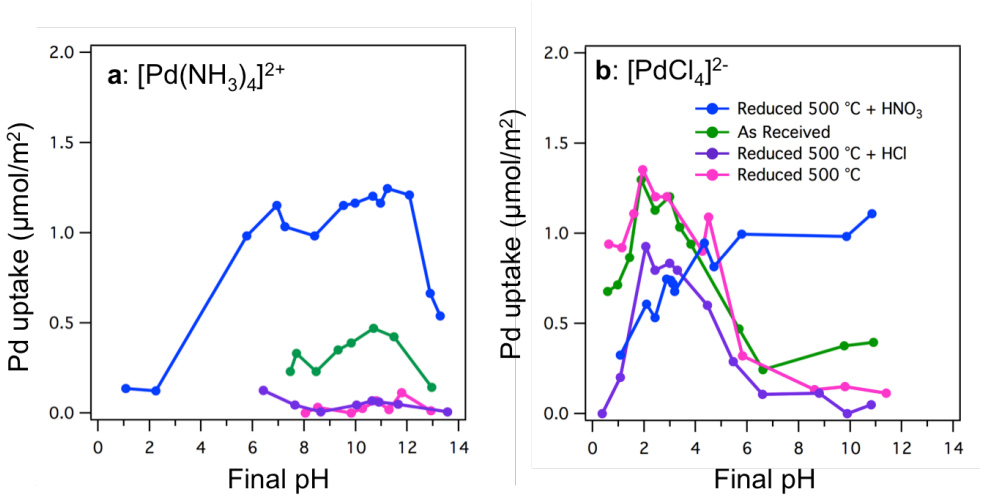

Figure 4.14: Uptake plots of a) $[Pd(NH_3)_4]^{2+}$ and b) $[PdCl_4]^{2-}$ adsorbed onto GN-Alfa supports exposed to a variety of acid and reduction treatments at a surface loading of 500 m^2/gram.

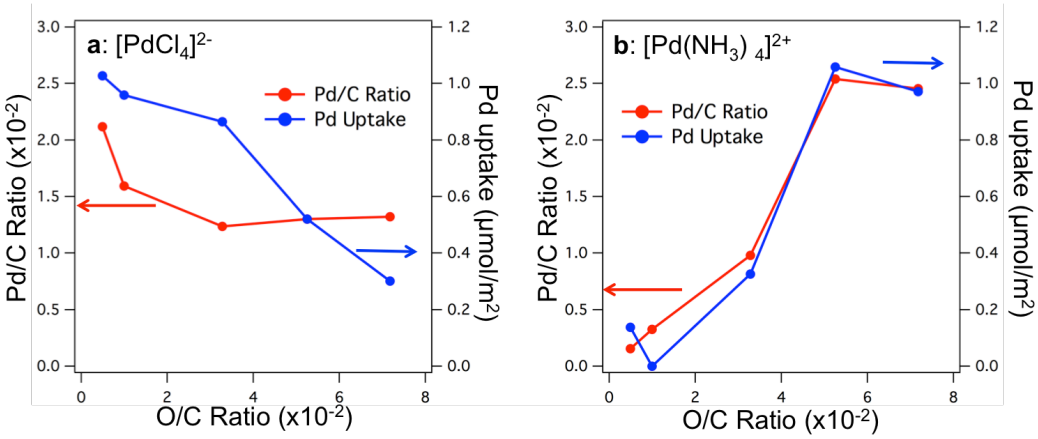

Figure 4.15: The top graphs depict the adsorption of $[PdCl_4]^{2-}$ (left) and $[Pd(NH_3)_4]^{2+}$ (right) on a series of GN-Alfa supports with varying levels of surface oxygen content, as expressed using the O(1s)/C(1s) ratio prior to uptake of Pd precursors. Uptake experiments were conducted at a pH of ~2.1 and 11 respectively.

www.manaraa.com

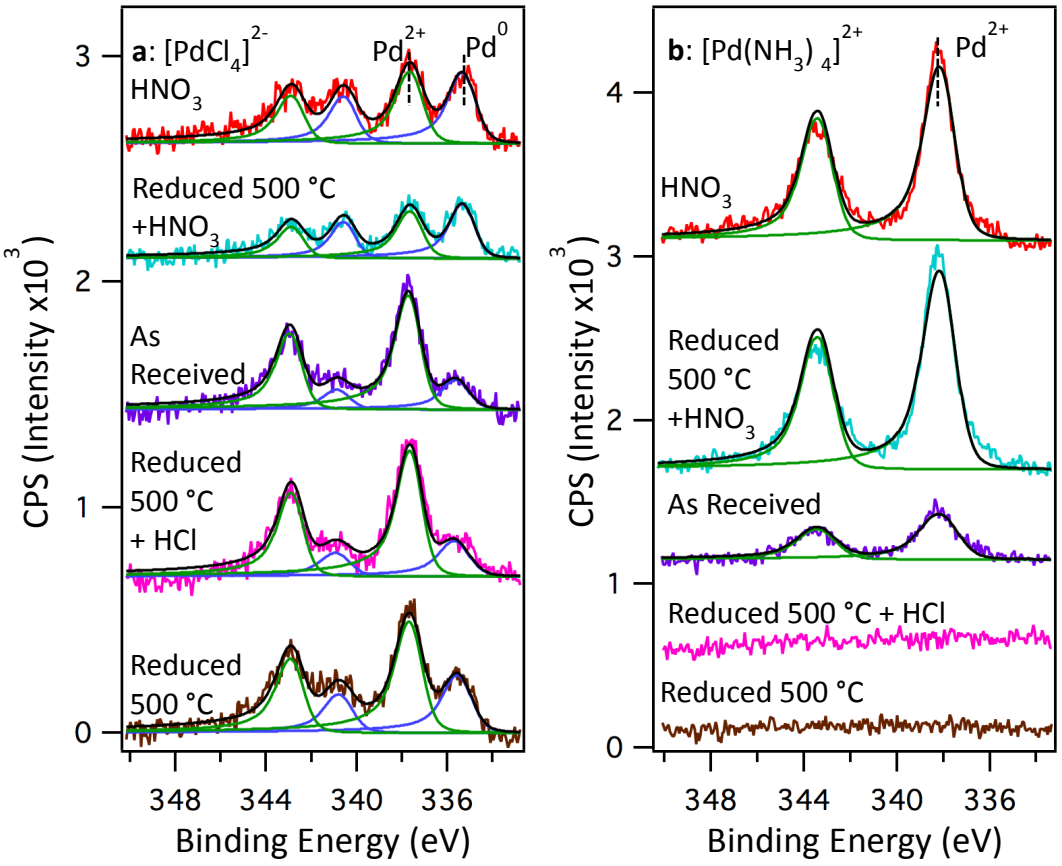

Figure 4.16: XPS of the Pd(3d) region for a) $[PdCl_4]^{2-}$ and b) $[Pd(NH_3)_4]^{2+}$ on a series of GN-Alfa supports with varying levels of surface oxygen content. Uptake experiments were conducted at a pH of ~2.1 and 11 respectively.

4.5 References

1. Crampton, A. S.; Rotzer, M. D.; Ridge, C. J.; Schweinberger, F. F.; Heiz, U.; Yoon, B.; Landman, U., Structure sensitivity in the nonscalable regime explored via catalysed ethylene hydrogenation on supported platinum nanoclusters. *Nature communications* **2016,** *7*, 10389.

2. Agashe, K. B.; Regalbuto, J. R., Revised physical adsorption model. *Journal of colloid and interface science* **1997,** *185*, 174-189.

www.manaraa.com

3. Hao, X.; Spieker, W. A.; Regalbuto, J. R., A further simplification of the revised physical adsorption (RPA) model. *Journal of colloid and interface science* **2003,** *267* (2), 259-264.

4. Park, J.; Regalbuto, J. R., A Simple, Accurate Determination of Oxide PZC and the Strong Buffering Effect of Oxide Surfaces at Incipient Wetness. *Journal of colloid and interface science* **1995,** *175*, 239-252.

5. Healy, T. W.; White, L. R., Ionizable surface group models of aqueous interfaces. *Advances in Colloid and Interface Science* **1978,** *9*, 303-345.

6. Dreyer, D. R.; Park, S.; Bielawski, C. W.; Ruoff, R. S., The chemistry of graphene oxide. *Chemical Society reviews* **2010,** *39* (1), 228-40.

7. Seuser, G. S.; Banerjee, R.; Metavarayuth, K.; Brandt, A. J.; Maddumapatabandi, T. D.; Karakalos, S.; Lin, Y.; Regalbuto, J. R.; Chen, D. A., Understanding Uptake of Pt Precursors During Strong Electrostatic Adsorption on Single-Crystal Carbon Surfaces. *Topics in Catalysis* **2018,** *61* (5-6), 379-388.

8. Hao, X.; Barnes, S.; Regalbuto, J. R., A fundamental study of Pt impregnation of carbon: Adsorption equilibrium and particle synthesis. *Journal of Catalysis* **2011,** *279*, 48-65.

9. Jia, R. L.; Wang, C. Y.; Wang, S. M., Preparation of carbon supported platinum catalysts: role of π sites on carbon support surface. *Journal of Materials Science* **2006,** *41* (20), 6881-6888.

10. Rodriguez-Reinoso, F., The role of carbon materials in heterogeneous catalysis. *Carbon* **1998,** *36* (3), 159-175.

www.manaraa.com

11. Montes-Morán, M. A.; Menéndez, J. A.; Fuente, E.; Suárez, D., Contribution of the Basal Planes to Carbon Basicity: An Ab Initio Study of the H3O+ - π Interaction in Cluster Models. *Journal of Physical Chemistry B* **1998,** *102*, 5595-5601.

12. Montes-Morán, M. A.; Suárez, D.; Menéndez, J. A.; Fuente, E., On the nature of basic sites on carbon surfaces: an overview. *Carbon* **2004,** *42* (7), 1219-1225.

13. Gilliland, S. E.; Tengco, J. M. M.; Yang, Y.; Regalbuto, J. R.; Castano, C. E.; Gupton, B. F., Electrostatic adsorption-microwave synthesis of palladium nanoparticles on graphene for improved cross-coupling activity. *Applied Catalysis A: General* **2018,** *550*, 168-175.

14. Lambert, S.; Job, N.; Dsouza, L.; Pereira, M.; Pirard, R.; Heinrichs, B.; Figueiredo, J.; Pirard, J.; Regalbuto, J., Synthesis of very highly dispersed platinum catalysts supported on carbon xerogels by the strong electrostatic adsorption method. *Journal of Catalysis* **2009,** *261* (1), 23-33.

15. Contescu, A.; Contescu, C.; Putyera, K.; Schwarz, J. A., Surface acidity of carbons characterized by their continuous pK distribution and Boehm titration. *Carbon* **1996,** *35* (1), 83-94.

16. Kim, Y. S.; Park, C. R., One-pot titration methodology for the characterization of surface acidic groups on functionalized carbon nanotubes. *Carbon* **2016,** *96*, 729-741.

17. Dimiev, A. M.; Alemany, L. B.; Tour, J. M., Graphene Oxide. Origin of Acidity, Its Instability in Water, and a New Dynamic Structural Model. *ACS Nano* **2013,** *7* (1), 576-588.

www.manaraa.com

18. Konkena, B.; Vasudevan, S., Understanding Aqueous Dispersibility of Graphene Oxide and Reduced Graphene Oxide through pKa Measurements. *The journal of physical chemistry letters* **2012,** *3* (7), 867-72.

19. Li, H.; Fu, A.; Xue, X.; Guo, F.; Huai, W.; Chu, T.; Wang, Z., Density functional theory prediction of pKa for carboxylated single-wall carbon nanotubes and graphene. *Chemical Physics* **2017,** *490*, 47-54.

20. Zaera, F., The Surface Chemistry of Metal-Based Hydrogenation Catalysis. *ACS Catalysis* **2017,** *7* (8), 4947-4967.

21. Xiao, J., Puddephatt, R. J., Pt-Re Clusters and Bimetallic Catalysts. *Coordination Chemistry Reviews* **1995,** *143*, 457-500.

22. Kašpar, J.; Fornasiero, P.; Hickey, N., Automotive catalytic converters: current status and some perspectives. *Catalysis Today* **2003,** *77* (4), 419-449.

23. Contescu, C.; Vass, M. I., The effect of pH on the adsorption of palladium (II) complexes on alumina. *Applied Catalysis* **1987,** *33*, 259-271.

24. Banerjee, R. The Oxidation And Decoration Chemistry Of Platinum And Palladium on Carbon Supports. University of South Carolina, 2016.

25. Kratzer, E. The Synthesis of Carbon Supported Palladium Catalysts by Strong Electrostatic Adsorption. University of Illinois at Chicago, 2006.

26. Cho, H.-R.; Regalbuto, J. R., The rational synthesis of Pt-Pd bimetallic catalysts by electrostatic adsorption. *Catalysis Today* **2015,** *246*, 143-153.

27. Tengco, J. M. M.; Lugo-José, Y. K.; Monnier, J. R.; Regalbuto, J. R., Chemisorption–XRD particle size discrepancy of carbon supported palladium: Carbon decoration of Pd? *Catalysis Today* **2015,** *246*, 9-14.

www.manaraa.com

28. Wagner, C. D.; Riggs, W. M.; Davis, L. E.; Moulder, J. F., *Handbook of X-ray Photoelectron Spectroscopy*. Perkin-Elmer Corporation: 1979.

29. Buono, C.; Davies, P. R.; Davies, R. J.; Jones, T.; Kulhavy, J.; Lewis, R.; Morgan, D. J.; Robinson, N.; Willock, D. J., Spectroscopic and atomic force studies of the functionalisation of carbon surfaces: new insights into the role of the surface topography and specific chemical states. *Faraday discussions* **2014,** *173*, 257-72.

30. Anslyn, E. V.; Dougherty, D. A., *Modern Physical Organic Chemistry*. University Science Books: 2006.

31. Dam, H. E. v.; Bekkum, H. v., Preparation of Platinum on Activated Carbon. *Journal of Catalysis* **1991,** *131*, 335-349.

32. Spieker, W. A.; Liu, J.; Miller, J. T.; Kropf, A. J.; Regalbuto, J. R., An EXAFS study of the co-ordination chemistry of hydrogen hexachloroplatinate(IV) 1. Speciation in aqueous solution. *Applied Catalysis A: General* **2002,** *232*, 219-235.

33. Schreier, M.; Regalbuto, J. R., A fundamental study of Pt tetraammine impregnation of silica: 1. The electrostatic nature of platinum adsorption. *Journal of Catalysis* **2004,** *225* (1), 190-202.

34. C. Moreno-Castilla, M. A. F.-G., J. P. Joly, I. Bautista-Toledo, F. Carrasco-Marin, and J. Rivera-Utrilla, Activated Carbon Surface Modifications by Nitric Acid, Hydrogen Peroxide, and Ammonium Peroxydisulfate Treatments. *Langmuir* **1995,** *1995*, 4386-4392.

35. Chen, X.; Wu, G.; Chen, J.; Chen, X.; Xie, Z.; Wang, X., Synthesis of "clean" and well-dispersive Pd nanoparticles with excellent electrocatalytic property on graphene oxide. *Journal of the American Chemical Society* **2011,** *133* (11), 3693-5.

www.manaraa.com

CHAPTER 5

NUCLEATION OF RE CLUSTERS ON HOPG: DISTIGUISHING BETWEEN CLUSTER SIZE EFFECTS AND OXYGEN COORDINATION

www.manaraa.com

5.1 Introduction

The addition of Re to Pt based catalysts enhances the activity and stability of catalysts for a variety of chemical reactions. Significant attention has been given to PtRe/Alumina catalysts due to its use by the oil industry in naphtha reforming.[1] More recently, PtRe/Carbon catalysts have been shown to be quite active in aqueous phase reforming (APR) of polyols[2-6], while PtRe/titania catalysts are superior to Pt based catalysts for low temperature water gas shift (WGS) reaction.[7, 8] A variety of explanations have been proposed for the enhanced activity of PtRe catalysts: weakened interaction between carbonaceous species and Pt due to changes in its electronic structure,[4] ReO_x species participating in WGS reaction,[7-9] and reduced sintering.[4] However, confirming these explanations through experiment has been hindered by difficulties in controlling the chemical composition of these complex, high surface area materials used in industrial applications.

To better understand the origin of the superiority of PtRe catalysts compared to their monometallic counterparts, the WGS reaction was studied using well characterized PtRe systems prepared on a TiO_2(110) single crystal surface.[10] Doing so required that the nucleation monometallic Re and Pt clusters on TiO_2(110) to be studied systematically. These studies suggested that Re interacts strongly with the titania support, as demonstrated by low diffusion length and reduction of titania.[11] The former is consistent with decreased diffusion length with increased affinity towards oxygen,[12] while the later suggests that Re strongly interacts with surface oxygen on titania, possibly becoming oxidized. Re has a relatively low heat of formation for Re oxide and lies on the border of transition metals that are oxidized when deposited onto titania at room temperature,

www.manaraa.com

which includes Re, Ru, and Co.[13] Ru does not oxidize on titania,[13] while Co is slightly oxidized, as evidence by the reduction of titania after Co deposition.[12, 13] Therefore, it is not obvious that Re should in fact become oxidized when deposited onto titania.

In principle, one should be able to identify the oxidation state of Re by examining binding energy position of the Re($4f_{7/2}$) peak; however the interpretation of XPS results for Re deposited on titania is not trivial. Figure 2.1 depicts XPS of the Re(4f) region at different coverages and the corresponding binding energies for the Re ($4f_{7/2}$) peak. At a coverage of 0.11 monolayer (ML), the Re($4f_{7/2}$) binding energy position shifted to 41.3 eV, +1.0eV from metallic Re, 40.3 eV, [14, 15]. The binding energy of Re decreases with increasing coverage, ultimately converging to the binding energy of metallic Re at 3.44 ML. One interpretation of this data is that at low coverages, most Re atoms are in direct contact with the titania interface, resulting in Re coordinating with surface oxygen and possibly becoming oxidized; at higher coverages, less Re is in direct contact with the titania surface, causing the binding energy of Re to shift to its metallic state. However, an alternative explanation is that the binding energy shift at low Re coverages is in fact a cluster size effect[16-18] that occur due to small clusters on the surface, which were found to be one atomic layer high on the 0.11 ML Re TiO_2(110) surface.[11] Small metal clusters are less effective at screening holes generated by ejected electrons, increasing the apparent binding energy of atoms in the cluster by lowering the energy of the final state. A positive shift in binding energy at low coverages has been reported for other metals deposited on titania, such as gold,[19] silver,[20] and platinum.[11] In these cases, the shift was attributed to a cluster size effect because none of these metals are expected to oxidize on titania.

www.manaraa.com

To distinguish between a cluster size effect and Re oxidation on titania, Re clusters of various sizes were grown on HOPG. HOPG was chosen because it is known for its weak interaction with metals [21-24] and lack of oxygen functionalities.[25] Furthermore, defects can be systematically introduced to the surface through sputtering, enabling the cluster size of Re to be controlled as a function of defect sites[26-32] while the coverage is kept constant. A positive binding energy shift was indeed observed as a function of Re particle size. However, there was also a binding energy shift that occurred when Re was deposited onto an HOPG sample that did not have all of the oxygen removed from the surface. Therefore, the binding energy shifts of Re deposited onto titania at low coverages cannot be fully attributed to a cluster size effect, and must also be due to a strong chemical interaction between titania and Re.

5.2 Experimental

All experiments were conducted in an ultrahigh vacuum (UHV) chamber that has previously been described.[33] The base pressure of the chamber is less than $1x10^{-10}$ torr and contains a variable–temperature STM (Omicron VT-25) and a hemispherical analyzer (Omicron EA125) for X-ray photoelectron spectroscopy and low energy ion scattering experiments. It also contains a sputter gun used for cleaning and sputtering surfaces with Argon ions (Omicron ISE 10).

HOPG was purchased from SPI, having the dimensions of 10 mm x 10 mm x 1 mm. The sample was mounted onto an Omicron tantalum sample plate using tantalum foil straps and heated via electron bombardment using a tungsten filament located behind the sample. Before each experiment, a clean HOPG surface was prepared by exfoliating

www.manaraa.com

the surface with tape. To generate defect sites in the surface of the HOPG, the surface was sputtered with Ar^+ at 500 eV using a current of 0.1 μA and an argon pressure of $3x10^{-7}$ torr for 30 seconds to 20 minutes. The surface was then annealed to 950 K for 12 minutes to remove surface oxygen species and Ar imbedded in the surface. Unless otherwise stated, the 950 K heat treatment was applied to every HOPG surface prior to Re deposition. In one cases, HOPG was annealed to 400 K for 3 minutes to remove residual contaminants, perhaps water, that may remain on the surface prior to Re deposition. This surface will be referred to as HOPG-O.

Re was deposited onto the surface from a Re rod (ESPI, 2 mm diameter, 99.99%) using a commercial Oxford Applied Research (EGC04) electron beam evaporator. The metal flux was monitored using a quartz crystal microbalance (QCM, Inficon XTM-2). One monolayer of Re is defined as the packing density of Re(0001), 1.52×10^{15} atoms/cm^2. Re was deposited at a rate of 0.05 ML/min. STM experiments were conducting in constant current mode using a voltage of 2.3 V and a current of 0.1 nA. XPS experiments were conducted using an Al Kα source with a dwell time of 0.2 s and a step size of 0.02 eV. Cluster heights were measured using an in-house program on an image area of 100 nm x 100 nm for the surfaces that were sputtered for less than 5 minutes, and 50 nm x 50 nm for surfaces sputtered for 5 minutes or longer. Reported cluster densities were all counted by hand. Cluster diameters were not measured since accurate values cannot be achieved due to tip convolusion effects.[16]

To locate the Re($4f_{7/2}$) peak maxima, residual Re deposited onto the tantalum straps had to be taken into consideration. To account for the residual Re signal, all Re(4f) data was processed by subtracting Re signal before deposition from the Re signal after

www.manaraa.com

deposition. The subtracted Re(4f) spectra was then used to determine the location of the Re($4f_{7/2}$) peak maxima.

5.3 Results and Discussion

Re nucleation occurred on both with basal plane and step edges of HOPG with a relatively broad size distribution, indicating that Re is highly mobile on the surface. Re nucleation on the HOPG support can be found in Figure 5.2a for 0.25 ML and 5.3a for 0.125 ML Re. For 0.25 ML Re on HOPG, the cluster size distribution was broad, with an average height of 10.7±3.8 Å and a cluster density of 1.33 $x10^{12}$ cm^{-2}. Decreasing the Re coverage to 0.125 ML slightly decreased the average cluster height (9.8±3.8 Å) and cluster density (0.96 $x10^{12}$ cm^{-2}), but the cluster size distribution was essentially the same. The broad cluster size distribution is expected for metals with high surface mobility, and is consistent with the weak interaction that transition metals have with HOPG.[34] As an example, investigations of the monometallic growth of Pt and Ru on HOPG showed that these metals are highly mobile.[26] However, the cluster density of Pt and Ru were an order of magnitude lower than that of Re for similar coverages, suggesting that Re has a stronger interaction with HOPG than Pt or Ru. These observations are consistent with DFT results examining the mobility of transition metal atoms on graphene.[35, 36]

Sputtering the surface of HOPG resulted in a decrease in average cluster size, an increase in the cluster density by up to an order of magnitude, and a narrowing of the cluster height distribution. STM images of 0.22-0.25 ML Re clusters on HOPG after sputtering for variable periods of time can be found in Figure 5.2a-d, images of the 0.11-

www.manaraa.com

0.125 ML coverages can be found in Figure 5.3a-d, and the overall cluster density and cluster height trends are displayed in Figure 5.4. Sputtering for 30 seconds results in only a slight increase in cluster density and decrease in cluster size relative to the unsputtered surface, but overall the cluster height distribution remained the same. Sputtering for 5-10 minutes decreased the average cluster height to the smallest values of 4.6±1.4 Å, increased the cluster density by an order of magnitude, and produced clusters with a narrow height distribution. The same trend in particle height, height distribution, and cluster density were observed when 0.11-0.125 ML Re was deposited onto HOPG. For the 0.11-0.125 ML Re surfaces, it was found that the smallest Re clusters (4.6 ±1.4 Å) were grown after sputtering the surface for 10 minutes, while sputtering for 20 minutes did not decrease the average particle height. Therefore, unlike TiO_2(110), it was not possible to grow approximately single layer high Re clusters, (2.23 Å),[37] on HOPG.[11, 38]

Lastly, Re was deposited onto an HOPG surface that contained oxygen functionalities on its surface, HOPG-O, opening up the possibility for Re to interact with oxygen functionalities on the surface. Oxygen functionalities were retained on the surface by annealing HOPG to 400 K for 3 minutes prior to Re deposition. As demonstrated in the XPS spectra of O(1s) in Figure 5.5a, the HOPG-O surface has more than double the amount of oxygen on the surface than does HOPG annealed to 950 K. However, the native oxide on the Ta straps used to mount the HOPG crystal may also be contributing to the oxygen signal. Separate experiments in which an X-ray source with a focused beam was used to examine HOPG, the oxygen to carbon ratio that was an order of magnitude lower than reported here.[39] Regardless, more oxygen functionalities are present on the HOPG-O surface compared to the surface annealed to 950 K. The average cluster height

www.manaraa.com

and distribution of Re on HOPG-O was 10.0±4.5 Å, similar to the oxygen free HOPG surface with the same coverage, and there was also a slight increase in cluster density up to $2.34x10^{12}$ cm^{-2}. These results indicate that the presence of oxygen functionalities did not affect the mobility of Re. However, separate experiments conducted in our laboratory suggested that the mobility of both Pt and Pd were decreased when deposited onto an HOPG surface that was hydroxylated with an HCl acid treatment. Therefore, it appears that the HOPG-O surface did not contain enough hydroxyl groups/oxygen functionalities to have a significant impact on the mobility of Re.

When 0.11-0.25 ML of Re clusters were grown on an HOPG surface sputtered for 5 minutes or longer, the average Re cluster size decreased while the Re($4f_{7/2}$) peak binding energy shifted by 0.2-0.3 eV with respect to the unsputtered surface. The Re($4f_{7/2}$) binding energy position as a function of sputter time and cluster size can be found in Figure 5.6 and 5.7 respectively; a full summary of all the Re/HOPG and Re/TiO_2(110) surfaces is located in Table 5.1. The binding energy shift maybe indicative of a strong interaction between Re and HOPG, but this possibility was ruled out because oxygen free HOPG tends to interact weakly with transition metals in general.[21-24] Thus, the positive binding energy shift that occurs with decreasing Re cluster size on HOPG was attributed to a cluster size effect.[16-18] Interestingly, the one exception to the shift in binding energy as a function of cluster size occurred when Re was deposited onto HOPG-O. In this case, the binding energy increased by 0.4 eV with respect to the 0.25 ML Re on oxygen free HOPG even though the average Re cluster size for the oxygen free and HOPG-O surfaces were similar. Therefore the binding energy shift for Re/HOPG-O

www.manaraa.com

cannot be attributed to a cluster size effect, and must instead be due to Re interacting strongly with oxygen functionalities on the surface of HOPG.

A similar trend in binding energy shift as a function of cluster size was observed for Re clusters on TiO_2(110) as well. However, the binding energy shift for Re/TiO_2(110) occurs at a much steeper rate than it did for Re/HOPG (see Figure 5.7), thus the binding energy shift that occurs on Re/ TiO_2(110) cannot be explained by a cluster size effect alone. An alternative explanation is that the shift is due, in part, to a strong chemical interaction between Re and TiO_2(110). The XPS experiment conducted on the Re/HOPG-O surface demonstrated that Re strongly interacts with oxygen functional groups. Therefore, it is expected that Re should interact strongly with surface oxygen on TiO_2(110) as well. The binding energy shift that occurs on TiO_2(110) is due to a combination of a cluster size effect and strong chemical interaction between Re and TiO_2(110). These conclusions are consistent with Re being an oxophilic metal that interacts strongly with the titania surface.[11, 12]

5.4 Conclusions

Introducing defect sites onto the surface of HOPG with Argon sputtering enabled the size of Re clusters to be systematically controlled. Re clusters grown on the unsputtered HOPG had a broad cluster height distribution, but the cluster size distribution narrowed and decreased in height when Re was deposited onto a surface sputtered for 5 minutes or longer. The Re clusters grown on the sputtered HOPG surfaces showed positive binding energy shift for their respective Re($4f_{7/2}$) peak, which was attributed to a cluster size effect. However, after depositing Re onto an HOPG surface with oxygen

www.manaraa.com

functional groups on the surface, the binding energy of Re increased in spite of the fact that the cluster height was essentially the same as it was on the oxygen free HOPG surface. These results indicate that Re strongly interacts with oxygen groups on the surface. Comparing the Re binding energy shift that occurred as a function of cluster size for HOPG and TiO_2(110) revealed that the shift was much more pronounce on the TiO_2(110). These results show that the binding energy shift that occurs for Re on TiO_2(110) cannot solely be attributed to a cluster size effect, but must also be due to Re interacting strongly with oxygen groups on the surface of TiO_2(110).

www.manaraa.com

Table 5.1: Summary of the average Re cluster height, cluster density and corresponding Re($4f_{7/2}$) peak position for Re deposited onto HOPG or TiO_2(110).

Surface	Avg. Height (Å)	Cluster density (10^{12} cm^{-2})	Re($4f_{7/2}$) (eV)
0.25 ML Re, HOPG	10.7±3.8	1.33	40.6
0.22 ML Re, HOPG-O	10.0±4.5	2.34	41.0
0.22 ML Re, sputtered 30 sec	8.7±3.7	3.34	40.6
0.22 ML Re, sputtered 5 min	6.4±1.7	11.18	40.9
0.22 ML Re, sputtered 10 min	4.6±1.4	12.31	40.9
0.125 ML Re, HOPG	9.8±3.8	0.96	40.6
0.11 ML Re, sputtered 5 min	5.7±1.7	11.17	40.8
0.125 ML Re, sputtered 10 min	4.7±1.4	13.89	40.8
0.11 ML Re, sputtered 20 min	4.6±1.4	15.08	40.8
0.11 ML Re, TiO_2(110)	2.9±1.1	31.44	41.3
0.22 ML Re, TiO_2(110)	3.2±1.1	28.16	41.1
0.43 ML Re, TiO_2(110)	4.0±1.3	25.76	41.0
1.7 ML Re, TiO_2(110)	4.7 ±1.0	15.49	40.6

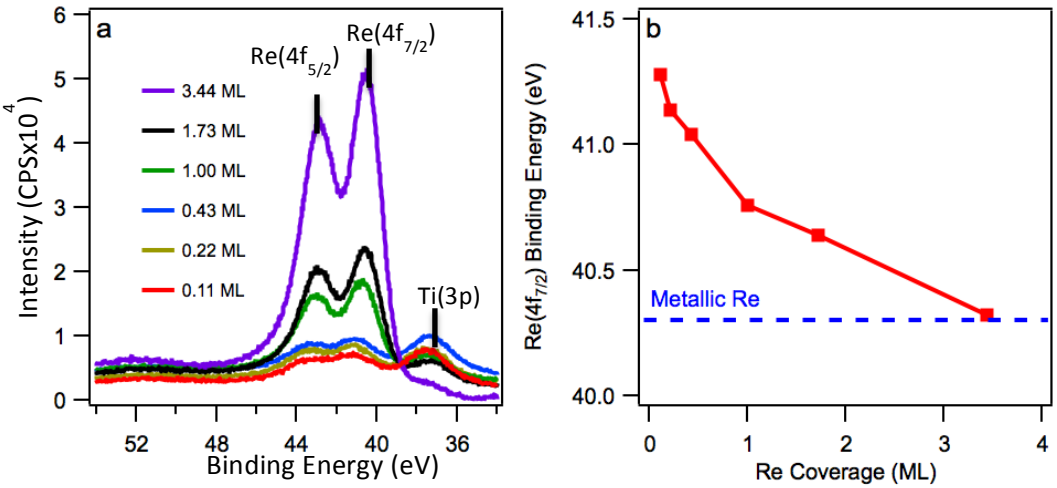

Figure 5.1: (a) Re(4f) region of for different monolayer coverages of Re deposited Ti(110) (b) Re($4f_{7/2}$) binding energy position as a function of coverage. The binding energy of metallic Re is represented by the dashed line at 40.3 eV.

www.manaraa.com

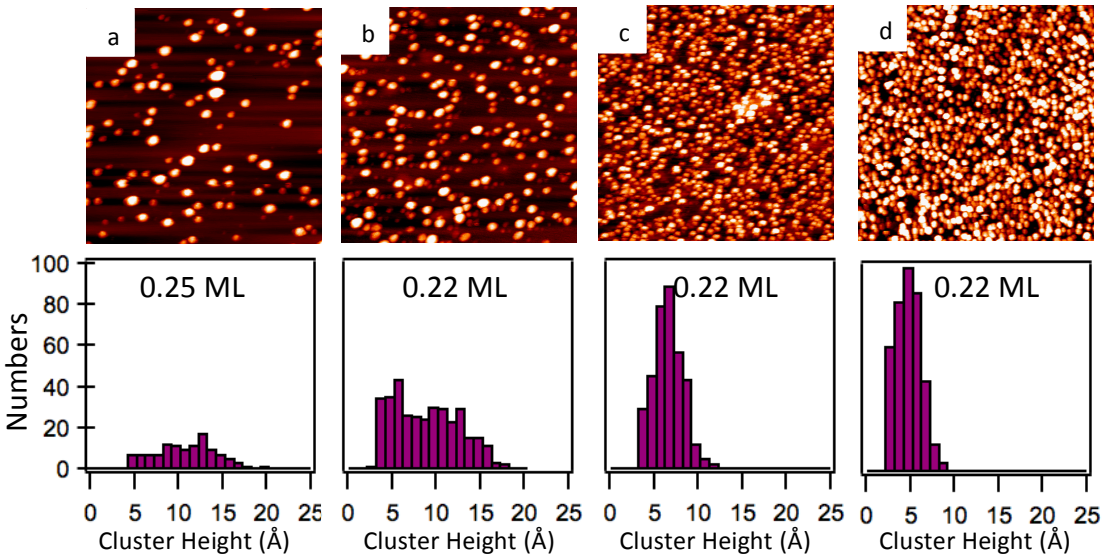

Figure 5.2: 0.25-0.22 ML of Re deposited onto HOPG that was sputtered for (a) 0 seconds, (b) 30 seconds, (c) 5 minutes and (d) 10 minutes. The histogram below each image corresponds to the Re cluster height distribution of that surface. All STM images are 100 nm x 100 nm.

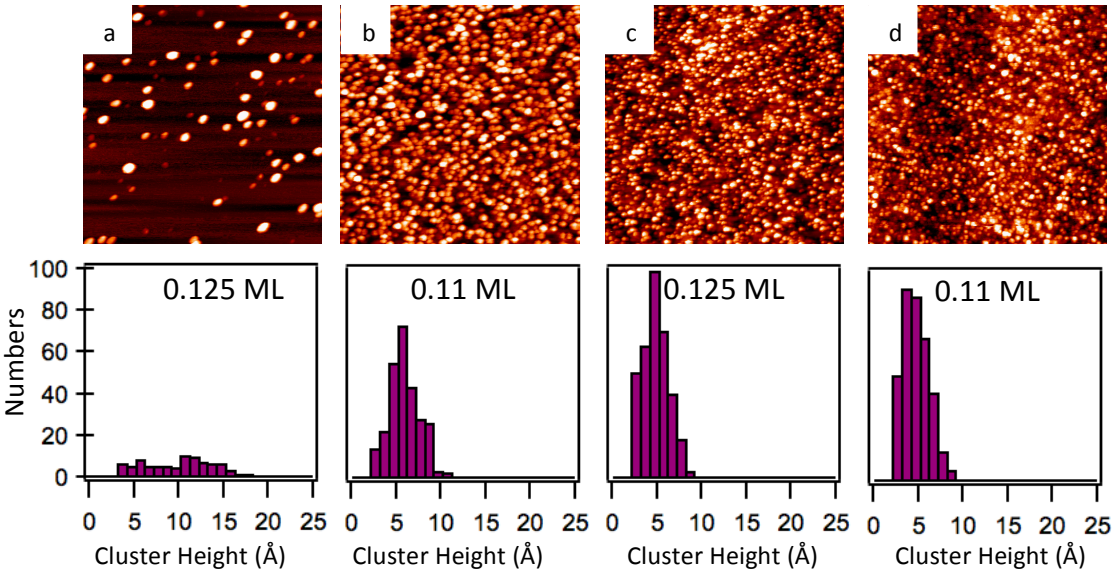

Figure 5.3: 0.11 – 0.125 ML of Re deposited onto HOPG that was sputter for (a) 0 seconds, (b) 5 minutes, (c) 10 minutes and (d) 20 minutes. The histograms below each image corresponds to the Re cluster height distribution for each image. All STM images are 100 nm x 100 nm.

www.manaraa.com

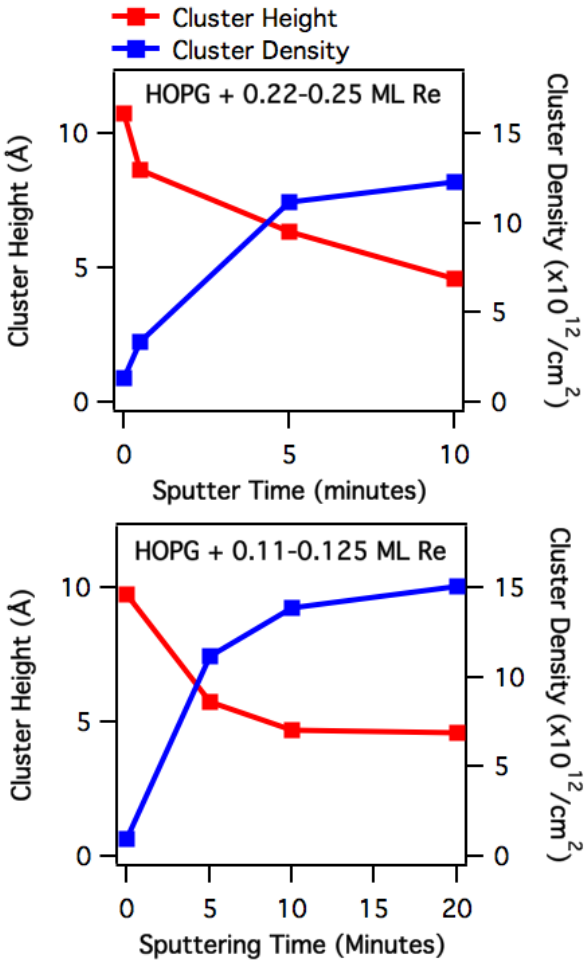

Figure 5.4: Top graph: cluster height and density for 0.22-0.25 ML Re/HOPG as a function of sputtering time. Bottom graph: cluster height and density for 0.11-0.125 ML Re/HOPG as a function of sputtering time.

www.manaraa.com

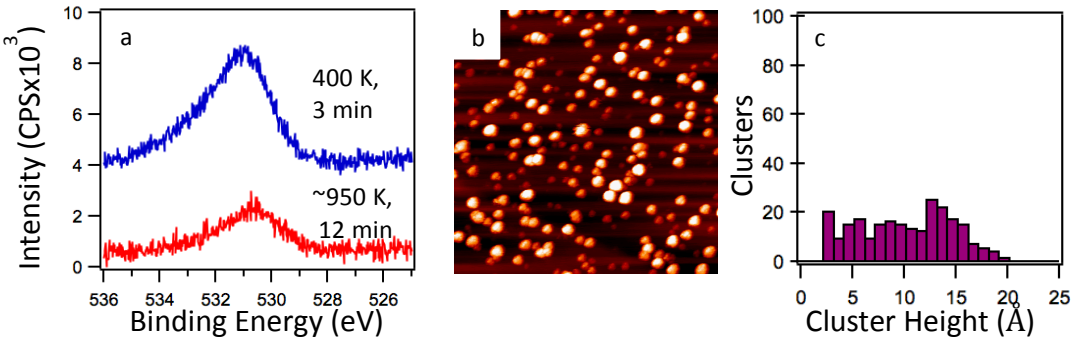

Figure 5.5: (a) the O(1s) region of HOPG after annealing to 400 K to 3 minutes (O/C ratio of 0.0479) and after annealing to 950 K for 12 minutes (O/C ratio of 0.0176). By annealing at lower temperature, HOPG retains oxygen functionality (b) STM image of 0.22 ML of Re deposited onto the HOPG-O (c) the cluster height distribution of Re. The STM image is 100 nm x 100 nm.

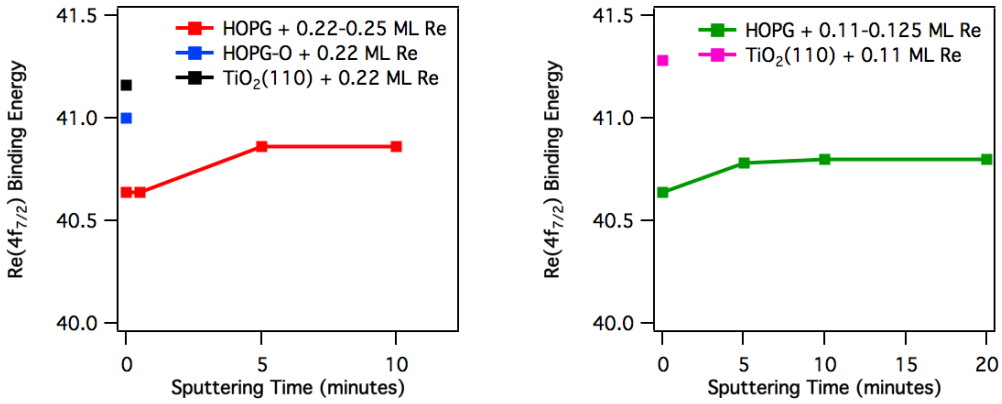

Figure 5.6: Left panel, binding energy position of Re for the 0.22-0.25 ML Re coverages as a function of sputtering time on HOPG and TiO_2(110). HOPG-O refers to the surface that was only annealed to 400 K prior to the deposition of Re. Right panel, binding energy position of Re for the 0.11-0.125 ML Re coverages on HOPG and TiO_2(110).

www.manaraa.com

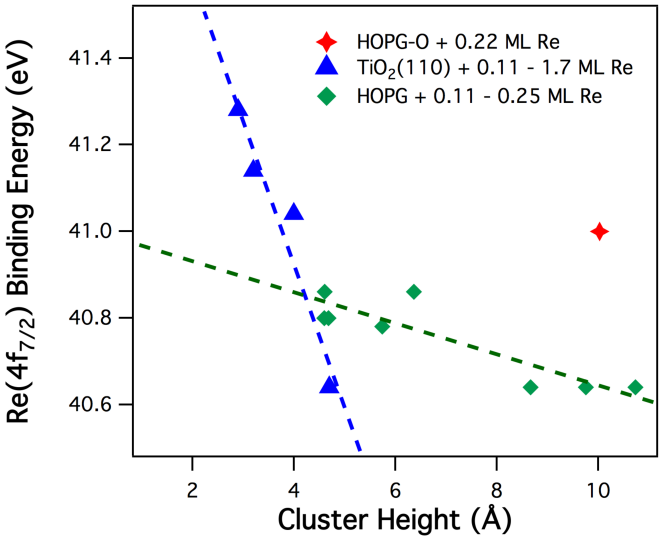

Figure 5.7: Binding energy of Re($4f_{7/2}$) plotted against the cluster height of Re on HOPG-O, HOPG, and TiO_2(110). The dashed blue and green lines offer a guide to indicate the general binding energy shift trends for Re grown on TiO_2(110) (blue) and HOPG (green).

References 5.5

1. Xiao, J., Puddephatt, R. J., Pt-Re Clusters and Bimetallic Catalysts. *Coordination Chemistry Reviews* **1995,** *143*, 457-500.

2. Cortright, R. D., R. R. Davda & J. A. Dumesic, Hydrogen from catalytic reforming of biomass-derived hydrocarbons in liquid water. *Nature* **2002,** *418*, 964-966.

3. Simonetti, D. A., E.L. Kunkes, J.A. Dumesic, Gas-phase conversion of glycerol to synthesis gas over carbon-supported platinum and platinum–rhenium catalysts. *Journal of Catalysis* **2007,** *247*, 298-306.

4. Kunkes, E. L., Dante A. Simonetti, James A. Dumesic, William D. Pyrz, Luis E. Murillo, Jingguang G. Chen, Douglas J. Buttrey, The role of rhenium in the conversion of

www.manaraa.com

glycerol to synthesis gas over carbon supported platinum–rhenium catalysts. *Journal of Catalysis* **2008,** *260*, 164-177.

5. Kim, Y. T., Dumesic, James A., Huber, George W., Aqueous-phase hydrodeoxygenation of sorbitol: A comparative study of Pt/Zr phosphate and PtReOx/C. *Journal of Catalysis* **2013,** *304*, 72-85.

6. Zhang, L., Ayman M. Karim, Mark H. Engelhard, Zhehao Wei, David L. King, Yong Wang, Correlation of Pt–Re surface properties with reaction pathways for the aqueous-phase reforming of glycerol. *Journal of Catalysis* **2012,** *287*, 37-43.

7. Azzam, K., I. Babich, I., K. Seshan, L. Lefferts, A bifunctional catalyst for the single-stage water–gas shift reaction in fuel cell applications. Part 2. Roles of the support and promoter on catalyst activity and stability. *Journal of Catalysis* **2007,** *251* (1), 163-171.

8. Sato, Y., Keisuke Terada, Satoshi Hasegawa, Toshihiro Miyao, Shuichi Naito, Mechanistic study of water–gas-shift reaction over TiO2 supported Pt–Re and Pd–Re catalysts. *Applied Catalysis A: General* **2005,** *296*, 80-89.

9. Iida, H., Akira Igarashi, Structure characterization of Pt-Re/TiO2 (rutile) and Pt-Re/ZrO2 catalysts for water gas shift reaction at low-temperature. *Applied Catalysis A: General* **2006,** *303* (2), 192-198.

10. Duke, A. S.; Xie, K.; Brandt, A. J.; Maddumapatabandi, T. D.; Ammal, S. C.; Heyden, A.; Monnier, J. R.; Chen, D. A., Understanding Active Sites in the Water–Gas Shift Reaction for Pt–Re Catalysts on Titania. *ACS Catalysis* **2017,** *7* (4), 2597-2606.

www.manaraa.com

11. Galhenage, R. P.; Xie, K.; Yan, H.; Seuser, G. S.; Chen, D. A., Understanding the Growth, Chemical Activity, and Cluster-Support Interactions for Pt-Re Bimetallic Clusters on TiO2(110). *The Journal of Physical Chemistry C* **2016,** *120*, 10866-10878.

12. Galhenage, R. P.; Yan, H.; Tenney, S. A.; Park, N.; Henkelman, G.; Albrecht, P.; Mullins, D. R.; Chen, D. A., Understanding the Nucleation and Growth of Metals on TiO2: Co Compared to Au, Ni, and Pt. *The Journal of Physical Chemistry C* **2013**.

13. Diebold, U., The surface science of Titania. *Surface Science Reports* **2003,** *48*, 53-229.

14. Ping, L., Shuh, D. K, Adsorption of O2 on Polycrystalline Rhenium Metal at Room Temperature Studied by Synchrotron X-ray Photoemission Spectroscopy. *Journal of Electron Spectroscopy and Related Phenomena* **2001,** *114-116*, 319-325.

15. Chan, A. S. Y.; Wertheim, G. K.; Wang, H.; Ulrich, M. D.; Rowe, J. E.; Madey, T. E., Surface atom core-level shifts of clean and oxygen-coveredRe(1231). *Physical Review B* **2005,** *72* (3).

16. Bäumer, M., Hans-Joachim Freund, Metal deposits on well-ordered oxide Films. *Surface Science* **1999,** *61*, 127-198.

17. Campbell, C. T., Ultrathin metal films and particles on oxide surfaces- structural, electronic and chemisorptive properties. *Surface Science Reports* **1997,** *27*, 1-111.

18. Mason, M. G., Electronic structure of supported small metal clusters. *Physical Review B* **1983,** *27* (2), 748-762.

19. Zhange, L.; Persaud, R.; Madey, T. E., Ultrathin metal films on a metal oxide surface: Growth of Au on TiO2(110). *Physical Review B* **1997,** *56* (16), 10549-10557.

www.manaraa.com

20. Luo, K.; Clair, T. P. S.; Lai, X.; Goodman, D. W., Silver Growth on TiO2(110) (1 × 1) and (1 × 2). *Journal of Physical Chemistry B* **2000,** *104*, 3050-3057.

21. Hövel, H.; Becker, T.; Bettac, A.; Reihl, B.; Tschudy, M.; Williams, E. J., Controlled cluster condensation into preformed nanometer-sized pits. *Journal of Applied Physics* **1997,** *81* (1), 154-158.

22. Howells, A. R.; Hung, L.; Chottiner, G. S.; Scherson, D. A., Effects of substrate defect density and annealing temperature on the nature of Pt clusters vapor deposited on the basal

plane of highly oriented pyrolytic graphite. *Solid State Ionics* **2002,** *150*, 53-62.

23. Yang, D. Q., E. Sacher, Ar+ induced surface defects on HOPG and their effect on the nucleation, coalescence and growth of evaporated copper. *Surface Science* **2002,** *516* (1-2), 43-55.

24. Yang, D.-Q.; Sacher, E., Initial- and final-state effects on metal cluster/substrate interactions, as determined by XPS: copper clusters on Dow Cyclotene and highly oriented pyrolytic graphite

. *Applied Surface Science* **2002,** *195*, 187-195.

25. Kwon, S.; Vidic, R.; Borguet, E., Enhancement of adsorption on graphite (HOPG) by modification of surface chemical functionality and morphology. *Carbon* **2002,** *40*, 2351-2358.

26. Galhenage, R. P.; Xie, K.; Diao, W.; Tengco, J. M.; Seuser, G. S.; Monnier, J. R.; Chen, D. A., Platinum-ruthenium bimetallic clusters on graphite: a comparison of vapor deposition and electroless deposition methods. *Physical chemistry chemical physics : PCCP* **2015,** *17* (42), 28354-63.

www.manaraa.com

27. Yuan, Z.; Hanf, M. C.; Stephan, R.; Dulot, F.; Denys, E.; Florentin, A.; Harbich, W.; Wetzel, P., Growth of palladium nanoparticles on nanostructured highly ordered pyrolytic graphite. *Surface and Interface Analysis* **2015,** *47* (1), 82-86.

28. Lopez-Salido, I.; Lim, D. C.; Kim, Y. D., Ag nanoparticles on highly ordered pyrolytic graphite (HOPG) surfaces studied using STM and XPS. *Surface Science* **2005,** *588* (1-3), 6-18.

29. Yang, D. Q.; Piyakis, K. N.; Sacher, E., The manipulation of Cu cluster dimensions on highly oriented pyrolytic graphite surfaces by low energy ion beam irradiation. *Surface Science* **2003,** *536* (1-3), 67-74.

30. Nielsen, R. M., S. Murphy , C. Strebel, M. Johansson, J.H. Nielsen,I. Chorkendorff, A comparative STM study of Ru nanoparticles deposited on HOPG by mass-selected gas aggregation versus thermal evaporation. *Surface Science* **2009,** *608*, 3420-3430.

31. Howells, A. R., Linda Hung, Gary S. Chottiner, Daniel A. Scherson Effects of substrate defect density and annealing temperature on the nature of Pt clusters vapor deposited on the basal plane of HOPG. *Solid State Ionics* **2002,** *150*, 53-62.

32. Lopez-Salido, I.; Lim, D. C.; Dietsche, R.; Bertram, N.; Kim, Y. D., Electronic and Geometric Properties of Au Nanoparticles on Highly Ordered Pyrolytic Graphite (HOPG) Studied Using X-ray Photoelectron Spectroscopy (XPS) and Scanning Tunneling Microscopy (STM). *Journal of Physical Chemistry B* **2006,** *110*, 1128-1136.

33. Tenney, S. A.; Cagg, B. A.; Levine, M. S.; He, W.; Manandhar, K.; Chen, D. A., Enhanced activity for supported Au clusters: Methanol oxidation on Au/TiO2(110). *Surface Science* **2012,** *606* (15-16), 1233-1243.

www.manaraa.com

34. Appy, D.; Lei, H.; Wang, C.-Z.; Tringides, M. C.; Liu, D.-J.; Evans, J. W.; Thiel, P. A., Transition metals on the (0 0 0 1) surface of graphite: Fundamental aspects of adsorption, diffusion, and morphology. *Progress in Surface Science* **2014,** *89* (3-4), 219-238.

35. Nakada, K.; Ishii, A., Migration of adatom adsorption on graphene using DFT calculation. *Solid State Communications* **2011,** *151* (1), 13-16.

36. Manadé, M.; Viñes, F.; Illas, F., Transition metal adatoms on graphene: A systematic density functional study. *Carbon* **2015,** *95*, 525-534.

37. Wagner, R., D. Schlatterbeck, K. Christmann, The interaction of copper with a rhenium(0001) surface: structure, energetics, and growth modes. *Surface Science* **1999,** *440*, 231–251.

38. Wagner, R.; Schlatterbeck, D.; Christmann, K., The interaction of copper with a rhenium(0001) surface- structure, energetics, and growth modes. *Surface Science* **1999,** *440*, 231-251.

39. Seuser, G. S.; Banerjee, R.; Metavarayuth, K.; Brandt, A. J.; Maddumapatabandi, T. D.; Karakalos, S.; Lin, Y.; Regalbuto, J. R.; Chen, D. A., Understanding Uptake of Pt Precursors During Strong Electrostatic Adsorption on Single-Crystal Carbon Surfaces. *Topics in Catalysis* **2018,** *61* (5-6), 379-388.

www.manaraa.com

CHAPTER 6

GROWTH AND OXIDATION OF RE FILMS ON PT(111)

www.manaraa.com

6.1 Introduction

Pt-Re catalysts have been used commercially for naphtha reforming since it was patented by Chevron in the 1960s.[1, 2] The superior activity and stability of bimetallic catalysts compared to their monometallic counterparts is typically attributed to changes in electronic structure, unique surface structures, or bifunctional sites.[3-5] More recently, Pt-Re catalysts have displayed superior catalytic activity towards the low temperature water-gas shift (LT-WGS) reaction[6-9] and the aqueous phase reforming (APR) of oxygenated hydrocarbons.[10-18] In both cases, the enhanced activity and stability is believed to be driven in part by the removal of CO and other carbonaceous species form the surface,[17-22] however the mechanism by which this occurs is not fully understood. One hypothesis is that the presence of Re changes the electronic structure of Pt, reducing the adsorption strength of CO and preventing the catalysts from becoming poisoned.[18, 22, 23] Pt and Re are known to form an alloy, and so the two metals are expected to have a strong chemical interaction.[23, 24] Another hypothesis is that the ReO_x species, which is believed to be present under reaction conditions, participates in the WGS reaction by oxidizing CO bound to Pt sites.[6-8, 17] Moreover, it has been proposed that ReO_x provides acid sites on the surface that facilitates C-O bond cleavage reactions in APR of oxygenated hydrocarbons.[10, 11, 15, 16] Because of the role that metallic Re and ReO_x may play in the chemistry of Pt-Re catalysts, it is critical to develop an understanding of the oxidation states of Re that are present during the reaction.

The presence of Pt can have a profound influence on the oxidation state of Re. For example, Re reduces at a lower temperature in the presence of Pt, most likely via the spillover of hydrogen from Pt onto Re.[11, 25-27] The reduction temperature has also been

www.manaraa.com

shown to play an important role in the formation of Pt-Re alloy particles.[25, 26] Interestingly, there is at least one report that suggests the presence of Pt facilitates the oxidation of Re on a carbon support exposed to steam at 225 °C. [15] However, these experiments were conducted on a traditional high surface area catalysts with an ill defined surface, making it difficult to come to a definitive conclusion about the results. In post-reaction XPS experiments conducted in our own lab, the presence of Pt in a model Pt-Re catalyst prepared on TiO_2(110) used for methanol oxidation at 100 °C increased the amount of Re in its higher oxidation states (+4, +6 and +7).[28] However, it was not possible to decouple the role that Pt and the titania support, which interacts strongly with Re,[29] may have on the oxidation state of Re.

To determine if Pt facilitates the oxidation of Re, Re films of varying thicknesses and chemical composition were prepared on a Pt(111) single crystal and then exposed to high pressures of O_2 at room temperature. By varying the thickness of the films, it was possible to test if direct contact between the Re film and Pt crystal increased the amount of Re that was oxidized. Pt-Re alloy surfaces were prepared by annealing the Re films to test how the alloy formation affects the oxidation state of Re. It was found that only Re at the surface of the films was oxidized upon exposure to O_2. Furthermore, the formation of a Pt-Re alloy surface suppresses the oxidation of Re due to the surface being Pt rich. Lastly, we found no correlation between the extent of Re oxidation and the thickness of the Re films; therefore direct contact of Re with Pt does not appear to facilitate the oxidation of Re.

www.manaraa.com

6.2 Experimental

All experiments were carried out in an ultrahigh vacuum (UHV) chamber that has been described previously.[30] The base pressure of the chamber is less than $1x10^{-10}$ torr and is equipped with a variable-temperature STM (Omicron, VT-25), a hemispherical analyzer (Omicron, EA125), a dual Al/Mg anode x-ray source for X-ray photoelectron spectroscopy (Omicron, DAR 400) and low energy ion scattering optics (Omicron, Spec3). The chamber also contains a sputter gun used for cleaning single crystals with Argon ions (Omicron ISE 10).

A Pt(111) single crystal (99.999%, Princeton Scientific Corp., 8 mm diameter, 2 mm thickness) was used for all the experiments. The configuration of the mounted Pt(111) crystal has been described in more detail elsewhere.[19] Briefly, the crystal was mounted onto a standard Omicron Ta plate with a window cut into the back and was held in place by two Ta wires that were spot welded to the plate. The Pt(111) crystal was heated through electron bombardment from a tungsten filament with a sample bias of +600 V. The Pt(111) crystal was cleaned by sputtering with 1 kV Ar^+ ions for 20 minutes, followed by annealing to 1000 K for 3 minutes. The temperature of the crystal was monitored using a Heitronics CT 18 pyrometer. The cleanliness of the surface was established using XPS, LEIS and STM.

Re was deposited between room temperature and 500 K from a 2 mm diameter Re rod (EPSI, 99.99%) using an Oxford Applied Research (EGC04) electron beam evaporator. The Re flux was monitored using a quartz crystal microbalance (QCM, Inficon XTM-2). One monolayer of Re is defined as the packing density of Re(0001), 1.52×10^{15} atoms/cm^2. Re was deposited onto the surface of Pt(111) at a rate of 0.02–

www.manaraa.com

0.05 ML/min. STM experiments were conducted in constant current mode using bias between +0.35-2.0 V and a tunneling current of 4 nA. The STM tips were prepared by electrochemically etching 0.38 mm the tungsten wire in with a NaOH solution and were later subjected to Ar^+ sputtering.

XPS experiments were conducted with 0.02 eV resolution and pass energy of 50 eV. "Regular" angle XPS experiments were done at 26° off-normal, while the grazing angle experiments were conducted at a 72° off-normal. Low energy ion scattering experiments were conducted using 600 eV He^+ ions. Previous work demonstrated that the ion bombardment did minimal damage to the Re films.[19] All peak fitting of the Re(4f) spectra were performed with XPSPeak software using a Shirley background and a Gaussian-Lorenztian peak shape with an asymmetry factor. The peak separation between the Re($4f_{7/2}$) and Re($4f_{5/2}$) was set to 2.45 ±0.1 eV and the area ratio between the two peaks was set to 4:3.

Oxidation treatments were conducted by transferring the prepared sample out of the main chamber into a load lock. The load lock was filled with 250 torr of ultra high pure oxygen gas (Matheson Gas, 99.98%) for two hours. After oxygen exposure, the load lock was pumped down overnight, at which time the sample was then transferred back into the chamber for post-oxidation XPS.

6.3 Results and Discussion

6.3.1 Growing Re films on Pt(111)

Figure 6.1 shows a series of STM images of Re films deposited onto Pt(111) at coverages of 0.4, 1.0, and 1.9 ML. At 0.4 ML (Figure 6.1a), the surface is predominantly covered with Re islands measuring between 2.2-2.8 Å high, corresponding to the height

www.manaraa.com

of one atomic layer of Re.[24] A small fraction of islands have a height greater than 4 Å, indicating that a second layer of Re begins to grow before the first layer is complete; overall the images are consistent with Re growing in an approximately layer-by-layer fashion.[24, 31] At 1.0 ML, the Re islands have begun to form a film that covers the majority of the Pt(111) surface, but there is significant Re island growth on the still incomplete first layer of Re. At 1.9 ML, the Re film has become contiguous and no longer appears to be growing in an approximately layer-by-layer mode, contrary to previous report that Re grows in a layer-by-layer mode up to 3 ML.[31] As more Re is deposited onto the surface, the film becomes more disordered. The significant growth of Re islands on the first layer of the Re film is attributed to the high step-down diffusion barrier associated with atoms descending down steps on the surface when depositing Re at room temperature.[32-37]

To grow smoother, atomically flat Re films, Re was deposited onto Pt(111) at higher temperatures. The STM images in Figure 6.2a-b compare a 1.0 ML Re film grown at room temperature (Figure 6.2a) and another grown at 500 K (Figure 6.2b). Both surfaces contained a significant number of Re islands occupying the second layer of the film, but there were fewer islands on the Re film deposited at 500 K, indicating that a more uniform film was grown. When Re was deposition at 600 K (Figure 6.2c), the Re islands had a more regular shape and no longer appeared to be growing in a layer-by-layer mode. The shape of the Re islands were similar to Re films that were annealed to 800 K, when significant alloy formation occurs.[19] From these images, it was concluded that deposition at 600 K led to significant Pt-Re alloy formation. Annealing the Re film grown at 500 K to 600 K for 10 minutes after film deposition led to even fewer second layer Re islands appearing on the surface. Upon annealing the film, perimeter Re atoms

www.manaraa.com

detach from existing islands and reattach to larger islands or descend down the step-edge to join the first Re layer.[4, 38]

To ensure that the Re films were not alloying upon annealing to 600 K after metal deposition, a series of low energy ion scattering (LEIS) and XPS experiments were conducted on annealed Re films to gain insight into the chemical composition of the surface. Pt-Re alloy formation of Re films on Pt(111) is known to lead to the diffusion of Pt to the surface,[24, 31] therefore monitoring the chemical composition of the surface can provide insight into whether or not an alloy was formed. Figure 6.3 tracks the LEIS signal of a 0.9 ML Re film deposited onto Pt(111) that was annealed to 500 K, 600 K, and 700 K for 1 minute. It was not possible to resolve the Pt and Re contributions to the signal, meaning that attaining quantitative information about the chemical composition of the top-most layer of the surface was not possible. However, previous work from our group showed that LEIS was 1.9 times more sensitive to a Pt foil as compared to a Re foil, enabling qualitative information to be extracted about the chemical composition of the surface.[20] Depositing 0.9 ML of Re onto the surface of Pt(111) decreased the LEIS signal by 60%, which was attributed to the top-most surface layer being composed primarily of Re. Annealing the Re film to 500 K and 600 K for 1 minute increased the LEIS signal slightly, while annealing to 700 K increased the signal to 70% of that observed for Pt(111). The sharp increase in signal after annealing to 700 K was attributed to Pt atoms diffusing to the surface and the formation of a Pt-Re surface alloy.[19, 23, 24] These results suggest that annealing the Re films to 600 K does not lead to the formation of an alloy.

www.manaraa.com

Grazing angle XPS experiments were performed to monitor the position of the Pt(4f) and Re(4f) binding energy positions as the Re film was grown and then subsequently annealed to 600 K, as shown in Figure 6.4. Upon deposition of 0.8 ML Re onto Pt(111) at 500 K, the binding energy position of Pt($4f_{7/2}$) shifted by +0.5 eV to ~71.1 eV. The binding energy shift is too large to be consistent with the surface core level shift of Pt, which is should be +0.4 eV.[24, 39] The binding energy position of Re($4f_{7/2}$) was 40.7 eV, higher than the position of pure metallic Re at 40.3 eV,[40, 41] which has no substantial surface core level shift.[41, 42] The positive shifts in binding energy for both Pt and Re is attributed to a strong chemical interaction between the two metals, consistent with previous observations for Re films grown on Pt(111) at room temperature.[19] Annealing to 600 K for 5 minutes increased the intensity of the Re(4f) and Pt(4f) signals by 15 and 18 percent respectively, while the binding energy positions of both metals remained unchanged. Because Re is known to diffuse into the surface upon alloy formation,[19, 24, 43, 44] the increase in Re(4f) signal is not consistent with alloy formation, but is consistent with the Re film becoming more atomically flat. Annealing to 600 K for an additional 5 minutes led to a less than 5% increase in intensity of both metals and no change in the binding energy positions. Similar to the LEIS experiments, these findings suggest that no significant alloying occurs when annealing Re films to 600 K.

Using these annealing procedures, two Re films were grown on Pt(111) that consisted of approximately 1 (0.8 ML) and 2 (1.8 ML) monolayers of Re, as shown in Figure 6.5. Both Re films were deposited onto Pt(111) at 500 K and then annealed to 600 K for 10 minutes. Re coverages of 0.8 and 1.8 ML were chosen to reduce the number of second and third layer Re islands that appeared on each respective surface. The 0.8 ML

www.manaraa.com

Re (Figure 6.5a) surface has noticeably less second layer Re islands as compared to its 1.0 ML Re counterpart (Figure 6.2b); however the first layer of Re almost completely covers the Pt(111) surface. For the 1.8 ML Re coverage film (Figure 6.5b), the first layer of Re is no longer visible, and only the second and third layer of Re islands can be seen. The second layer of Re covers significantly less of the surface than the first layer of the 0.8 ML Re film; however the film is still approximately 2 ML thick. The 0.8 and 1.8 ML Re films were used to test how Pt influences the oxidation of Re, the results of which will be discussed in section 6.3.3.

6.3.2 Pt-Re Alloy formation

STM images in Figure 6.6 depict a clean Pt(111) surface and a 1.9 ML Re film that was annealed to 1000 K for 5 minutes. Figure 6.6a shows that Pt(111) surface is an atomically flat surface with steps. The annealed 1.9 ML Re/Pt(111) surface has much fewer islands than Re films grown at room temperature[20] and has irregularly shaped steps. These results indicate that the Re islands have diffused into the surface of Pt(111) surface after annealing.

The surface composition of a 1.9 ML Re film on Pt(111) undergoing alloy formation by annealing to 1000 K for 5 minutes was monitored using XPS, as shown in Figure 6.7. XPS measurements were taken at 26°, "regular" angle, and 72° off-normal, grazing angle, which is more surface sensitive. Using the Seah-Dench equation, the sampling depth of the "regular" and grazing angle XPS measurements were estimated to be 5 nm (20 monolayers) and 1.5 nm (7 monolayers) respectively.[45] Depositing 1.9 ML Re onto the surface of Pt(111) decreased the Pt(4f) intensity of the "regular" and grazing angle XPS signals by 24 and 51 percent respectively. The more dramatic decrease in the

www.manaraa.com

Pt(4f) intensity in the grazing angle experiment is consistent with the top most layers of the surface being composed of a Re film. After annealing to 1000 K, the "regular" and grazing angle Pt(4f) intensity increased by 14 and 66 percent respectively, while the "regular" and grazing angle Re(4f) intensities decreased by 12 and 41 percent respectively. These results are consistent with Re diffusing into the bulk and the surface becoming more Pt rich upon annealing, a phenomenon that has been noted by others studying Pt-Re alloys.[23, 24, 43, 44] Previous LEIS experiments conducted in our group showed that upon annealing to 1000 K, the top-most layer of Re/Pt(111) surface consisted of virtually all Pt.[19] Diffusion of Pt to the surface in Pt-Re alloys is consistent with Pt having a lower surface free energy than Re, 2.5 J/m^2 and 3.6 J/m^2 respectively,[46] meaning that a Pt surface should be more thermodynamically stable than a Re surface.

The position of the Pt($4f_{7/2}$) peak in the grazing angle XPS spectra shifts from 70.7 eV on the pristine Pt(111) surface to 71.1 eV, which was attributed to a combination of an electronic interaction between the two metals and a surface-core level shift (SCLS). The SCLS occurs when adsorbates or adatoms are deposited onto the surface of a metal, causing the surface atoms to become bulk like.[24, 39, 47] Interestingly, the Pt($4f_{7/2}$) peak position shifted from 71.1 eV to 70.9 eV after annealing to 1000 K, but this shift was not observed in the less surface sensitive "regular" angle XPS spectra. The shift to lower binding energy is attributed to the diffusion of Pt to the surface, meaning that there is no longer a positive shift associated with the SCLS.[24] After alloy formation, the Pt($4f_{7/2}$) peak remains above 70.7 eV due to the electronic interaction with Re.

www.manaraa.com

6.3.3 Oxidation of Pt, Pt-Re alloy and Re films

Grazing angle XPS was used to characterize the adsorption of oxygen onto Pt(111) , the 1.9 ML Pt-Re alloy, and the 0.8 and 1.8 ML Re films after exposure to 250 torr O_2 for 2 hours at room temperature. The post-oxidation XPS results of the Pt(4f) and Re(4f) regions for Pt(111) and the Pt-Re alloy surface are shown in Figure 6.8. For the Pt-Re alloy surface, Re remained in the metallic state. The XPS spectra of the Pt(4f) region indicates that Pt was not oxidized by the oxygen treatment. The Pt($4f_{7/2}$) of the Pt(111) surface shifted from 70.7 to 70.9 eV after being exposed to O_2, which was attributed to the surface core level shift.[24, 47] For the Pt-Re alloy surface, there was a small shift in the Re($4f_{7/2}$) peak from 40.4 to 40.6 eV, but this shift is too small to be attributed to a change in oxidation state. The lack of Re oxidation in the Pt-Re alloy is attributed to the top-most layer of the surface being covered predominantly by Pt, which prevents subsurface Re from being oxidized. However, Re does not stay subsurface in Pt-Re alloys at higher temperatures in an oxidizing environment. In ambient pressure (AP)-XPS studies conducted by Duke et al., it was reported that Re remained in the metallic state up to a temperature of 450 K in 500 mtorr of O_2, but was oxidized at 500 K.[19] Similarly, Tysoe et al. exposed a Pt-Re alloy surface to 700 torr oxygen at 475 K, which lead to extensive oxidation of Re.[48]

The O(1s) spectra of the oxidized Pt-Re surfaces are shown in Figure 6.9. The intensities of the O(1s) of the Pt(111) an Pt-Re alloy surface after O_2 exposure are within 2 percent of one another, indicating that the same amount of oxygen was adsorbed on both surfaces. The O(1s) on both surfaces is assigned to atomic oxygen.[19, 47, 49] The intensity of the O(1s) signal of the 0.8 and 1.8 ML Re films is a factor of 2 times greater

www.manaraa.com

than that seen the Pt(111) or Pt-Re alloy surface. The larger oxygen content on the Re films is consistent with Re being a more oxophilic metal than Pt. The O(1s) signal intensities of the 0.8 and 1.8 ML Re are within 6% of one another, meaning that about the same amount of oxygen adsorbed onto each film. The binding energy position of the O(1s) peak on Pt(111), the 1.9 ML Re/Pt(111) alloy, and the Re films were 531.1, 530.7 and 530.3 eV respectively. The peak position of the Pt(111) is about +1 eV higher than previous reports,[49, 50] an inconsistency that has still not been fully explained. The 530.3 eV peak position for the Re film is close to previously reported values of dissociated O_2 on Re(0001)[51] and on Re films deposited on Pt(111) in AP-XPS experiments.[19] There appears to be a correlation between the binding energy of the O(1s) peak and the presence of Re.

Figure 6.10 shows the Re(4f) signals before and after exposure of the 0.8 and 1.8 ML Re films were exposed to 250 torr O_2 at room temperature, demonstrating extensive oxidation of Re. The binding energy positions of the Re($4f_{7/2}$) peak fits appearing at 40.7, 41.1, 43.0-43.2, and 44.6-44.7 eV were assigned to Re^0, Re^{2+}, Re^{+4} and Re^{+6} respectively. The +0.8 binding energy shift of the 41.1 eV peak with respect to metallic Re (40.3 eV) is slightly too high to be attributed to a Re species coordinated with oxygen, for which binding energy shifts of +0.3-0.7 eV have been reported.[40, 41] Therefore, the 41.1 eV peak was assigned to Re^{2+}, corresponding to a ReO phase.[40, 42] The peak at 43.0-43.2 was assigned to Re^{4+}, in agreement with reported values that range between 42.5-43.3. [48, 52-54] The binding energy is on the high end of the range, but the binding energy is too low to be assigned to Re^{5+}, which has been reported between 43.7-44.1 eV.[19, 20] Finally, the peak at 44.6-44.7 eV was assigned to Re^{6+}, which has been reported in the binding energy

www.manaraa.com

range between 44.8-45.4 eV.[48, 52, 53] Although the binding energy falls in the low range of previously reported values for Re^{6+}, the binding energy is too low to be assigned to Re^{7+} (46.5 – 47 eV),[52, 55, 56] and is too high be assigned to Re^{5+}. Furthermore, there are few reports of Re^{5+},[19, 20] most likely due to its instability, making it unlikely that such a species was formed during the experiment.

As more Re is deposited onto the surface, the fraction of Re in the Re^0 and Re^{2+} oxidation states increases. The percentage Re^0 and Re^{2+} on the surface increased from 57 to 78% on the 0.8 and 1.8 ML Re surfaces respectively. The percentage increased further to 85% on a 2.6 ML Re film, and the same trend was also observed for Re films grown on TiO_2(110) (Table 6.1). These results are consistent with only the Re at the surface of the films being oxidized by O_2, while the subsurface Re atoms remain in the metallic state.

The distribution of Re species in the higher oxidation states, Re^{4+} and Re^{6+}, was used to determine if Re being in contact with Pt influenced the oxidation state of Re. When compared to the 0.8 ML Re surface, there was 11% less Re in the higher oxidation states (4+ and 6+) on the 1.8 ML Re film based on the integrated areas derived from the Re(4f) peak fits. However, there was 20% more Re in the higher oxidation states on a 2.6 ML Re film (Table 6.1). Oxidation experiments on a number of Re films showed mixed results, as shown in Table 6.1. There maybe a correlation between the oxidation states present on the surface and the number of edge sites on the surface, but we were unable to draw a definitive correlation. Therefore, there is no clear trend indicating that direct contact between Pt and Re influences the oxidation of Re. The discrepancy between our

www.manaraa.com

results and previously observed enhanced oxidation of Re maybe related to a combination of Re interacting with both Pt and the support.

6.4 Conclusions

When Re films were alloyed with Pt(111), Re did not oxidized after exposure to O_2 because most of the Re was subsurface. A similar amount of oxygen adsorbed on the Pt-Re alloy, consistent with the surface of the alloy being Pt rich. Significantly more oxygen adsorbed onto the Re films deposited onto Pt(111), which was expected since Re is more oxophilic than Pt. Furthermore, the surface of the Re films were oxidized while the subsurface Re remained in the metallic phase. There was no clear correlation between the thickness of the Re film and the extent of oxidation, meaning that direct contact between Pt and Re does not enhance the oxidation of Re. These results suggest that the previously observed enhanced oxidation of Re for Pt-Re clusters on TiO_2(110) is not solely due to the presence of Pt.

Acknowledgments

I would like to thank Dr. Randima Galhenage for collecting some of the STM images of Re films deposited on Pt(111).

www.manaraa.com

Table 6.1: The integrated area and total fraction associated with each Re oxidation state determined by XPS for Re films on TiO_2(110) and Pt(111) exposed to 250 torr of O_2 at room temperature.

Sample	Re^0 Area (fraction)	Re^{2+} Area (fraction)	Re^{4+} Area (fraction)	Re^{6+} Area (fraction)
TiO_2(110) + 0.4 ML Re room temperature	0 (0)	6114 (0.314)	6663 (0.343)	6665 (0.343)
TiO_2(110) + 1.0 ML Re room temperature	28802 (0.520)	8992 (0.162)	3516 (0.064)	14086 (0.254)
TiO_2(110) + 2.0 ML Re room temperature	78879 (0.664)	14345 (0.121)	7355 (0.062)	18198 (0.153)
TiO_2(110) + 4.0 ML Re room temperature	132227 (0.730)	28038 (0.155)	0 (0)	20778 (0.115)
Pt(111) + 0.8 ML Re 500 K + 600 K 10 min	15015 (0.348)	9421 (0.218)	6026 (0.139)	12757 (0.295)
Pt(111) + 1.8 ML Re 500 K + 600 K 10 min	39105 (0.535)	17987 (0.246)	4690 (0.064)	11261 (0.155)
Pt(111) + 2.6 ML Re 500 K + 600 K 10 min	92266 (0.621)	33341 (0.224)	7603 (0.051)	15357 (0.104)
Pt(111) + 1.0 ML Re 500 K + 600 K 10 min	19555 (0.399)	10103 (0.206)	4168 (0.085)	15237 (0.310)
Pt(111) + 1.0 ML Re room temperature	14449 (0.317)	9685 (0.212)	5664 (0.124)	15816 (0.347)

www.manaraa.com

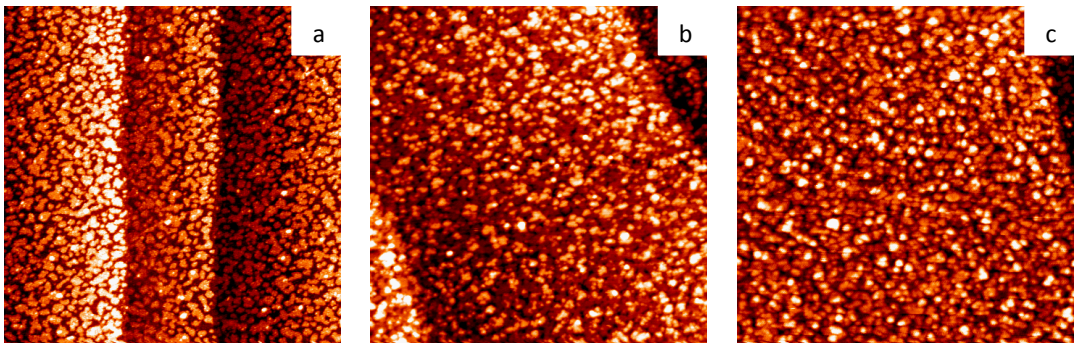

Figure 6.1: Re films grown on Pt(111) surface at coverages of a) 0.4 ML, b) 0.9 ML and c) 1.9 ML. All STM images are 100 nm x 100 nm.

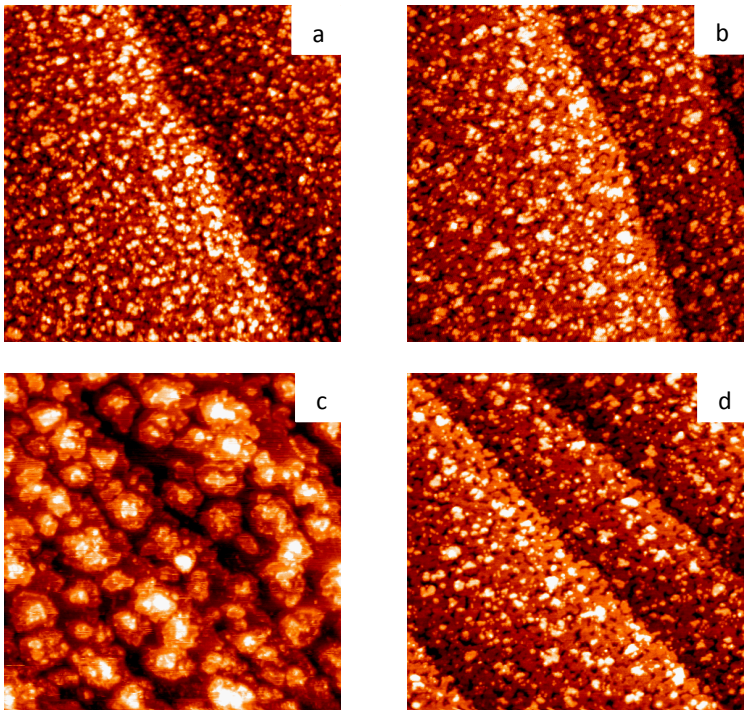

Figure 6.2: STM images of 1.0 ML Re films grown on Pt(111) at a) room temperature, b) 500 K and c) a 0.8 ML Re film at 600 K. The image shown in d) is the same surface as c) after annealing 600 K for 10 minutes. Both STM images are 100 nm x 100 nm.

www.manaraa.com

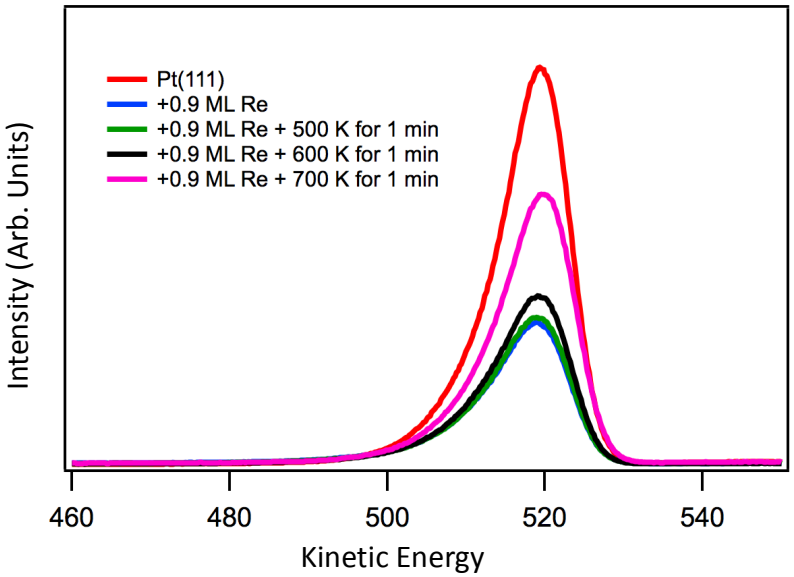

Figure 6.3: Low energy ion scattering (LEIS) data of 0.9 ML Re film deposited on Pt(111) followed by annealing to 500, 600, and 700 K for 1 minutes each.

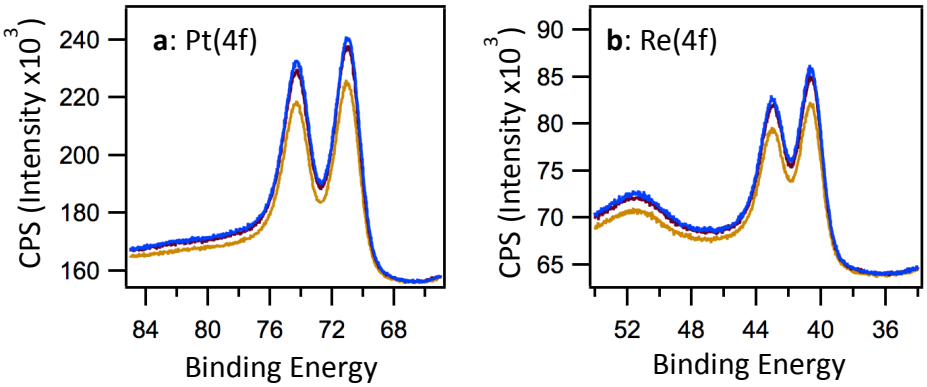

Figure 6.4: XPS of the a) Pt(4f) and b) Re(4f) regions of 0.8 ML Re deposited at 500 K. The gold traces corresponds to the 0.8 ML Re film after deposition; the maroon traces was taken after annealing the film to 600 K for 5 minutes; and blue traces corresponds to the surface after annealing for an addition 5 minutes at 600 K.

www.manaraa.com

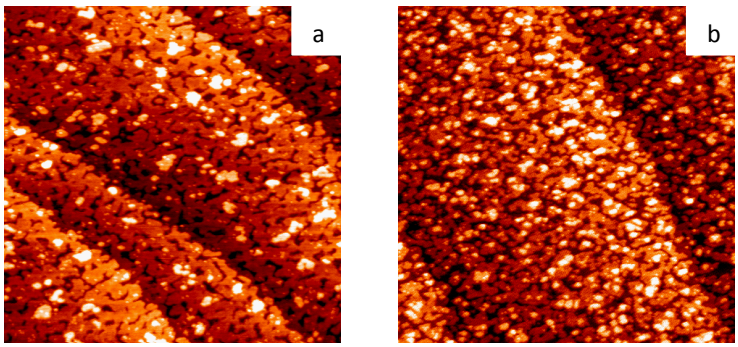

Figure 6.5: STM images of a) 0.8 ML Re film deposited at 500 K followed by annealing to 600 K for 10 minutes and b) addition 1.0 ML Re deposited onto the surface at 500 K followed by annealing to 600 K for 10 minutes. Both STM images are 100 nm x 100 nm.

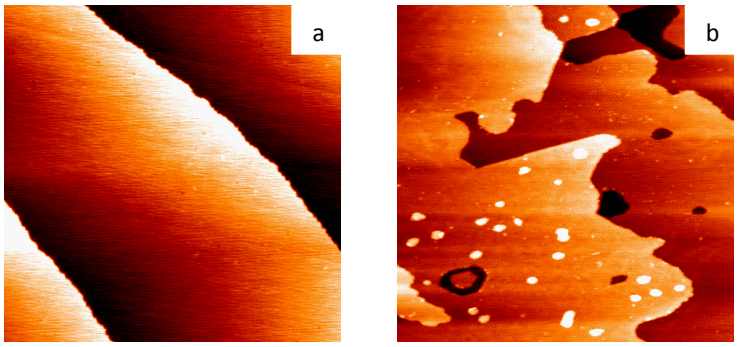

Figure 6.6: STM images of a) clean Pt(111) surface and b) Pt(111) + 1.9 ML Re annealed to 1000 K for 5 minutes. Both STM images are 100 nm x 100 nm.

www.manaraa.com

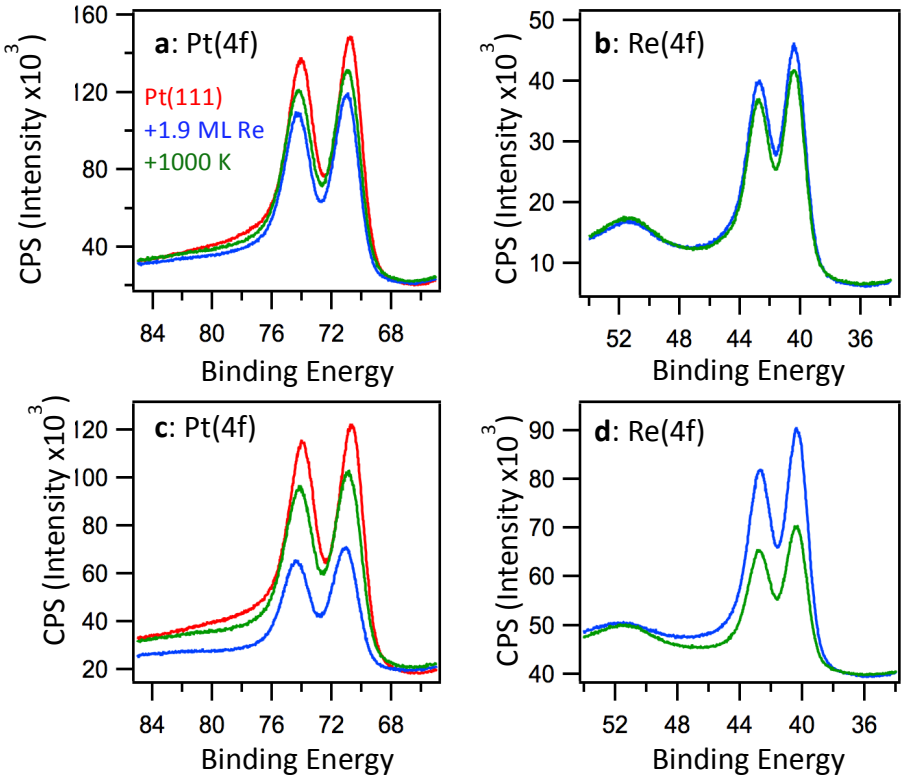

Figure 6.7: XPS done at a 26° off-normal for the a) Pt(4f) and b) Re(4f) regions following the formation of Pt-Re alloy formation process on Pt(111). Grazing angle XPS done at a 72° off-normal for the c) Pt(4f) and d) Re(4f) regions. The red traces correspond to the pristine Pt(111) surface, the blue traces are the 1.9 ML Re surface, and the green traces represent the 1.9 ML Re surface annealed to 1000 K for 5 minutes.

www.manaraa.com

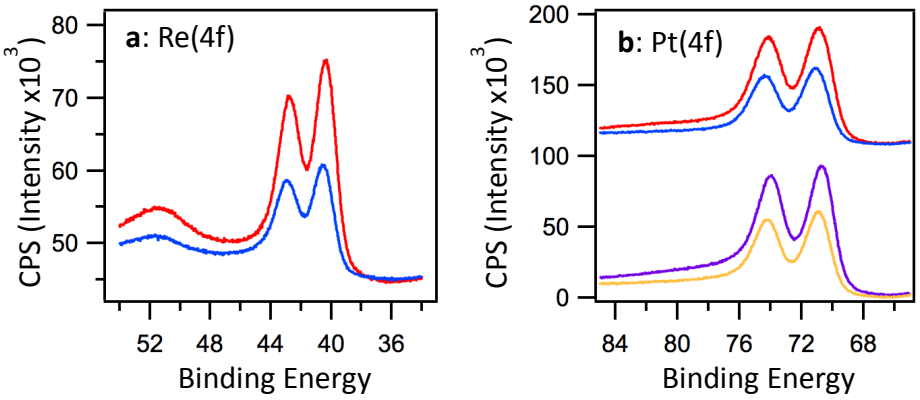

Figure 6.8: XPS of a) Re(4f) and b) Pt(4f) region of a Pt(111) and a 1.9 ML Re/Pt(111) surface annealed to 1000 K before, purple and red traces respectively, and after exposure to 250 torr O_2, yellow-orange and blue traces respectively. All XPS measurements were conducted at 72° off-normal.

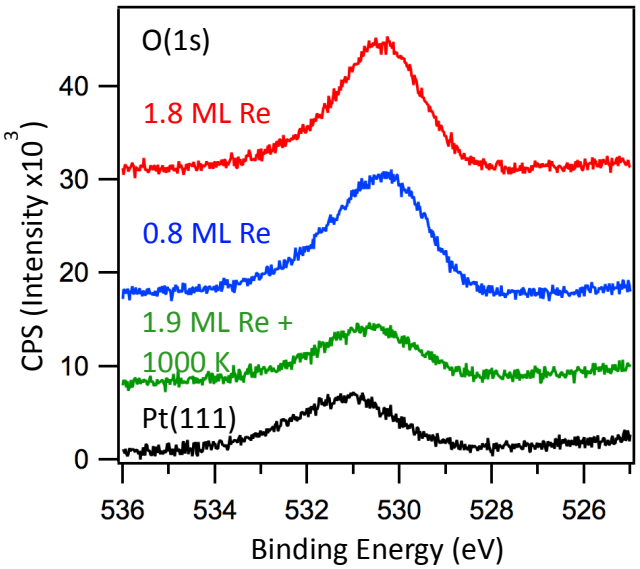

Figure 6.9: XPS of the O(1s) region of Pt(111), 1.9 ML Re film annealed to 1000 K for 5 minutes, 0.8 ML Re film, and 1.8 ML Re exposed to 250 torr of O_2 for 2 hours.

www.manaraa.com

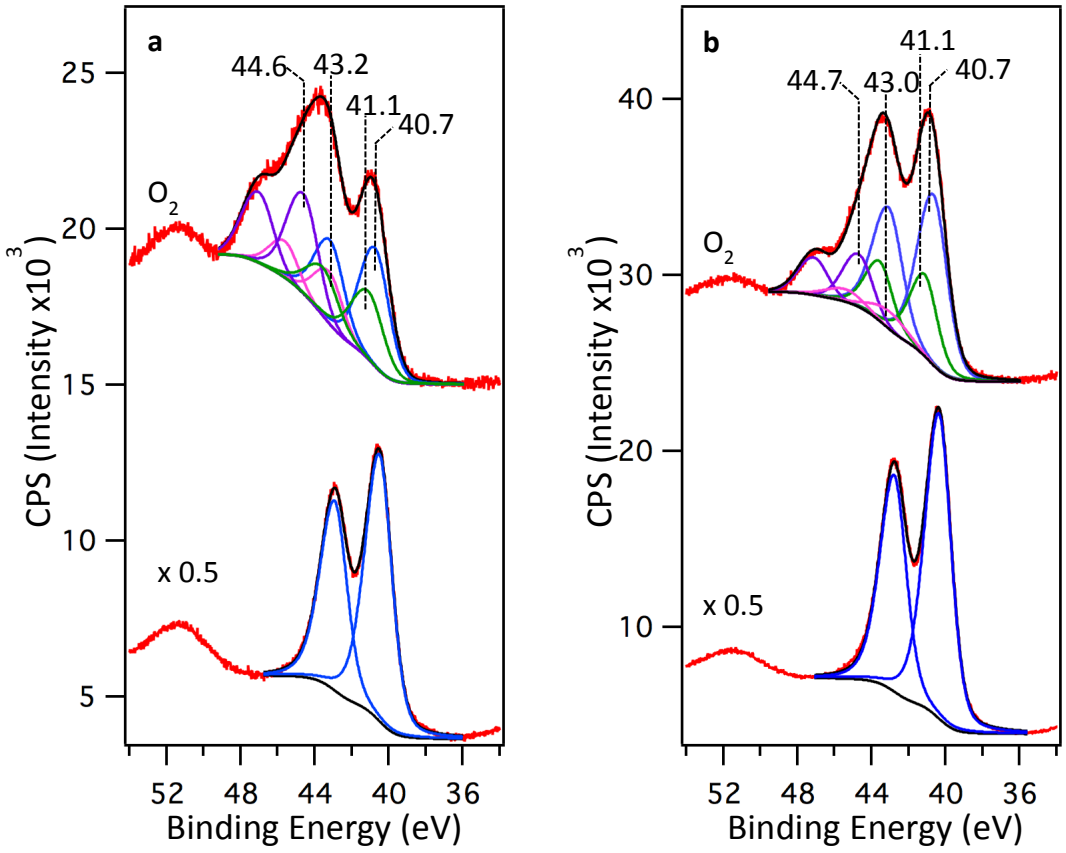

Figure 6.10: XPS of Re(4f) pre and post exposure to 250 torr O_2 for 2 hours for the a) 0.8 ML Re and b) 1.8 ML Re films deposited on Pt(111).

6.5 References

1. Xiao, J., Puddephatt, R. J., Pt-Re Clusters and Bimetallic Catalysts. *Coordination Chemistry Reviews* **1995,** *143*, 457-500.

2. Kluksdahl, H. E. Reforming a sulfur-free naphtha with a platinum-rhenium catalyst. 1968.

3. Rodriguez, J. A., Goodman, D. Wayne, Surface Science Studies of the Electronic and Chemical Properties of Bimetallic Systems. *J. Phys. Chem.* **1991,** *95*, 4196-4206.

4. Rodriguez, J. A., Physical and chemical properties of bimetallic surfaces. *Surface Science Reports* **1996,** *24*, 223-287.

www.manaraa.com

5. Campbell, C. T., Bimetallic Surface Chemistry. *Annu. Rev. Phys. Chem.* **1990,** *41*, 775-837.

6. Azzam, K., I. Babich, I., K. Seshan, L. Lefferts, A bifunctional catalyst for the single-stage water–gas shift reaction in fuel cell applications. Part 2. Roles of the support and promoter on catalyst activity and stability. *Journal of Catalysis* **2007,** *251* (1), 163-171.

7. Iida, H., Akira Igarashi, Structure characterization of Pt-Re/TiO2 (rutile) and Pt-Re/ZrO2 catalysts for water gas shift reaction at low-temperature. *Applied Catalysis A: General* **2006,** *303* (2), 192-198.

8. Iida, H., Akira Igarashi, Difference in the reaction behavior between Pt–Re/TiO2 (Rutile) and Pt–Re/ZrO2 catalysts for low-temperature water gas shift reactions. *Applied Catalysis A: General* **2006,** *303* (1), 48-55.

9. Sato, Y., Keisuke Terada, Satoshi Hasegawa, Toshihiro Miyao, Shuichi Naito, Mechanistic study of water–gas-shift reaction over TiO2 supported Pt–Re and Pd–Re catalysts. *Applied Catalysis A: General* **2005,** *296*, 80-89.

10. Wei, Z.; Karim, A.; Li, Y.; Wang, Y., Elucidation of the Roles of Re in Aqueous-Phase Reforming of Glycerol over Pt–Re/C Catalysts. *ACS Catalysis* **2015,** *5* (12), 7312-7320.

11. Falcone, D. D.; Hack, J. H.; Klyushin, A. Y.; Knop-Gericke, A.; Schlögl, R.; Davis, R. J., Evidence for the Bifunctional Nature of Pt–Re Catalysts for Selective Glycerol Hydrogenolysis. *ACS Catalysis* **2015,** *5* (10), 5679-5695.

www.manaraa.com

12. Ciftci, A.; Ligthart, D. A. J. M.; Sen, A. O.; van Hoof, A. J. F.; Friedrich, H.; Hensen, E. J. M., Pt-Re synergy in aqueous-phase reforming of glycerol and the water–gas shift reaction. *Journal of Catalysis* **2014,** *311*, 88-101.

13. Ciftci, A.; Ligthart, D. A. J. M.; Hensen, E. J. M., Aqueous phase reforming of glycerol over Re-promoted Pt and Rh catalysts. *Green Chem.* **2014,** *16* (2), 853-863.

14. Kim, Y. T., Dumesic, James A., Huber, George W., Aqueous-phase hydrodeoxygenation of sorbitol: A comparative study of Pt/Zr phosphate and PtReOx/C. *Journal of Catalysis* **2013,** *304*, 72-85.

15. Zhang, L., Ayman M. Karim, Mark H. Engelhard, Zhehao Wei, David L. King, Yong Wang, Correlation of Pt–Re surface properties with reaction pathways for the aqueous-phase reforming of glycerol. *Journal of Catalysis* **2012,** *287*, 37-43.

16. King, D. L., Zhang, Liang, Xia, Gordon, Karim, Ayman M., Heldebrant, David J., Wang, Xianqin, Peterson, Tom, Wang, Yong, Aqueous phase reforming of glycerol for hydrogen production over Pt–Re supported on carbon. *Applied Catalysis B: Environmental* **2010,** *99* (1-2), 206-213.

17. Kunkes, E. L., Dante A. Simonetti, James A. Dumesic, William D. Pyrz, Luis E. Murillo, Jingguang G. Chen, Douglas J. Buttrey, The role of rhenium in the conversion of glycerol to synthesis gas over carbon supported platinum–rhenium catalysts. *Journal of Catalysis* **2008,** *260*, 164-177.

18. Simonetti, D. A., E.L. Kunkes, J.A. Dumesic, Gas-phase conversion of glycerol to synthesis gas over carbon-supported platinum and platinum–rhenium catalysts. *Journal of Catalysis* **2007,** *247*, 298-306.

www.manaraa.com

19. Duke, A. S.; Galhenage, R. P.; Tenney, S. A.; Sutter, P.; Chen, D. A., In Situ Studies of Carbon Monoxide Oxidation on Platinum and Platinum–Rhenium Alloy Surfaces. *The Journal of Physical Chemistry C* **2015,** *119* (1), 381-391.

20. Duke, A. S.; Galhenage, R. P.; Tenney, S. A.; Ammal, S. C.; Heyden, A.; Sutter, P.; Chen, D. A., In Situ Ambient Pressure X-ray Photoelectron Spectroscopy Studies of Methanol Oxidation on Pt(111) and Pt–Re Alloys. *The Journal of Physical Chemistry C* **2015,** *119* (40), 23082-23093.

21. Duke, A. S.; Xie, K.; Monnier, J. R.; Chen, D. A., Superior long-term activity for a Pt-Re alloy compared to Pt in methanol oxidation reactions. *Surface Science* **2017,** *657*, 35-43.

22. Duke, A. S.; Xie, K.; Brandt, A. J.; Maddumapatabandi, T. D.; Ammal, S. C.; Heyden, A.; Monnier, J. R.; Chen, D. A., Understanding Active Sites in the Water–Gas Shift Reaction for Pt–Re Catalysts on Titania. *ACS Catalysis* **2017,** *7* (4), 2597-2606.

23. Ramstad, A., F. Strisland, S. Raaen, A. Borg, C. Berg, CO and O2 adsorption on the Re/Pt(111) surface studied by photoemission and thermal desorption. *Surface Science* **1999,** *440*, 290-300.

24. Ramstad, A., F. Strisland, S. Raaen, T. Worren, A. Borg, C. Berg, Growth and alloy formation studied by photoelectron spectroscopy and STM. *Surface Science* **1999,** *425*, 57-67.

25. Prestvik, R., Moljord, K., Grande, K., Holmen, A., Influence of Pretreatment on the Metal Function of a Commercial Pt-Re/Al2O3 Catalyst. *Journal of Catalysis* **1998,** *174*, 119-129.

www.manaraa.com

26. Prestvik, R., Totdal, B., Lyman, C. E., Holmen, A., Bimetallic Particle Formation in Pt-Re/Al2O3 Reforming Catalyst Revealed by Energy-Dispersive X-Ray Spectrometry in the Analytical Electron Microscope. *Journal of Catalysis* **1998,** *176*, 246-252.

27. Daniel, O. M.; DeLaRiva, A.; Kunkes, E. L.; Datye, A. K.; Dumesic, J. A.; Davis, R. J., X-ray Absorption Spectroscopy of Bimetallic Pt-Re Catalysts for Hydrogenolysis of Glycerol to Propanediols. *ChemCatChem* **2010,** *2* (9), 1107-1114.

28. Xie, K. Understanding The Activity Of Model Catalyst Surfaces: Ultrahigh Vacuum and Atmospheric Pressure Studies. University of South Carolina, 2016.

29. Galhenage, R. P.; Xie, K.; Yan, H.; Seuser, G. S.; Chen, D. A., Understanding the Growth, Chemical Activity, and Cluster-Support Interactions for Pt-Re Bimetallic Clusters on TiO2(110). *The Journal of Physical Chemistry C* **2016,** *120*, 10866-10878.

30. Tenney, S. A.; Cagg, B. A.; Levine, M. S.; He, W.; Manandhar, K.; Chen, D. A., Enhanced activity for supported Au clusters: Methanol oxidation on Au/TiO2(110). *Surface Science* **2012,** *606* (15-16), 1233-1243.

31. Somorjai, G. A., Godbey, D. J., The Preparation and Characterization of Rhenium Modified Pt(111) and Pt(100), and Platinum Modified Re(0001) Single Crystal Surfaces. *Surface Science* **1988,** *202*, 204-226.

32. Reason, M.; Rudawski, N. G.; McKay, H. A.; Weng, X.; Ye, W.; Goldman, R. S., Mechanisms of GaAsN growth: Surface and step-edge diffusion. *Journal of Applied Physics* **2007,** *101* (8), 083520.

33. Esch, S.; Hohage, M.; Michely, T.; Comsa, G., Origin of oxygen induced layer-by-layer growth in homoepitaxy on Pt(111). *Phys Rev Lett* **1994,** *72* (4), 518-521.

www.manaraa.com

34. Michely, T.; Hohage, M.; Esch, S.; Comsa, G., The effect of surface reconstruction on the growth mode in homoepitaxy. *Surface Science Letters* **1996,** *349*, L89-L94.

35. Kalff, M.; Šmilauer, P.; Comsa, G.; Michely, T., No coarsening in Pt(111) homoepitaxy. *Surface Science* **1999,** *426*, L447-L453.

36. Kolasinski, K. W., *Surface Science: Foundations of Catalysis and Nanoscience*. Third Edition ed.; John Wiley & Sons, Ltd: 2012.

37. Vrijmoeth, J.; van der Vegt, H. A.; Meyer, J. A.; Vlieg, E.; Behm, R. J., Surfactant-induced layer-by-layer growth of Ag on Ag(111): Origins and side effects. *Phys Rev Lett* **1994,** *72* (24), 3843-3846.

38. Roder, H.; Brune, H.; Kern, K., Roughening and fragmentation of strained Ag islands on Pt(111). *Phys Rev Lett* **1994,** *73* (15), 2143.

39. Baetzold, R. C.; Apai, G.; Shustorovich, E.; Jaeger, R., Surface core-level shifts for Pt single-crystal surfaces. *Physical Review B* **1982,** *26* (8), 4022-4027.

40. Ping, L., Shuh, D. K, Adsorption of O2 on Polycrystalline Rhenium Metal at Room Temperature Studied by Synchrotron X-ray Photoemission Spectroscopy. *Journal of Electron Spectroscopy and Related Phenomena* **2001,** *114-116*, 319-325.

41. Chan, A. S. Y.; Wertheim, G. K.; Wang, H.; Ulrich, M. D.; Rowe, J. E.; Madey, T. E., Surface atom core-level shifts of clean and oxygen-coveredRe(1231). *Physical Review B* **2005,** *72* (3).

42. Ducros, R.; Fusy, J., Core level binding energy shifts of rhenium surface atoms for a clean and oxygenated surface. *Journal of Electron Spectroscopy and Related Phenomena* **1987,** *42*, 305-312.

www.manaraa.com

43. Detwiler, M. D.; Majumdar, P.; Gu, X.-K.; Delgass, W. N.; Ribeiro, F. H.; Greeley, J.; Zemlyanov, D. Y., Characterization and theory of Re films on Pt(111) grown by UHV-CVD. *Surface Science* **2015,** *640*, 2-9.

44. Mun, B. S., M. Rossi, P. N. Ross Jr., The study of surface segregation of Re(3)Pt polycrystalline alloy with photoelectron spectroscopy. *The Journal of chemical physics* **2008,** *129* (17), 174707.

45. *Surface Analysis – The Principal Techniques*. 2nd ed.; John Wiley & Sons, Ltd: 2009.

46. Vitos , A. V., H. L. Ruban , H.L. Skriver , J. Kolla´r, The surface energy of metals. *Surface Science* **1998,** *411*, 186-202.

47. Björneholm, O.; Nilsson, A.; Tillborg, H.; Bennich, P.; Sandell, A.; Hernnäs, B.; Puglia, C.; Mårtensson, N., Overlayer structure from adsorbate and substrate core level binding energy shifts: CO, CCH3 and O on Pt(111). *Surface Science* **1994,** *315*, L983-L989.

48. Tysoe, W. T.; Zaera, F.; Somorjai, G. A., An XPS study of the oxidation and reduction of the Rhenium-Platinum system under atmospheric conditions. *Surface Science* **1988,** *200*, 1-14.

49. Puglia, C.; Nilsson, A.; Hernnäs, B.; Karis, O.; Bennich, P.; Mårtensson, N., Physisorbed, chemisorbed and dissociated 02 on Pt(111) studied by different core level spectroscopy methods. *Surface Science* **1995,** *342*, 119-133.

50. Miller, D. J.; Oberg, H.; Kaya, S.; Sanchez Casalongue, H.; Friebel, D.; Anniyev, T.; Ogasawara, H.; Bluhm, H.; Pettersson, L. G.; Nilsson, A., Oxidation of Pt(111) under near-ambient conditions. *Phys Rev Lett* **2011,** *107* (19), 195502.

www.manaraa.com

51. Drucos, R.; Alnot, M.; Ehrhardt, J. J.; Housley, M.; Piquard, G.; Cassuto, A., A study of the adsorption of several oxygen-containing molecules (O2, CO, NO, H2O) on Re(0001) by XPS, UPS and temperature programmed desorption. *Surface Science* **1980,** *94*, 154-168.

52. Okal, J., Oxidation and redispersion of a low-loaded Re/γ-Al2O3 catalyst. *Journal of Catalysis* **2003,** *219* (2), 362-371.

53. Shpiro, E. S.; Avaev, V. I.; Antoshin, G. V.; Ryashentseva, M. A.; Micachev, K. M., XPS Studies of the Rhenium State in Supported Re Catalysts. *Journal of Catalysis* **1978,** *55*, 402-406.

54. Kirlin, P. S.; Strohmeier, B. R.; Gates, B. C., The effect of carbon on the reducibility of Rhenium in Pt-Re/Al2O3 Catalysts. *Journal of Catalysis* **1986,** *98*, 308-316.

55. Okal, J., Tylus, W., Kepinski, L., XPS study of oxidation of rhenium metal on γ-Al2O3 support. *Journal of Catalysis* **2004,** *225* (2), 498-509.

56. Okal, J., A study of effect of particle size on the oxidation of rhenium in the Re/γ-Al2O3 catalysts. *Applied Catalysis A: General* **2005,** *287* (2), 214-220.

www.manaraa.com

APPENDIX A

SUPPLEMENTAL TABLE FOR CHAPTER 3

Vendors for the carbon and metal oxide supports used for experiments in Figure 3.10, Figure 3.2 and Table A.1 are as follows: Darco G60 (Cabot Corporation), Ketjen Black EC300 (AkzoNobel), Timrex HSAG 300 (Imerys Graphite and Carbon), Darco S51 (Cabot Corporation), and Darco KBM (Cabot Corporation). Vendors for the oxide supports were: Aerosil 300 hydrophilic fumed silica (Evonik Industries) and Puralox/Catalox g-alumina SBa200 (Sasol).

www.manaraa.com

Table A.1: Experimental details for SEA studies on carbon supports.

Precursor	Support	PZC	pH (initial)	Concentration (ppm)	Experiment	Associated Figure
$H_2[PtCl_6]$	HOPG	---	2.5[a]	100	XPS	3.3a
$H_2[PtCl_6]$	GNPs	7-8	3	300	XPS	3.3b
$H_2[PtCl_6]$	HOPG	---	2.5[a]	100	AFM	3.5
$H_2[PtCl_6]$	GNPs	7-8	3	300	STEM	3.6
$[Pt(NH_3)_4](OH)_2$	HOPG	----	11	100	XPS	3.7a
$[Pt(NH_3)_4](OH)_2$	GNPs	7-8	11.5[b]	300	XPS	3.7b
$[Pt(NH_3)_4](OH)_2$	HOPG	----	11	100	AFM	3.8
$[Pt(NH_3)_4](OH)_2$	GNPs	7-8	11	300	STEM	3.9
$Na_2[PtCl_4]$	HOPG	----	2.2	100	XPS	3.10a, i
$Na_2[PtCl_4]$	GNPs	7-8	3	300	XPS	3.10a, ii
$Na_2[PtCl_4]$	Darco G60	8.5	3	300	XPS	3.10a, iii
$Na_2[PtCl_4]$	Ketjen black	9.4	3	200	XPS	3.10a, iv
$[Pt(NH_3)_4](OH)_2$	Timrex HSG300	4.5	11	300	XPS	3.10b, i
$[Pt(NH_3)_4](OH)_2$	Darco S51	4.7	11	300	XPS	8b, ii
$[Pt(NH_3)_4](OH)_2$	Darco KBM	2.8	11	300	XPS	8b, iii
$[Pt(NH_3)_4](Cl)_2$	Silica	4.1[c]	11	300	XPS	None
$Na_2[PtCl_4]$	g-Alumina	8.3[c]	3	200	XPS	None

www.manaraa.com

[a]Although the absolute uptakes of $H_2[PtCl_6]$ on HOPG may depend on pH (2.5 vs. 3), the uptake trends as a function of pH are the same on the untreated and HCl-treated GNP surfaces (Figure 3.4a).

[b]Based on the uptake vs. pH curve for $[Pt(NH_3)_4](OH)_2$ on GNPs, the uptakes are nearly identical at pHs of 11 and 11.5 (Figure 3.4b).

[c]Initial and final pHs during SEA were the same except on silica and alumina, where the final values were 8.7 and 4.2, respectively.

www.manaraa.com

APPENDIX B
PERMISSION TO PRINT FOR CHAPTER 3

SPRINGER NATURE LICENSE
TERMS AND CONDITIONS

Jul 03, 2018

This Agreement between Mr. Grant Seuser ("You") and Springer Nature ("Springer Nature") consists of your license details and the terms and conditions provided by Springer Nature and Copyright Clearance Center.

License Number	4363270474886
License date	Jun 06, 2018
Licensed Content Publisher	Springer Nature
Licensed Content Publication	Topics in Catalysis
Licensed Content Title	Understanding Uptake of Pt Precursors During Strong Electrostatic Adsorption on Single-Crystal Carbon Surfaces
Licensed Content Author	Grant S. Seuser, Ritubarna Banerjee, Kamolrat Metavarayuth et al
Licensed Content Date	Jan 1, 2017
Licensed Content Volume	61
Licensed Content Issue	5
Type of Use	Thesis/Dissertation
Requestor type	academic/university or research institute
Format	print and electronic
Portion	full article/chapter
Will you be translating?	no
Circulation/distribution	<501
Author of this Springer Nature content	yes
Title	Understanding the adsorption and nucleation of transition metals on model carbon supports
Instructor name	Donna A. Chen
Institution name	University of South Carolina

www.manaraa.com

Terms and Conditions

Springer Nature Terms and Conditions for RightsLink Permissions

Springer Customer Service Centre GmbH (the Licensor) hereby grants you a non-exclusive, world-wide licence to reproduce the material and for the purpose and requirements specified in the attached copy of your order form, and for no other use, subject to the conditions below:

1. The Licensor warrants that it has, to the best of its knowledge, the rights to license reuse of this material. However, you should ensure that the material you are requesting is original to the Licensor and does not carry the copyright of another entity (as credited in the published version).

   If the credit line on any part of the material you have requested indicates that it was reprinted or adapted with permission from another source, then you should also seek permission from that source to reuse the material.

2. Where **print only** permission has been granted for a fee, separate permission must be obtained for any additional electronic re-use.

3. Permission granted **free of charge** for material in print is also usually granted for any electronic version of that work, provided that the material is incidental to your work as a whole and that the electronic version is essentially equivalent to, or substitutes for, the print version.

4. A licence for 'post on a website' is valid for 12 months from the licence date. This licence does not cover use of full text articles on websites.

5. Where **'reuse in a dissertation/thesis'** has been selected the following terms apply: Print rights for up to 100 copies, electronic rights for use only on a personal website or institutional repository as defined by the Sherpa guideline (www.sherpa.ac.uk/romeo/).

6. Permission granted for books and journals is granted for the lifetime of the first edition and does not apply to second and subsequent editions (except where the first edition permission was granted free of charge or for signatories to the STM Permissions Guidelines http://www.stm-assoc.org/copyright-legal-affairs/permissions/permissions-guidelines/), and does not apply for editions in other languages unless additional translation rights have been granted separately in the licence.

7. Rights for additional components such as custom editions and derivatives require additional permission and may be subject to an additional fee. Please apply to Journalpermissions@springernature.com/bookpermissions@springernature.com for these rights.

8. The Licensor's permission must be acknowledged next to the licensed material in print. In electronic form, this acknowledgement must be visible at the same time as the figures/tables/illustrations or abstract, and must be hyperlinked to the journal/book's homepage. Our required acknowledgement format is in the Appendix below.

9. Use of the material for incidental promotional use, minor editing privileges (this does not include cropping, adapting, omitting material or any other changes that affect the meaning, intention or moral rights of the author) and copies for the disabled are permitted under this licence.

10. Minor adaptations of single figures (changes of format, colour and style) do not require the Licensor's approval. However, the adaptation should be credited as shown in Appendix below.

www.manaraa.com